Effects Of The Relativistic Correction To The Electron Mass On Electron Cyclotron Current Drive

J.A. Owen

THESIS SUBMITTED FOR THE DEGREE OF DOCTOR OF PHILOSOPHY OF THE UNIVERSITY OF ST ANDREWS

EFFECTS OF THE RELATIVISTIC CORRECTION TO THE ELECTRON MASS ON ELECTRON CYCLOTRON CURRENT DRIVE

Abstract

Electron cyclotron resonance heating (ECRH) has a number of advantages over similar schemes for heating tokamaks. Recently, it has been proposed, by Fisch and Boozer, as a method for driving the electric current necessary for the stability of tokamaks. The mechanism relies on preferential heating of electrons which are moving in one direction along the magnetic field lines. In this thesis we investigate the effect of including the relativistic correction to the electron mass on the mechanism and the efficiency of ECRH current drive.

First of all, the propagation and absorption of waves at the fundamental electron cyclotron frequency and its second harmonic are studied, using the weakly relativistic dielectric tensor. The relativistic resonance condition is then investigated. This differs from the non-relativistic one in a number of important ways. The resonance condition is now asymmetric about the resonance point. Also, the scaling of resonant velocity and the ratio of current density to power density with distance are changed, so that the position of the current layer is significantly altered.

Current drive efficiency, measured in terms of the ratio of total current driven to total power absorbed, is then calculated using the theory of Fisch and Boozer, and some representative results are given. Finally, the linear theory on which the current drive

calculation is based is examined, and it is found that for power densities typical of present day tokamaks, the linear theory is invalid.

ACKNOWLEDGEMENTS

I would like to thank Drs R.A. Cairns and J.J. Sanderson of the Applied Mathematics Department and Dr C.N. Lashmore-Davies of Culham Laboratory for their supervision during my period as a research student.

I would also like to thank the staff of Culham Laboratory for their help and, in particular, Dr T.J. Martin for the use of his routine for calculating the plasma dispersion.

I wish to thank Miss Shiela Wilson for typing this thesis.

I am grateful to Culham Laboratory and the Science and Engineering Research Council for financial support.

CERTIFICATE

I certify that John A. Owen has satisfied the conditions of the Ordinance and Regulations and is thus qualified to submit the accompanying application for the degree of Doctor of Philosophy.

POSTGRADUATE CAREER

I was admitted into the University of St Andrews as a research student under Ordinance General No.12 in October 1981 to work on Electron Cyclotron Current Drive under the supervision of Dr J.J. Sanderson. I was admitted under the above resolution as a candidate for the degree of Ph.D. in October 1982.

DECLARATION

I declare that the following thesis is a record of research work carried out by me, that the thesis is my own composition, and that it has not been previously presented in application for a higher degree.

CONTENTS

CHAPTER 1

INTRODUCTION

Heating in Tokamaks

Ever since the confirmation of the results obtained on the T-3 tokamak in Moscow (Peacock *et al.*, 1969), there have been tokamak research programmes in many countries. These programmes have proved successful and have led to the design and construction of a new generation of large tokamaks such as JET and TFTR which, it is hoped, will produce plasma in conditions close to those required in a thermonuclear fusion reactor.

At present, the tokamak is a pulsed device in which an electric current is driven inductively. This current serves two purposes. Firstly, it creates the poloidal magnetic field which is necessary for equilibrium of the tokamak. Secondly, due to the electrical resistance of the plasma, the current heats the plasma ohmically. However, as the temperature of the plasma increases, its resistance decreases since the ions and electrons collide less often at higher velocities. This reduces the effectiveness of ohmic heating at high temperatures. It is then quite clear that in order to heat the plasma to the temperature required for fusion ($\gtrsim 10^8$K), some additional heating will be required.

Several methods have been proposed for providing this additional heating and these can be divided into three groups.

The one which has received most attention to date is neutral beam injection heating. The principle is simply to inject a beam of high energy neutral atoms into the plasma. The neutral atoms readily cross the confining magnetic fields and are ionised once they are in the plasma. The resulting ions give up their energy as they are slowed down. It is arranged that the mean free path for ionization of the neutral beam is approximately the same as the plasma radius, so that the heating is distributed over the plasma volume and there is virtually complete absorption of the beam. Neutral beam heating at power levels up to 3MW has proved to be successful (Eubank *et al.*, 1979; Roberts, 1979) and its importance to the fusion programme is clear.

Other heating methods use low frequency or non-oscillatory electromagnetic fields. One such method is magnetic compression in minor radius (Furth and Yoshikawa, 1970). This can be achieved either by increasing the toroidal magnetic field, or (better, since less power is required) reducing the major radius by using an increasing vertical field. The latter method has been used successfully at Princeton University (Robinson, 1981). Another method in this group is transit-time magnetic pumping (TTMP). In this scheme (Berger *et al.*, 1958), the plasma passes through a solenoid in which the magnetic field is sinusoidally modulated, or "pumped". The modulation frequency is chosen so that the period is comparable with the transit-time of a particle through the solenoid. However, at these frequencies, nonlinear parametric

instabilities (Canobbio, 1975) can be excited, and this may have been the cause of the phenomenon of "pump-out" observed in some experiments (Lees *et al.*, 1972). A high power heating experiment using TTMP has been carried out in Grenoble (Parlange *et al.*, 1978).

The final group of methods for heating tokamaks consists of methods which use high frequency electromagnetic waves. In order of increasing frequency, these are heating in the ion cyclotron range of frequencies (ICRF), lower hybrid resonance heating (LHRH), and electron cyclotron resonance heating (ECRH). In ICRF, the range of frequencies used is 25 to 100 MHz. Several natural resonances exist in the plasma in this frequency range which enable power to be absorbed from an applied electromagnetic field. These are the ion cyclotron frequency Ω_i $\left(= \frac{qB}{m_i}\right.$, where q is the ion charge, B is the magnetic field and m_i is the ion mass$\left.\right)$ and its harmonics, and the ion-ion hybrid resonance, which can exist if there are two ion species in the plasma with differing charge to mass ratio. The applied electromagnetic field excites the "fast" magnetosonic wave in the plasma, and this is absorbed by one of several mechanisms. There has been much interest in schemes where there is a small proportion of one of the ion species (Stix, 1975), and significant ion heating has been obtained in this way in PLT (Hosea, 1980) and TFR (Equipe TFR, 1980).

In LHRH, the plasma is heated by resonance with waves at the lower hybrid frequency ($\omega_{LH}^2 = \omega_{pi}^2/(1 + \omega_{pe}^2/\Omega_e^2)$, where ω_{pi} and ω_{pe} are the ion and electron plasma frequencies and Ω_e is the electron

cyclotron frequency). The waves are transformed at the lower hybrid resonance to slow plasma waves which are then strongly damped. Ion temperatures of close to 10^7K have been achieved using this method (Suzuki *et al.*, 1980; Schuss *et al.*, 1979).

In ECRH, waves at the electron cyclotron frequency $\Omega_e \left(= \frac{eB}{m_e}\right)$ or its harmonics are used. As with other electromagnetic resonance schemes, resonance does not occur through the whole plasma, but just around the resonance layer at which, in this case, the wave frequency ω equals Ω_e. Around this layer the electrons gain energy from the waves and their perpendicular velocity is increased. The ions in the plasma gain energy from collisions with the electrons. For a typical tokamak toroidal magnetic field of 3T, the cyclotron frequency is 84 GHz. This is the main problem with ECRH, namely to be able to produce high power waves of this frequency efficiently. Only with the recent development of the gyrotron source (Manheimer and Granatstein, 1977; Alikaev *et al.*, 1978; Jory *et al.*, 1980) has ECRH in tokamaks become practicable.

The main advantages of ECRH are as follows (Fidone *et al.*, 1978; Arunasalam *et al.*, 1983; Manheimer, 1979)

(1) The electromagnetic waves can penetrate easily to the core of the plasma.

(2) This penetration is largely independent of density, temperature and other conditions at the plasma edge.

(3) Power deposition can be localised in the plasma at any desired position.

(4) No complicated antenna structure is necessary for production of the waves.

(5) Wave reflection by the plasma can be avoided, which eliminates the dangerous plasma-wave interaction at the edge.

(6) ECRH is a very clean scheme, in that virtually nothing seems to go into the plasma except power.

(7) The theory of ECRH is relatively simple.

Effective heating has been obtained using ECRH in experiments on TM-3 (Alikaev *et al.*, 1976) and T10 (Strelkov, 1979) both at the fundamental cyclotron frequency and the second harmonic ($\omega = 2\Omega_e$). However, experiments have yet to be performed on tokamaks with large magnetic fields because of the lack of high frequency sources.

Current drive in tokamaks

In its present form the tokamak is necessarily a pulsed device due to the inductive mechanism used for driving the plasma current. The desirability of maintaining a steady current has long been recognised, and various methods have been proposed for doing this, (Fisch, 1980).

Ohkawa (1970) suggested that ion beams could be used for driving currents. High velocity neutral beams enter the plasma and are ionised, producing ions of disparate charge states. Electrons in the plasma collide preferentially with the ions with the higher charge state and consequently drift in the streaming direction of these ions, producing net current.

Wort (1971) proposed the use of travelling Alfvén waves to impart momentum to resonant electrons (those with parallel velocity $v_{//}$ equal to the wave parallel phase velocity $\omega/k_{//}$). The idea is to impart momentum with as little as possible energy expenditure to the resonant electrons and thence, by collisions, to produce a drift of the electron fluid.

One of the most promising schemes is to launch waves at the lower hybrid frequency in one direction around the tokamak (Fisch, 1978). High energy electrons are preferentially driven one way by Landau damping. A number of experiments have obtained current in this way (Wong *et al.*, 1980; Yamamoto *et al.*, 1980).

The common feature of the three schemes outlined above is that net toroidal momentum is delivered to either the electrons or the ions by an external source and a current is thereby created. A basically different method, which is the subject of this thesis, was proposed by Fisch and Boozer (1980), in which no net toroidal momentum is injected. Instead, the collisionality of the plasma is altered so that, for example, electrons moving to the right collide more frequently with the ions than do electrons moving to the left. There is then a net current with ions moving to the right and electrons moving to the left. A feature of this scheme is that collisions are an integral part and without them there would be no current, whereas in the earlier methods, collisions between electrons and ions will reduce the current.

The means of achieving this altered collisionality of the plasma is to preferentially heat electrons travelling to the left so that, being hotter, they collide less. An electron cyclotron

wave can do this, as will be described in Chapter 4. It is suggested that, despite their low parallel momentum content, electron cyclotron waves can drive currents with a similar efficiency to other methods, this efficiency being measured in terms of the total current driven per unit power dissipated in the plasma.

Due to the advent of the gyrotron and the corresponding interest in ECRH, there was a fair amount of early theoretical work on ECRH current drive. Cordey *et al.* (1982) balanced the effect of waves on the electron distribution function with a Fokker-Planck collision operator and included the effects of toroidally trapped electrons. They used a linearised method in which the perturbation to the distribution function is assumed to be small. Chan *et al.* (1982) also used a linearised method, but based on the equation for drift of the guiding centre in toroidal coordinates. More recently, Start and O'Brien (1982) combined the Fokker-Planck code of Cordey *et al.* with a ray tracing code to compute current profiles in toroidal coordinates. Karney and Fisch (1981) numerically checked the formula for the current to power ratio given by Fisch and Boozer and considered nonlinear effects. Fisch (1981) extended the model of Fisch and Boozer to include relativistic dynamics.

Finally, it should be noted that ECRH current drive has been obtained on the Levitron at Culham Laboratory (Start *et al.*, 1982). A current of about 30 mA per Watt, which varied linearly with the microwave power and flowed in opposite directions on opposite sides of the resonance layer, was observed.

Outline of this thesis

It is well-known that the relativistic correction to the electron mass can strongly affect propagation and absorption of electromagnetic waves (Shkarofsky, 1966; Bornatici and Engelmann, 1979; Fidone *et al.*, 1978). This correction has been shown to be important for a wide range of angles of incidence of waves (Fidone *et al.*, 1982) and not just for propagation nearly perpendicular to the magnetic field. It is thus of interest to see whether ECRH current drive is also affected by the correction, and in what way. This is the subject of this thesis.

First of all, the propagation and absorption of electromagnetic waves at the cyclotron frequency and its second harmonic are investigated. For this purpose, the elements of the relativistic dielectric tensor, as given by Shkarofsky (1966), are calculated in Chapter 2. In Chapter 3, these are then used to solve the dispersion relation, and dispersion curves of the results are plotted. In Chapter 4, the theory of ECRH current drive is outlined with particular emphasis on the relativistic resonance condition. Our method of calculating the ratio of current driven to power absorbed is then given in detail. The results of the computer program which calculates the above ratio are presented in Chapter 5. Chapter 6 is an investigation of the validity of the linear approximation used in the current drive calculation. The final chapter summarises the results of the previous chapters and gives suggestions for further work.

CHAPTER 2

Shkarofsky's F_q function

In order to investigate the dispersion of electromagnetic waves as they propagate through a plasma, we require to solve the dispersion relation, which is the condition that the following equation has non-trivial solutions

$$\underset{\sim}{n} \times (\underset{\sim}{n} \times \underset{\sim}{E}) + \underset{\approx}{\varepsilon}.\underset{\sim}{E} = 0 \qquad (1)$$

where $\underset{\sim}{n}$ is the refractive index, $\frac{\underset{\sim}{k}c}{\omega}$, $\underset{\sim}{E}$ is the electric field and $\underset{\approx}{\varepsilon}$ is the dielectric tensor. When the frequency of the waves is close to one of the harmonics of the electron cyclotron frequency, a relativistic expression for $\underset{\approx}{\varepsilon}$ is necessary (Shkarofsky, 1966). Such an expression was derived by Trubnikov (1959), but was exceedingly complicated.

For the case of $n_z = 0$, i.e. wave propagation perpendicular to the magnetic field, a simplification was obtained by Dnestrovskii *et al.* (1964). The first simplification to include non-zero n_z was obtained by Shkarofsky (1966). His expression was restricted to the weakly relativistic case ($v_t^2 << c^2$) and the case of small transverse wave numbers ($\lambda \equiv k_x^2 v_t^2/\Omega^2 < 1$), where v_t is the electron thermal velocity, $(kT_e/m)^{\frac{1}{2}}$, and Ω is the electron cyclotron frequency. This suits our purposes since, at the temperatures we will be considering, $v_t/c \lesssim 1/10$. For thermonuclear reactors, however, this will not be the case.

Shkarofsky's expression for $\underset{\approx}{\varepsilon}$ involves a function, $\mathcal{F}_q$, which is defined as follows

$$\mathcal{F}_q\left(\frac{\mu n\Omega}{\omega}, n_z\right) = -i \int_0^\infty \frac{dt \exp\left\{\mu - \mu[(1-it)^2 + n_z^2 t^2]^{\frac{1}{2}} - in\mu \frac{\Omega}{\omega} t\right\}}{[(1-it)^2 + n_z^2 t^2]^{q/2}} \qquad (2)$$

where $\mu = c^2/v_t^2$ and n is the harmonic number.

Calculation of the $\mathcal{F}_q$ function

Despite the reference to Shkarofsky's expression for the dielectric tensor as a simplification, it is by no means a trivial task to evaluate the $\mathcal{F}_q$ function. $\mathcal{F}_q$ cannot be calculated analytically, so we must resort to numerical methods. There are, however, problems in doing so.

Firstly, except in the situation in which the integral may be made real (see below), the integrand is a rapidly oscillating function of t. This will require a small step width in the numerical integration scheme used, in order to follow the oscillations, and consequently a large number of evaluations of a non-trivial function.

Secondly, the range of integration is infinite. The standard technique for avoiding this problem is to make a substitution such as $u = t/(1+t)$, so that the infinite range is converted to the range [0,1]. For the $\mathcal{F}_q$ function, however, the effect of this will be to give an integrand which has oscillations which get more rapid, without limit, as $u \to 1$. This will make the first problem even more

serious.

In order to circumvent these problems, we use an approximation to $\mathcal{F}_q$ which does not require the direct integration of the integrand of $\mathcal{F}_q$. Three such approximations are described below. Also, under certain conditions, $\mathcal{F}_q$ can be turned into a real integral so that the problem of oscillations doesn't arise.

The "tractable" expression for $\mathcal{F}_q$

Subject to the condition $n_z^2 << 1$, the denominator of (2) can be written as $(1 - it)^q$. The numerator of (2) is

$$\exp \mu \left\{ 1 - (1 - it) \left[1 + \frac{n_z^2 t^2}{(1 - it)^2} \right]^{1/2} - in \frac{\Omega}{\omega} t \right\}.$$

For small values of n_z, we expand $\left[1 + \frac{n_z^2 t^2}{(1 - it)^2} \right]^{1/2}$ by the binomial theorem to obtain

$$\exp \mu \left\{ 1 - (1 - it) - \frac{1}{2} \frac{n_z^2 t^2}{1 - it} + R - in \frac{\Omega}{\omega} t \right\}$$

where the remainder R is given by $R = \frac{1}{8} \frac{\mu n_z^4 t^4}{(1 - it)^3} - \frac{3}{48} \frac{\mu n_z^6 t^6}{(1 - it)^5} + \ldots$

We wish to neglect the remainder R. This will be possible if $\exp \mu R \approx 1$. When t is not large, $\exp \mu R \approx 1$ if $\mu n_z^4 << 1$. When t is large, the real part of the exponential part of the integrand tends

to a constant value (see Appendix). Thus the only variation in the magnitude of the integrand will be through the $(1 - it)^q$ factor in the denominator, so that the integrand is an oscillating function whose magnitude is small and only slowly varying. There will then be cancellation of positive and negative contributions to the integral, and so a negligible net contribution. We may therefore ignore large values of t when considering the integrand.

Our conclusion is, then, that we may neglect the remainder R provided that $\mu n_z^4 << 1$. In this case the numerator becomes

$$\exp \mu \left\{ 1 - (1 - it) - \frac{1}{2} \frac{n_z^2 t^2}{(1 - it)} - in \frac{\Omega}{\omega} t \right\}$$

$$= \exp \mu \left\{ i\delta t - \frac{1}{2} \frac{n_z^2 t^2}{(1 - it)} \right\}, \quad \text{where} \quad \delta = 1 - \frac{n\Omega}{\omega} .$$

The integral is then

$$\mathcal{F}_q = -i \int_0^\infty \frac{dt \exp \mu \left\{ i\delta t - \frac{1}{2} \frac{n_z^2 t^2}{1 - it} \right\}}{(1 - it)^q} \tag{3}$$

subject to

$$\mu n_z^4 << 1 \quad \text{and} \quad n_z^2 << 1. \tag{4}$$

Equation (3) is Shkarofsky's equation (15).

We note that at this point we differ from Shkarofsky. He uses the conditions $\mu n_z^2 << 1$ and $|\mu n_z (2\delta - n_z^2)| << 1$ in order to obtain (3). While these conditions are sufficient, they are by no means

necessary. Shkarofsky does use these conditions to obtain a later equation, but again we do not find that they are necessary (see method 2 below).

Equation (3) is referred to as the "tractable" expression for $\mathcal{F}_q$ by Airoldi and Orefice (1982). Furthermore they show that "only the 'tractable' relativistic form of the function $\mathcal{F}_q$ is needed to obtain the most general dielectric tensor for electromagnetic waves, avoiding all hypotheses and limitations". Equation (3) is therefore used as a starting point for a number of methods for evaluating $\mathcal{F}_q$, without demanding that conditions (4) are satisfied. The justification for this is investigated later.

Method 1 - The method of Krivenski and Orefice

Airoldi and Orefice (1982) show that the tractable expression for $\mathcal{F}_q$ may be written

$$\mathcal{F}_q = \left(\frac{\mu}{2\pi}\right)^{\frac{1}{2}} \int_{-\infty}^{\infty} d\rho \exp(-\tfrac{1}{2}\mu\rho^2) F_{q-\frac{1}{2}}(\mu\beta_n) \qquad (5)$$

$$\text{where} \quad \beta_n = 1 - \frac{n\Omega}{\omega} + \tfrac{1}{2}\rho^2 - \rho n_z \quad \text{and} \quad F_q(z) = -i \int_0^{\infty} \frac{dt\, e^{izt}}{(1-it)^q} \qquad (6)$$

F_q is just the $\mathcal{F}_q$ function in the case of $n_z = 0$ (Dnestrovskii *et al.*, 1964).

Airoldi and Orefice claim that equation (5) is itself a convenient form for the evaluation of $\mathcal{F}_q$, but it involves an integral

over an infinite range of a non-trivial function, so it is not used here.

Krivenski and Orefice (1983) start with an alternative expression for F_q, namely

$$F_q(z) = \frac{1}{(q-1)!} \int_0^\infty dx \, \frac{x^{q-1}\exp(-x)}{x+z} . \tag{7}$$

This is used to derive the following recurrence relations for F_q

$$\begin{aligned} d\,F_{q+1}(z)/dz &= F_{q+1}(z) - F_q(z) \\ F_{q+1}(z) &= [1 - z\,F_q(z)]/q \end{aligned} \tag{8}$$

Equations (8) and (5) are combined to give a recurrence relation for $\mathcal{F}_q$:

$$\mathcal{F}_q = [1 + \phi^2\mathcal{F}_{q-2} - (q-2)\mathcal{F}_{q-1}]/\psi^2 \tag{9}$$

where $\phi^2 = \mu\alpha_n$, $\alpha_n = \frac{1}{2}n_z^2 - \left(1 - \frac{n\Omega}{\omega}\right)$ and $\psi^2 = \frac{1}{2}\mu n_z^2$.

Finally, Krivenski and Orefice give expressions for $\mathcal{F}_{1/2}$ and $\mathcal{F}_{3/2}$ as follows

$$\mathcal{F}_{1/2} = -\tfrac{1}{2}[Z(\psi - \phi) + Z(-\psi - \phi)]/\phi \tag{10}$$

$$\mathcal{F}_{3/2} = -\tfrac{1}{2}[Z(\psi - \phi) - Z(-\psi - \phi)]/\psi \tag{11}$$

$$\text{where} \quad Z(z) = 2i \exp(-z^2) \int_{-\infty}^{iz} \exp(-y^2)\,dy.$$

$Z(z)$ is the well-known plasma dispersion function (Fried and Conte, 1961), routines for the calculation of which are widely available, so that this method for evaluating $\mathcal{F}_q$ is very simple.

Applicability of Method 1

Since this method is based on the tractable expression (3) for $\mathcal{F}_q$, it would seem that the method is only applicable when $\mu n_z^4 \ll 1$ and $n_z^2 \ll 1$. However, according to Airoldi and Orefice, such conditions are not necessary. We investigate this by calculating $\mathcal{F}_q$ and its derivatives for a wide range of parameters by two different methods, namely Simpson's rule (see below) and method 1. Some representative results are presented below.

Table 2.1

Comparison of Simpson's rule and method 1 for the evaluation of $\mathcal{F}_q$ and $\frac{\partial \mathcal{F}_z}{\partial\left(\mu n \frac{\Omega}{\omega}\right)}$. We take $\mu = 511$, $q = 7/2$, $n = 1$, $\frac{\Omega}{\omega} = 0.996$. Results are in the form (real part, imaginary part).

$\mathcal{F}_q$

n_z	Simpson's rule	Method 1
0.001	(0.200, 0)	(1.01, 0)
0.01	(0.201, 0)	(0.200, 0)
0.1	$(0.269, -1.22 \times 10^{-2})$	$(0.269, -1.18 \times 10^{-2})$
0.3	$(8.86 \times 10^{-2}, -0.150)$	$(8.90 \times 10^{-2}, -0.150)$

$\frac{\partial \mathcal{F}_q}{\partial\left(\mu n \frac{\Omega}{\omega}\right)}$

n_z	Simpson's rule	Method 1
0.001	$(4.42\times 10^{-2},\ 0)$	$(-8.61\times 10^{-2},\ 0)$
0.01	$(4.44\times 10^{-2},\ 0)$	$(4.45\times 10^{-2},\ 0)$
0.1	$(0.114,\ -5.18\times 10^{-2})$	$(0.108,\ -5.38\times 10^{-2})$
0.3	$(-1.53\times 10^{-2},\ -1.44\times 10^{-2})$	$(-1.54\times 10^{-2},\ -1.45\times 10^{-2})$

The results are quite contrary to what would be expected. We find that for values of n_z which do not satisfy (4), there is nevertheless good agreement between the two methods. On the other hand, for very small values of n_z where we would expect method 1 to be most accurate we find that it is not.

In order to see the reason for the failure of method 1 for small n_z, we must consider the recurrence relation (9) which is used to calculate $\mathcal{F}_q$ functions with values of q other than $\frac{1}{2}$ and $\frac{3}{2}$. Inevitably there will be some error in the calculation of $\mathcal{F}_{1/2}$ and $\mathcal{F}_{3/2}$. Suppose the error in $\mathcal{F}_{3/2}$ is Δ. Then the error in $\mathcal{F}_{5/2}$ due to this error alone is $-\frac{1}{2}\frac{\Delta}{\psi^2}$. There will be a similar error in $\mathcal{F}_{5/2}$ due to the error in $\mathcal{F}_{1/2}$. Now $2\psi^2 = \mu n_z^2$, so that when $\mu n_z^2 \ll 1$, the error in $\mathcal{F}_{5/2}$ will be much greater than that in $\mathcal{F}_{3/2}$. The error will multiply at each application of the recurrence relation. We therefore find that when condition (4) is well satisfied, application of (9) gives inaccuracy for $q \geq \frac{5}{2}$. For $q = \frac{1}{2}$ and $q = \frac{3}{2}$, small values of n_z yield good results:

Table 2.2

Comparison of Simpson's rule and method 1 for the evaluation of $\mathcal{F}_q$.

We take $\mu = 511$, $q = 3/2$, $n = 1$, $\frac{\Omega}{\omega} = 1.001$.

$\mathcal{F}_q$ n_z	Simpson's rule	Method 1
0.001	(0.528145, -1.51988)	(0.528148, -1.51990)
0.01	(0.4881, -1.49369)	(0.4882, -1.49367)
0.1	$(4.1\times 10^{-3}$, -0.5413)	$(4.3\times 10^{-3}$, -0.5417)
0.3	$(-1.8\times 10^{-4}$, -0.1842)	$(-1.6\times 10^{-4}$, -0.1843)

The minor discrepancies in the real part of $\mathcal{F}_{3/2}$ for $n_z = 0.1$ and $n_z = 0.3$ are due to inaccuracy in the Simpson's rule method, rather than in Method 1.

Our conclusion is that we may use method 1 in all cases except when n_z is small and $q \geq 5/2$.

Method 2 - An approximation to $\mathcal{F}_q$ valid for very small n_z

Again we start from the tractable expression (3) for $\mathcal{F}_q$. Using $-t^2 = (1-it)^2 - 2(1-it) + 1$, we write the numerator as

$$\exp \mu\left\{i\delta t + \frac{n_z^2}{2}\left[(1-it) - 2 + \frac{1}{1-it}\right]\right\}$$

When $\frac{\mu n_z^2}{2} << 1$, we expand the second part of this to obtain

$$\mathcal{F}_q = \int_0^\infty \frac{\exp(i\mu\delta t)}{(1-it)^q}\left[1 + \frac{\mu n_z^2}{2}\left[(1-it) - 2 + \frac{1}{1-it}\right]\right].$$

This will be justified if t is not large and, as before, we may neglect contributions to the integral from large values of t. We also require that $\frac{n_z^2}{2} << |\delta|$ since otherwise the periods of oscillation of the above two expressions would be quite different, and there would be inaccuracy as a result. The requirement that $\frac{n_z^2}{2} << |\delta|$ can be seen clearly from the results of the next section where a full expansion is made.

We now use the definition of the F_q function (6) to obtain

$$\mathcal{F}_q = F_q + \frac{\mu n_z^2}{2}\left[F_{q-1} - 2F_q + F_{q+1}\right] \tag{12}$$

subject to

$$\frac{\mu n_z^2}{2} << 1 \quad \text{and} \quad \frac{n_z^2}{2} << |\delta| \tag{13}$$

where the argument of the F_q function is $\mu\delta$ in each case. Equation (12) is just Shkarofsky's equation (16).

We have now reduced the problem of calculating $\mathcal{F}_q$ to that of calculating $F_q(z)$ where $z = \mu\delta$. For values of z less than 15 in magnitude, we express $F_q(z)$ in terms of the plasma dispersion function as follows

$$F_q(z) = \sum_{p=0}^{q-3/2} (-z)^p \frac{(q-p-2)!}{(q-1)!} + \frac{\pi^{1/2}}{(q-1)!}(-z)^{q-3/2}\, iz^{1/2}\, Z(iz^{1/2}) \tag{14}$$

where the general form of the factorial function is used, namely

$$x! = \int_0^\infty t^x e^{-t}\, dt.$$

The expression (14) does not work well for large values of z because of inaccuracy due to cancellation of large terms. For large values of z we use an asymptotic expansion of the plasma dispersion function to obtain

$$F_q(z) \sim \frac{-\pi\sigma\,(-z)^{q-3/2}\, z^{1/2}\, e^z}{(q-1)!} - \sum_{p=0}^{\infty} \frac{(p+q-1)!}{(-z)^{p+1}(q-1)!} \qquad (15)$$

where $\sigma = 0,1,2$ for $\mathrm{Im}(iz^{1/2})$ greater, equal or less than zero, respectively.

We find that we never need take more than five terms of the asymptotic series to obtain good results.

Finally we note (as mentioned above) that Shkarofsky's conditions for the validity of this approximation, $\frac{\mu n_z^2}{2} << 1$ and $|\mu n_z(2\delta - n_z^2| << 1$ do not agree with ours. We find that the second of these is neither a necessary nor a sufficient condition. This is demonstrated in the following table in which results using Method 2 are compared with those obtained with Method 1, using parameters for which Method 1 is accurate.

Table 2.3

A comparison of Shkarofsky's condition and our condition for the validity of Method 2.

We take $\mu = 500$, $q = 3/2$, $n = 1$, $n_z = 0.02$.

F_q	δ	Method 1	Method 2	Method 2 accurate?	$n_z^2 << \lvert\delta\rvert$?	$\lvert\mu n_z(2\delta - n_z^2)\rvert << 1$?
	-5×10^{-5}	(1.47, -1.01)	(1.39, -1.53)	×	×	✓
	-5×10^{-4}	(0.882, -1.37)	(0.837, -1.40)	×	×	✓
	-5×10^{-3}	(-0.531, -0.454)	(-0.529, -0.454)	✓	?	×
	-5×10^{-2}	(-0.0427, ≈ 0)	(-0.0427, ≈ 0)	✓	✓	×

Method 3 - An approximation to $\mathcal{F}_q$ valid for small n_z

We start again from the tractable expression (3). We write

$$-\frac{1}{2}\frac{\mu t^2 n_z^2}{1-it} = -\tfrac{1}{2}it\mu n_z^2 + \frac{1}{2}\frac{\mu n_z^2}{1-it} - \tfrac{1}{2}\mu n_z^2$$

so that

$$\mathcal{F}_q = -i\exp(-\tfrac{1}{2}\mu n_z^2)\int_0^\infty \frac{\exp\mu\left(i\delta t - \frac{itn_z^2}{2}\right)\exp\left(\frac{\frac{1}{2}\mu n_z^2}{1-it}\right)dt}{(1-it)^q}. \qquad (16)$$

We expand $\exp\left(\frac{\frac{1}{2}\mu n_z^2}{1-it}\right)$ in a power series to obtain

$$\mathcal{F}_q = \exp(-\tfrac{1}{2}\mu n_z^2)\sum_{p=0}^{\infty}\left(\frac{\mu n_z^2}{2}\right)^p\frac{1}{p!}F_{q+p}\left(\mu\delta - \frac{\mu n_z^2}{2}\right) \qquad (17)$$

subject to

$$\mu n_z^2 \lesssim 1. \qquad (18)$$

Equation (17) is an unnumbered equation in Shkarofsky, between his equations (17) and (18).

If (17) is expanded to first order in $\frac{\mu n_z^2}{2}$, using a Taylor series for $F_{q+p}\left(\mu\delta - \frac{\mu n_z^2}{2}\right)$ in conjunction with equation (8), equation (12) is obtained. It is now quite clear that $\frac{n_z^2}{2} << |\delta|$ is a necessary condition for the validity of Method 2.

For Method 3, Shkarofsky requires that $n_z^2 < |\delta|$. We find that this is unnecessary. For example, methods 1 and 3 have been found to agree to at least 3 decimal places for the same range of

parameters as in Table 2.3 even when $n_z^2 > |\delta|$.

Simpson's Rule

As explained above, there are problems involved in the direct numerical calculation of F_q, so this method will merely provide a check on the other methods in some instances.

First of all, we have to convert the infinite range in (2) into a finite one. As has been shown, we can neglect large values of t, so we may simply cut off the range of integration at some finite point. The main problem is that the integrand is oscillating rapidly, coupled with the fact that it is decaying only slowly, so that a very large number of evaluations are necessary before the range of integration can be cut off.

In order to get round this problem, we change the contour of integration, from A to B in Fig. 2.1. We may do this since the singularities of the integrand are close to $t = -i$, and the integrand is zero on C. As a result, the integrand now decays exponentially as $t \to \infty$, and the range of integration can be cut considerably.

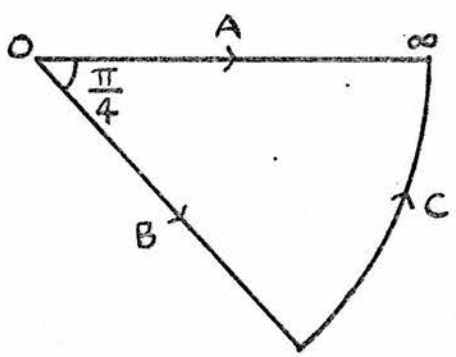

Figure 2.1

The remaining problem is that of determining the cut off point. Due to the complex nature of the integrand, it is not possible to determine this point *a priori*. The procedure, then, is to choose a suitable step length for the application of Simpson's rule, start integrating at the lower limit and continue until the integrand has decayed to a sufficiently small value.

Now as $t \to \infty$, the imaginary part of the exponential part of the integrand becomes (see Appendix)

$$in_z t\left[(1 - n_z^2)^{\frac{1}{2}} - n\frac{\Omega}{\omega}\right].$$

Thus we can use

$$\tau = \frac{2\pi}{n_z\left[(1 - n_z^2)^{\frac{1}{2}} - n\frac{\Omega}{\omega}\right]}$$

as a guide to the period of oscillation of the integrand.

We want, say, 100 evaluations of the integrand in each period, so we take the step length to be $\tau/100$. However, when $(1-n_z^2)^{\frac{1}{2}} \approx n\frac{\Omega}{\omega}$, this step length becomes very large, but the integrand still decays fairly quickly, partly on account of the denominator which we have so far ignored. Thus the number of points of evaluation in the important part of the range becomes vanishingly small. To prevent this happening, we insist that the step length be no more than 0.1, and that there always be at least 40 points of evaluation in total.

We wish to cut off the range of integration at the point where the integrand has decayed to approximately 10^{-6} of its maximum

absolute value. However, we know that the maximum absolute value is normally of order unity, so we simply cut off the integration when the absolute value of the integrand is less than 10^{-6}. The assumption behind this is that the absolute value of the integral will be of order unity, so that we are neglecting only a small fraction. If, as the result of our calculation, we find that the absolute value of the integrand is small, then the calculation is repeated with a correspondingly smaller absolute value of the integrand at which we cut off the integration.

A special case : $\mathcal{F}_q$ is real

If $n\frac{\Omega}{\omega} < (1-n_z^2)^{\frac{1}{2}}$, then $\mathcal{F}_q$ can be turned into a real integral by means of the substitution $y = -it$. We obtain

$$\mathcal{F}_q = \int_0^{-i\infty} \frac{dy \exp\mu\left\{1 - [(1+y)^2 - n_z^2y^2]^{\frac{1}{2}} + n\frac{\Omega}{\omega}y\right\}}{[(1+y)^2 - n_z^2y^2]^{q/2}} . \qquad (19)$$

Now the singularities of the integrand are at $y = \frac{-1}{1 \pm n_z}$ which are both on the negative real axis (n_z being less than 1), and the integral is zero on the contour from $-i\infty$ to ∞. Hence we may replace the upper limit of integration by ∞. We now use Simpson's rule as above, but with some important differences.

The integrand is not oscillatory, so our step length can no longer be determined by the period of oscillation. The exponential part of the integrand becomes, for large y, $\exp\left\{-\mu y\left[(1-n_z^2)^{\frac{1}{2}} - n\frac{\Omega}{\omega}\right]\right\}$. We now identify a region of interest $[0,y_c]$ as that within which the exponential part is greater than e^{-10} ($\approx 5 \times 10^{-5}$). Then

$$y_c = \frac{10}{\mu\left[(1 - n_z^2)^{\frac{1}{2}} - n\frac{\Omega}{\omega}\right]} .$$

In order to have, say, 100 points of evaluation in this region, we take the step length to be $y_c/100$. The cut off point is that at which the integrand has decayed in absolute magnitude to 10^{-5}.

The non-relativistic limit of $\mathcal{F}_q$

In the non-relativistic limit given by $n_z^2 >> |2\delta|$ and $n_z >> \mu^{-\frac{1}{2}}$, $\mathcal{F}_q$ becomes (Shkarofsky, 1966; Fidone *et al.*, 1978)

$$\mathcal{F}_q\left(\mu n\frac{\Omega}{\omega},\ n_z\right) = -\frac{1}{(2\mu)^{\frac{1}{2}} n_z} Z(z_n) \qquad (20)$$

where $$z_n = \frac{\left(1 - n\frac{\Omega}{\omega}\right)\mu^{\frac{1}{2}}}{\sqrt{2}\ n_z} .$$

Some notes on the computation of $\mathcal{F}_q$ and its derivatives

In order to determine the relativistic dielectric tensor we require to calculate $\mathcal{F}_q$, $n_z \frac{\partial \mathcal{F}_q}{\partial n_z}$, and $\frac{\partial \mathcal{F}_q}{\partial\left(\mu n \frac{\Omega}{\omega}\right)}$. First of all, if $n_z = 0$, we have

$$\mathcal{F}_q = F_q(\mu\delta);\quad n_z \frac{\partial \mathcal{F}_q}{\partial n_z} = 0;\quad \frac{\partial \mathcal{F}_q}{\partial\left(\mu n \frac{\Omega}{\omega}\right)} = \frac{\partial F_q(\mu\delta)}{\partial\left(\mu n \frac{\Omega}{\omega}\right)} .$$

We use equations (8) to calculate the derivative of the F_q function.

Next, we use Method 2 when equations (13) are satisfied. It would be convenient to use equation (8) to express F_{q+1} and F_{q-1} in terms of F_q, so that the calculation of only one F_q function would be necessary in (12). This, however, would give rise to inaccuracy for, respectively, large and small values of $\mu\delta$, due to inexact cancellation of terms of large magnitude. If $q = \frac{1}{2}$ we substitute for $F_{-\frac{1}{2}}$ in terms of $F_{\frac{1}{2}}$ since our method for calculating F_q does not work for negative q.

Method 3 is the next choice, provided $\mu n_z^2 < 1$. We use equation (17) for $\mathcal{F}_q$. For the derivatives of $\mathcal{F}_q$ we obtain

$$n_z \frac{\partial \mathcal{F}_q}{\partial n_z} = 2 \exp(-\tfrac{1}{2}\mu n_z^2) \sum_{p=0}^{\infty} \left(\frac{\mu n_z^2}{2}\right)^{p-1} \frac{1}{p!} \left\{\left[-\mu n_z^2 + p - \frac{\mu n_z^2}{2}\left(\frac{q+p-1}{z}\right)\right] F_{q+p} + \frac{\mu n_z^2}{2z}\right\}$$

and

$$\frac{\partial \mathcal{F}_q}{\partial\left(\mu n \frac{\Omega}{\omega}\right)} = -\exp(-\tfrac{1}{2}\mu n_z^2) \sum_{p=0}^{\infty} \left(\frac{\mu n_z^2}{2}\right)^{p} \frac{1}{p!} \left\{\left[1 + \frac{q+p-1}{z}\right] F_{q+p} - \frac{1}{z}\right\}.$$

If $\mu n_z^2 \geq 1$, we check to see whether $\mathcal{F}_q$ may be made real. If this is possible, we use Simpson's rule as described above. If not, then we use the method of Krivenski and Orefice (Method 1).

Some results have already been presented in Tables 2.1, 2.2 and 2.3. It should be mentioned that other results have been obtained which agree with those of other authors (Drestrovskii *et al.*, 1964; Airoldi and Orefice, 1982). We note here that there is an error in equation VIII of Drestrovskii *et al.*: the sign of the last term should be negative, in agreement with Shkarofsky (1966).

CHAPTER 3

Dispersion Relations

We consider propagation in the x-z plane, so that $k_y = 0$. Then the dispersion relation (1) may be written

$$\begin{vmatrix} \varepsilon_{11} - n_z^2 & \varepsilon_{12} & \varepsilon_{13} + n_x n_z \\ \varepsilon_{12} & \varepsilon_{22} - n_x^2 - n_z^2 & \varepsilon_{23} \\ n_x n_z + \varepsilon_{31} & \varepsilon_{32} & -n_x^2 + \varepsilon_{33} \end{vmatrix} = 0. \qquad (21)$$

The Relativistic Dielectric Tensor

The dielectric tensor elements are given in equations (4) of Shkarofsky (1966). These are

$$\left.\begin{aligned}
\varepsilon_{11} - 1 &= \varepsilon_{22} - 1 = -\frac{\omega_p^2}{\omega^2}\,\mu \sum_{n=0}^{\infty} \frac{n^2 \lambda^{n-1}}{2^n\, n!}\, \mathcal{F}^a_{n+3/2} \\
i\varepsilon_{12} &= -i\varepsilon_{21} = -\frac{\omega_p^2}{\omega^2}\,\mu \sum_{n=0}^{\infty} \frac{n^2 \lambda^{n-1}}{2^n\, n!}\, \mathcal{F}^b_{n+3/2} \\
\varepsilon_{33} - 1 &= -\frac{\omega_p^2}{\omega^2}\,\mu \left\{ \frac{\partial}{\partial n_z}\left[n_z\, \mathcal{F}_{5/2}(0, n_z)\right] + \sum_{n=0}^{\infty} \frac{\lambda^n}{2^n\, n!} \frac{\partial}{\partial n_z}\left(n_z\, \mathcal{F}^a_{n+5/2}\right) \right\} \\
\varepsilon_{13} &= \varepsilon_{31} = -\frac{\omega_p^2}{\omega^2}\,\mu\, \frac{n_x n_z}{\Omega/\omega} \sum_{n=0}^{\infty} \frac{n\lambda^{n-1}}{2^n\, n!} \frac{\partial}{\partial(n\mu\Omega/\omega)}\, \mathcal{F}^a_{n+5/2} \\
-i\varepsilon_{23} &= i\varepsilon_{32} = -\frac{\omega_p^2}{\omega^2}\,\mu\, \frac{n_x n_z}{\Omega/\omega} \sum_{n=0}^{\infty} \frac{n\lambda^{n-1}}{2^n\, n!} \frac{\partial}{\partial(n\mu\Omega/\omega)}\, \mathcal{F}^b_{n+5/2}
\end{aligned}\right\} \qquad (22)$$

where $\mathcal{F}^a_q = \mathcal{F}_q\left(\mu n \frac{\Omega}{\omega},\ n_z\right) + \mathcal{F}_q\left(-\mu n \frac{\Omega}{\omega},\ n_z\right)$

$$\mathcal{F}^b_q = \mathcal{F}_q\left(\mu n \frac{\Omega}{\omega},\ n_z\right) - \mathcal{F}_q\left(-\mu n \frac{\Omega}{\omega},\ n_z\right)$$

$$\lambda = \frac{n_x^2}{(\Omega/\omega)^2 \mu}$$

First of all, we make approximations regarding $\mathcal{F}_q^a$ and $\mathcal{F}_q^b$. For waves at the fundamental cyclotron frequency $\mathcal{F}_q\left(\mu\frac{\Omega}{\omega},\ n_z\right)$ will be much larger in magnitude than $\mathcal{F}_q\left(-\mu\frac{\Omega}{\omega},\ n_z\right)$. The reason is that the integrand of the second $\mathcal{F}_q$ function is oscillating much more rapidly than that of the first one, but the magnitudes of the integrands are similar, so that cancellation of positive and negative contributions will be more effective. This is because, as we saw in the last chapter, the period of oscillations is inversely proportional to $(1-n_z^2)^{\frac{1}{2}} - n\frac{\Omega}{\omega}$ (at least approximately) and $(1-n_z^2)^{\frac{1}{2}} \approx 1$ for the range of angles which we will be considering. We may then write $\mathcal{F}_q^a\left(\frac{\mu\Omega}{\omega},\ n_z\right) \approx \mathcal{F}_q^b\left(\frac{\mu\Omega}{\omega},\ n_z\right) \approx \mathcal{F}_q\left(\frac{\mu\Omega}{\omega},\ n_z\right)$. At the second harmonic ($\omega \approx 2\Omega$), $\mathcal{F}_q\left(2\mu\frac{\Omega}{\omega},\ n_z\right)$ will be the $\mathcal{F}_q$ function of the largest magnitude, for the same reason as above.

Next we use the small Larmor radius approximation, i.e. we assume that $\lambda << 1$. This means that at the fundamental, we need only consider the $n = 0$ and $n = 1$ terms in each series. Fortunately, all the $n = 0$ terms, apart from the one in ϵ_{33} are zero. At the second harmonic we must consider $n = 0$, $n = 1$ and $n = 2$ terms and keep only those of the greatest magnitude. We can neglect $\mathcal{F}_q\left(-\frac{2\mu\Omega}{\omega},\ n_z\right)$ in comparison with $\mathcal{F}_q\left(\frac{2\mu\Omega}{\omega},\ n_z\right)$, but not $\mathcal{F}_q\left(-\frac{\mu\Omega}{\omega},\ n_z\right)$ in comparison with $\mathcal{F}_q\left(\frac{\mu\Omega}{\omega},\ n_z\right)$, nor $\mathcal{F}_q\left(\frac{\mu\Omega}{\omega},\ n_z\right)$ in comparison with $\lambda\mathcal{F}_q\left(\frac{2\mu\Omega}{\omega},\ n_z\right)$. This gives the dielectric tensor elements a rather more complicated form, at the second harmonic. The dielectric tensor elements are as follows.

Fundamental

$$\left.\begin{aligned}
&\varepsilon_{11} = 1 + P; \quad \varepsilon_{22} = 1 + P \\
&i\varepsilon_{12} = Q; \quad -i\varepsilon_{21} = Q \\
&\varepsilon_{33} = 1 + R + Sn_x^2 \\
&\varepsilon_{13} = Tn_x; \quad \varepsilon_{31} = Tn_x \\
&-i\varepsilon_{23} = Un_x; \quad i\varepsilon_{32} = Un_x
\end{aligned}\right\} \qquad (23)$$

where

$$P = Q = -\frac{\omega_p^2}{\omega^2}\,\mu\,\frac{1}{2}\,F_{5/2}\left(\frac{\mu\Omega}{\omega},\ n_z\right)$$

$$R = -\frac{\omega_p^2}{\omega^2}\,\mu\,\frac{\partial}{\partial n_z}\left[n_z\,F_{5/2}(0,n_z)\right]$$

$$S = -\frac{\omega_p^2}{\omega^2}\,\frac{1}{2(\Omega/\omega)^2}\,\frac{\partial}{\partial n_z}\left[n_z\,F_{7/2}\left(\frac{\mu\Omega}{\omega},\ n_z\right)\right]$$

$$T = U = -\frac{\omega_p^2}{\omega^2}\,\mu\,\frac{n_z}{\Omega/\omega}\,\frac{1}{2}\,\frac{\partial}{\partial\left(\frac{\mu\Omega}{\omega}\right)}\,F_{7/2}\left(\frac{\mu\Omega}{\omega},\ n_z\right)$$

Second Harmonic

$$\left.\begin{aligned}
&\varepsilon_{11} = 1 + A + B + Cn_x^2; \quad \varepsilon_{22} = 1 + A + B + Cn_x^2 \\
&i\varepsilon_{12} = A - B + Cn_x^2; \quad -i\varepsilon_{21} = A - B + Cn_x^2 \\
&\varepsilon_{33} = 1 + D \\
&\varepsilon_{13} = n_x(E + F + Gn_x^2); \quad \varepsilon_{31} = n_x(E + F + Gn_x^2) \\
&-i\varepsilon_{23} = n_x(E - F + Gn_x^2); \quad i\varepsilon_{32} = n_x(E - F + Gn_x^2)
\end{aligned}\right\} \qquad (24)$$

where

$$A = -\frac{\omega_p^2}{\omega^2}\,\mu\,\frac{1}{2}\,\mathcal{F}_{5/2}\left(\mu\,\frac{\Omega}{\omega},\ n_z\right)$$

$$B = -\frac{\omega_p^2}{\omega^2}\,\mu\,\frac{1}{2}\,\mathcal{F}_{5/2}\left(-\mu\,\frac{\Omega}{\omega},\ n_z\right)$$

$$C = -\frac{\omega_p^2}{\omega^2}\,\frac{1}{2(\Omega/\omega)^2}\,\mathcal{F}_{7/2}\left(2\mu\,\frac{\Omega}{\omega},\ n_z\right)$$

$$D = -\frac{\omega_p^2}{\omega^2}\,\mu\,\frac{\partial}{\partial n_z}\left[n_z\,\mathcal{F}_{5/2}(0,n_z)\right]$$

$$E = -\frac{\omega_p^2}{\omega^2}\,\frac{\mu n_z}{2(\Omega/\omega)}\,\frac{\partial}{\partial\left(\mu\,\frac{\Omega}{\omega}\right)}\,\mathcal{F}_{7/2}\left(\mu\,\frac{\Omega}{\omega},\ n_z\right)$$

$$F = -\frac{\omega_p^2}{\omega^2}\,\frac{\mu n_z}{2(\Omega/\omega)}\,\frac{\partial}{\partial\left(\mu\,\frac{\Omega}{\omega}\right)}\,\mathcal{F}_{7/2}\left(-\mu\,\frac{\Omega}{\omega},\ n_z\right)$$

$$G = -\frac{\omega_p^2}{\omega^2}\,\frac{n_z}{4(\Omega/\omega)^3}\,\frac{\partial}{\partial\left(2\mu\,\frac{\Omega}{\omega}\right)}\,\mathcal{F}_{9/2}\left(2\mu\,\frac{\Omega}{\omega},\ n_z\right)$$

Non-relativistic limit

To obtain the non-relativistic dielectric tensor elements, we simply substitute equation (20) of Chapter 2 into (23) and (24). We obtain

$$\left.\begin{aligned} P = Q &= \frac{\omega_p^2}{\omega^2}\,\frac{\mu^{\frac{1}{2}}}{2\sqrt{2}\,n_z}\ Z(z_1) \\ R &= -\frac{\omega_p^2}{\omega^2}\,\frac{\mu^{\frac{1}{2}}\,z_0}{\sqrt{2}\,n_z}\,\frac{\partial Z(z_0)}{\partial z_0} \\ S &= -\frac{\omega_p^2}{\omega^2}\,\frac{z_1}{\mu^{\frac{1}{2}}2\sqrt{2}\,n_z\,(\Omega/\omega)^2}\,\frac{\partial Z(z_1)}{\partial z_1} \\ T = U &= -\frac{\omega_p^2}{\omega^2}\,\frac{1}{4(\Omega/\omega)n_z}\,\frac{\partial Z(z_1)}{\partial z_1} \end{aligned}\right\} \qquad (25)$$

and

$$\left.\begin{aligned}
A &= \frac{\omega_p^2}{\omega^2}\,\frac{z_0}{2}\,Z(z_1)\\
B &= \frac{\omega_p^2}{\omega^2}\,\frac{z_0}{2}\,Z(z_{-1})\\
C &= \frac{\omega_p^2}{\omega^2}\,\frac{1}{2\sqrt{2}\,\mu^{\frac{1}{2}}\,n_z(\Omega/\omega)^2}\,Z(z_2)\\
D &= -\frac{\omega_p^2}{\omega^2}\,z\,\frac{\partial Z(z_0)}{\partial z_0}\\
E &= -\frac{\omega_p^2}{\omega^2}\,\frac{1}{4(\Omega/\omega)n_z}\,\frac{\partial Z(z_1)}{\partial z_1}\\
F &= -\frac{\omega_p^2}{\omega^2}\,\frac{1}{4(\Omega/\omega)n_z}\,\frac{\partial Z(z_{-1})}{\partial z_{-1}}\\
G &= -\frac{\omega_p^2}{\omega^2}\,\frac{1}{8\mu(\Omega/\omega)^3 n_z}\,\frac{\partial Z(z_2)}{\partial z_2}
\end{aligned}\right\} \qquad (26)$$

Dispersion relation at the fundamental

We combine equations (21) and (23) to obtain

$$n_x^4\{(1-S)(1+P-n_z^2) + (T+n_z)^2\} +$$

$$n_x^2\{2QUn_z + 2QUT - (T+n_z)^2(1+P-n_z^2) + Q^2(1-S) - (1+P-n_z^2)(U^2 + (1+P-n_z^2)(1-S)$$

$$+ 1 + R)\} + (1+P-n_z^2)^2(1+R) - Q^2(1+R) = 0. \qquad (27)$$

This is a quadratic for n_x^2, one root of which corresponds to the O-mode and the other to the X-mode. We use an ad hoc method to determine which is which, based on the Appleton-Hartree dispersion relation for a cold plasma. This is (Fielding, 1981)

$$n^2 = n_x^2 + n_z^2 = 1 - \frac{2\omega^2(\omega^2 - \omega_p^2)}{2\omega^2(\omega^2 - \omega_p^2) - \omega^2\Omega^2\sin^2\theta \pm \omega\Gamma}$$

where $\Gamma = [\omega^2\Omega^4\sin^4\theta + 4\Omega^2(\omega^2 - \omega_p^2)^2\cos^2\theta]^{\frac{1}{2}}$.

The + sign gives the O-mode and the - sign the X-mode.

We find that n_x^2 is greater for the X-mode than for the O-mode if $(2\omega^2(\omega^2 - \omega_p^2) - \omega^2\Omega^2\sin^2\theta)^2 - \omega^2\Gamma^2 < 0$ (provided that $\omega^2 > \omega_p^2$ which is true when the O-mode propagates). This condition reduces to

$$\omega^2(\omega^2 - \omega_p^2 - \Omega^2) - \omega_p^2\Omega^2\cos^2\theta < 0. \qquad (28)$$

This condition is just that the frequency be below the resonant frequency for the X-mode ($(\omega_p^2 + \Omega^2)^{\frac{1}{2}}$ when $\theta = \pi/2$, and Ω when $\theta = 0$). This is the case when the X-mode propagates. Thus for the Appleton-Hartree dispersion relation, n_x is greater for the X-mode.

For the relativistic dispersion relation, we then take n_x for the X-mode to be the root of n_x^2 with the larger real part (we always take the real part of n_x to be positive).

Graphs are plotted in Figs 3.1, 3.2 and 3.3 of some representative results. We note here that throughout this thesis we will present results based on a linear magnetic field gradient, that is we assume

$$B = B_0\left(1 + \frac{x}{R}\right) \qquad (29)$$

where R is the major radius of the tokamak.

As a consequence, $\Omega = \Omega_0\left(1 + \frac{x}{R}\right)$, where $\omega = \Omega_0$ for the fundamental resonance and $\omega = 2\Omega_0$ at the second harmonic.

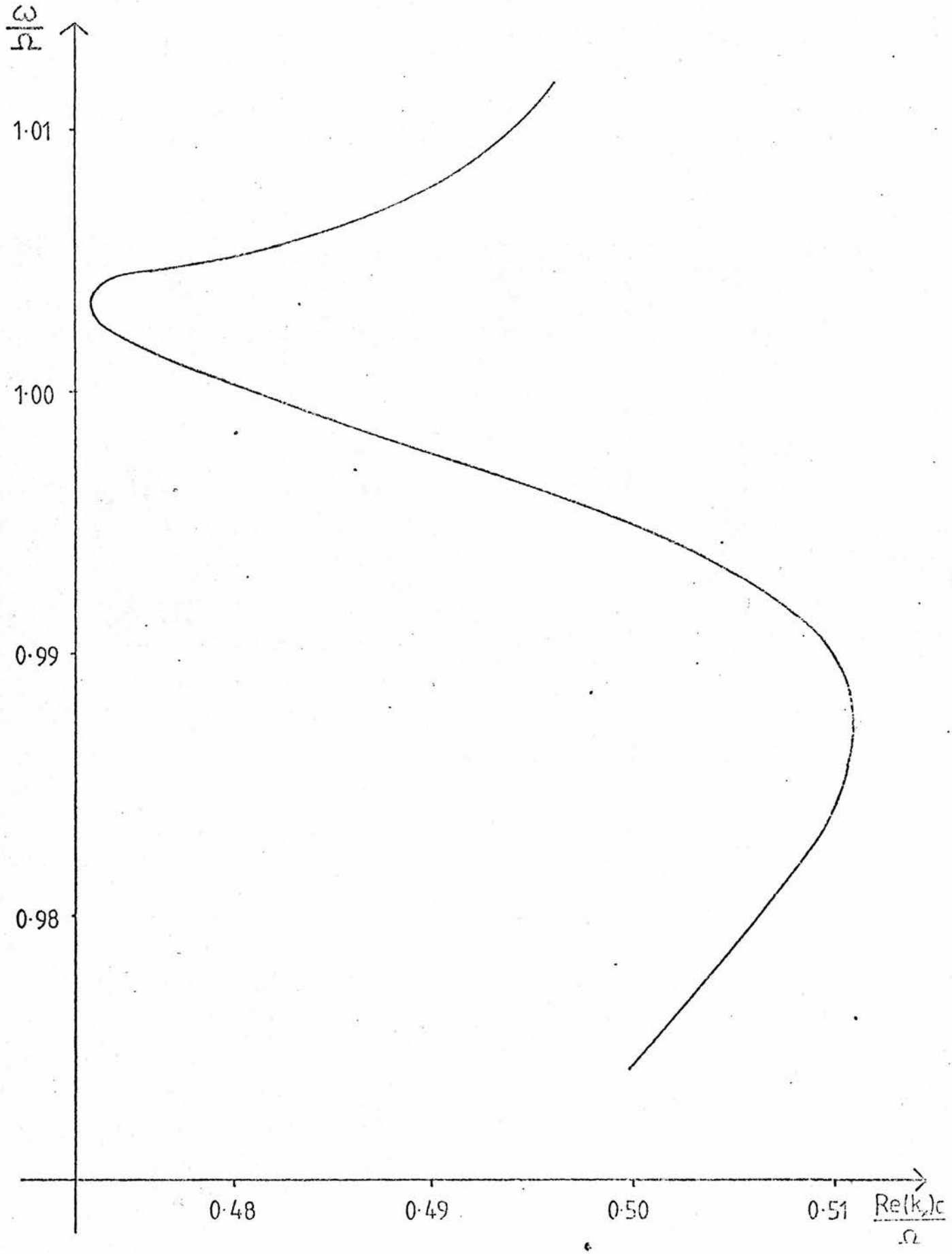

Figure 3.1

Dispersion curve for the O mode in the relativistic case with $T = 1.0$ keV, $\omega_p^2/\omega^2 = 0.75$, $n = 1$, $n_z = 0.1$, $R = 1.2$m.

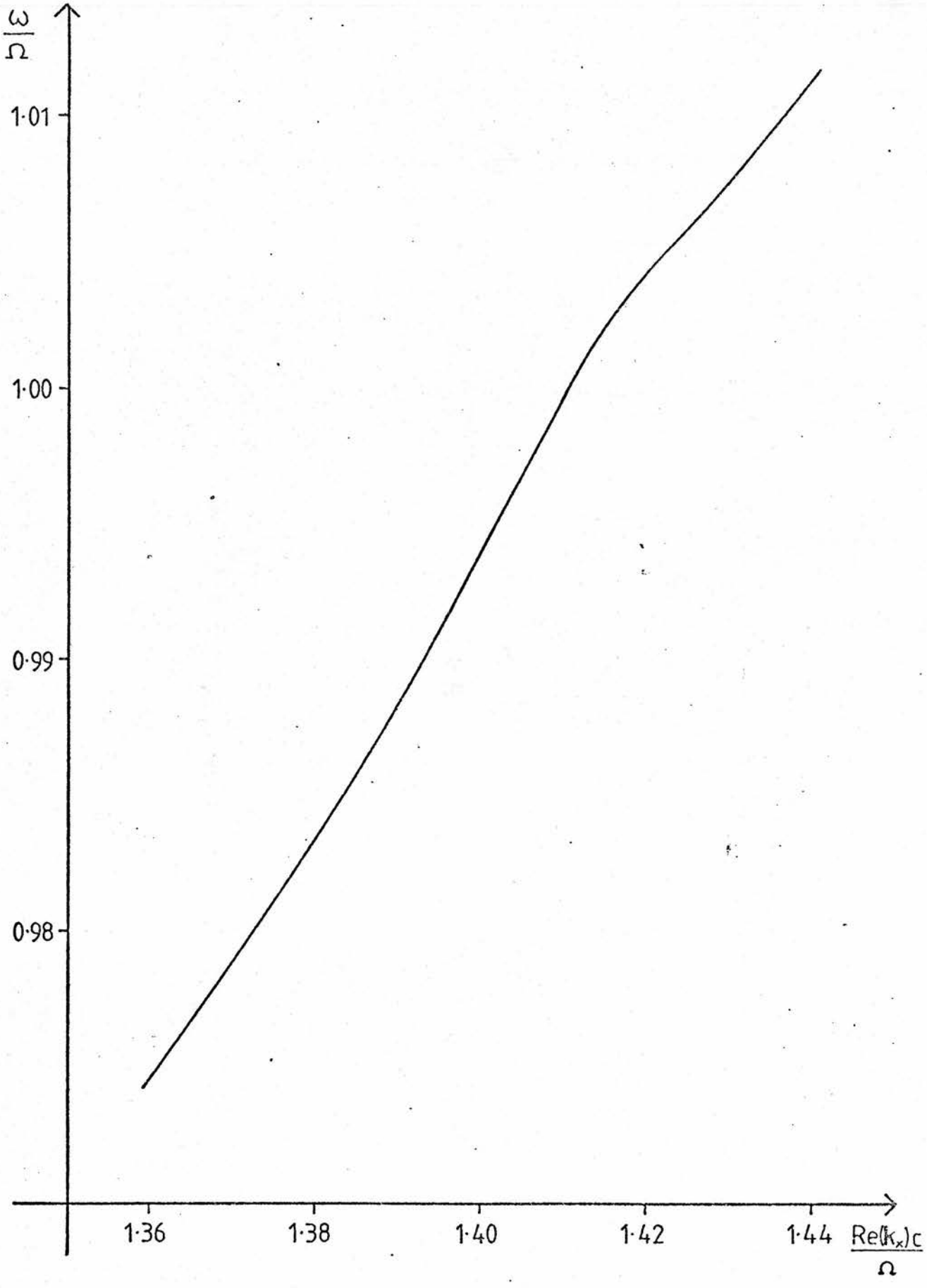

Figure 3.2

Dispersion curve for the X mode in the relativistic case with the same parameters as for Fig. 3.1.

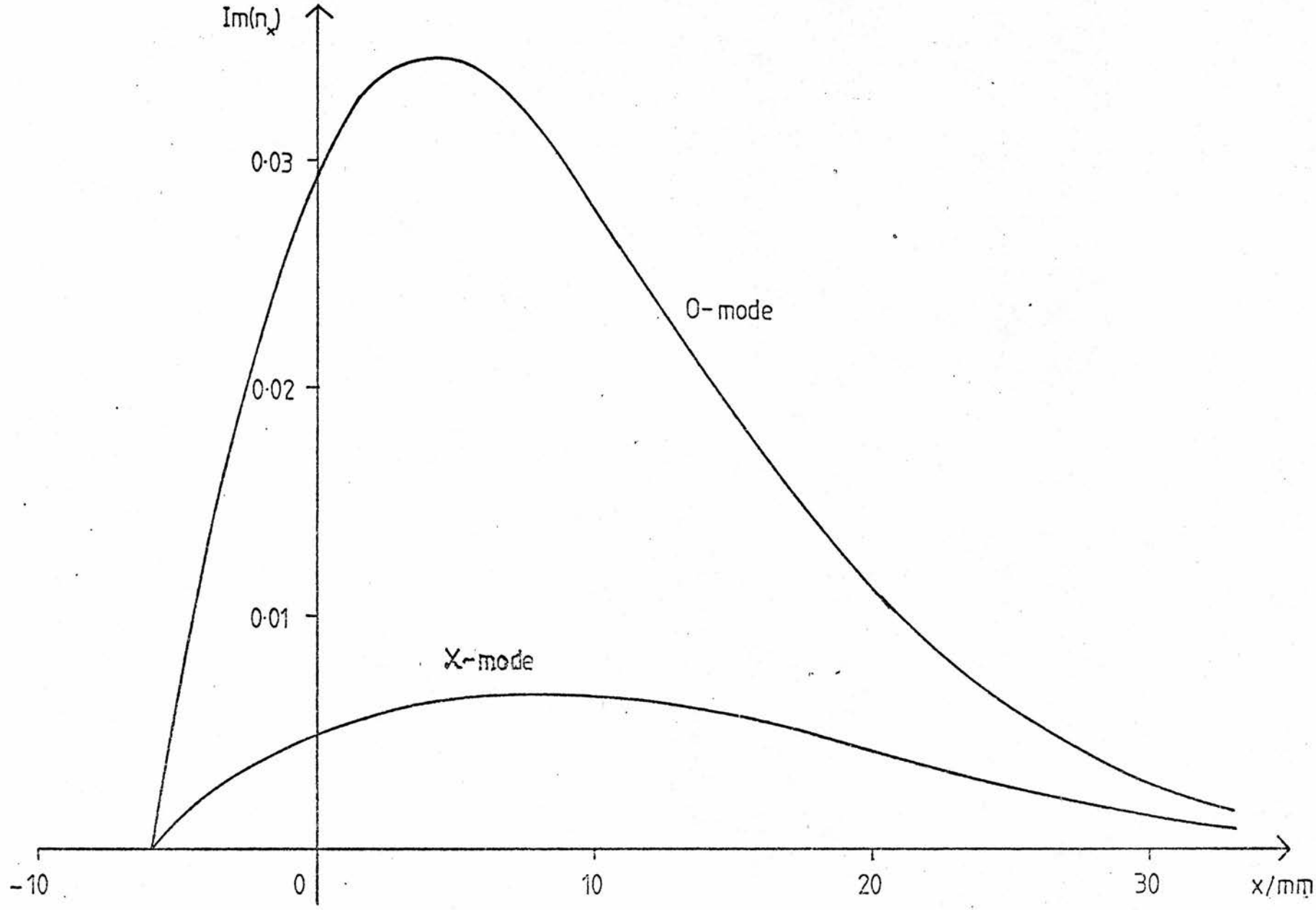

Figure 3.3

Variation of Im(n_x) with distance for the O and X modes in the relativistic case with the same parameters as for Fig. 3.1.

Fig 3.1 is a dimensionless form of an ω-k diagram, ω/Ω being plotted against $R_e(k_x c/\Omega)$. This diagram is for the O-mode. Fig 3.2 presents the same results for the X-mode. In Fig 3.3 the imaginary part of n_x is plotted against x for both the O and X modes. As will be explained in the next chapter, the imaginary part of n_x gives the damping rate of the wave as it passes through the plasma. The graphs for the non-relativistic case, corresponding to Figs 3.1, 3.2 and 3.3 are plotted in Figs 3.4, 3.5 and 3.6.

It will be seen from Fig 3.3 that in the relativistic case there is a point on the low field ($x < 0$) side beyond which there is no wave damping, since $\mathrm{Im}(n_x) = 0$ beyond this point. This is the point at which $1 - \frac{\Omega}{\omega} = \frac{n_z^2}{2}$, i.e. $\frac{x}{R} = -\frac{n_z^2}{2}$. This is a consequence of the fact that $\mathcal{F}_q$ is real when $\frac{\Omega}{\omega} < (1 - n_z^2)^{\frac{1}{2}} \approx 1 - \frac{n_z^2}{2}$. That no wave damping occurs for $\frac{x}{R} < -\frac{n_z^2}{2}$ will also be evident in the next chapter when we consider the resonance condition in detail. We call this point the low field cut-off point. Thus, waves will propagate freely on the low field side of the resonance and will be damped on the high field side.

This is, however, subject to certain limitations (Antonsen and Manheimer, 1978; Manheimer, 1979; Fielding, 1981). In the case of the O-mode, there is an upper limit on the density at resonance, since the O-mode cut-off will be encountered unless $\omega_p^2/\omega^2 < 1$. The upper limit is given by $n_{max} \approx 10^{19} B^2 m^{-3}$ where B is in Tesla. Thus ECRH imposes constraints on the operating range of density in low field tokamaks with $B \lesssim 1T$, but not on those with $B \gtrsim 5T$. In the case of the X mode, waves can propagate from the low field side only

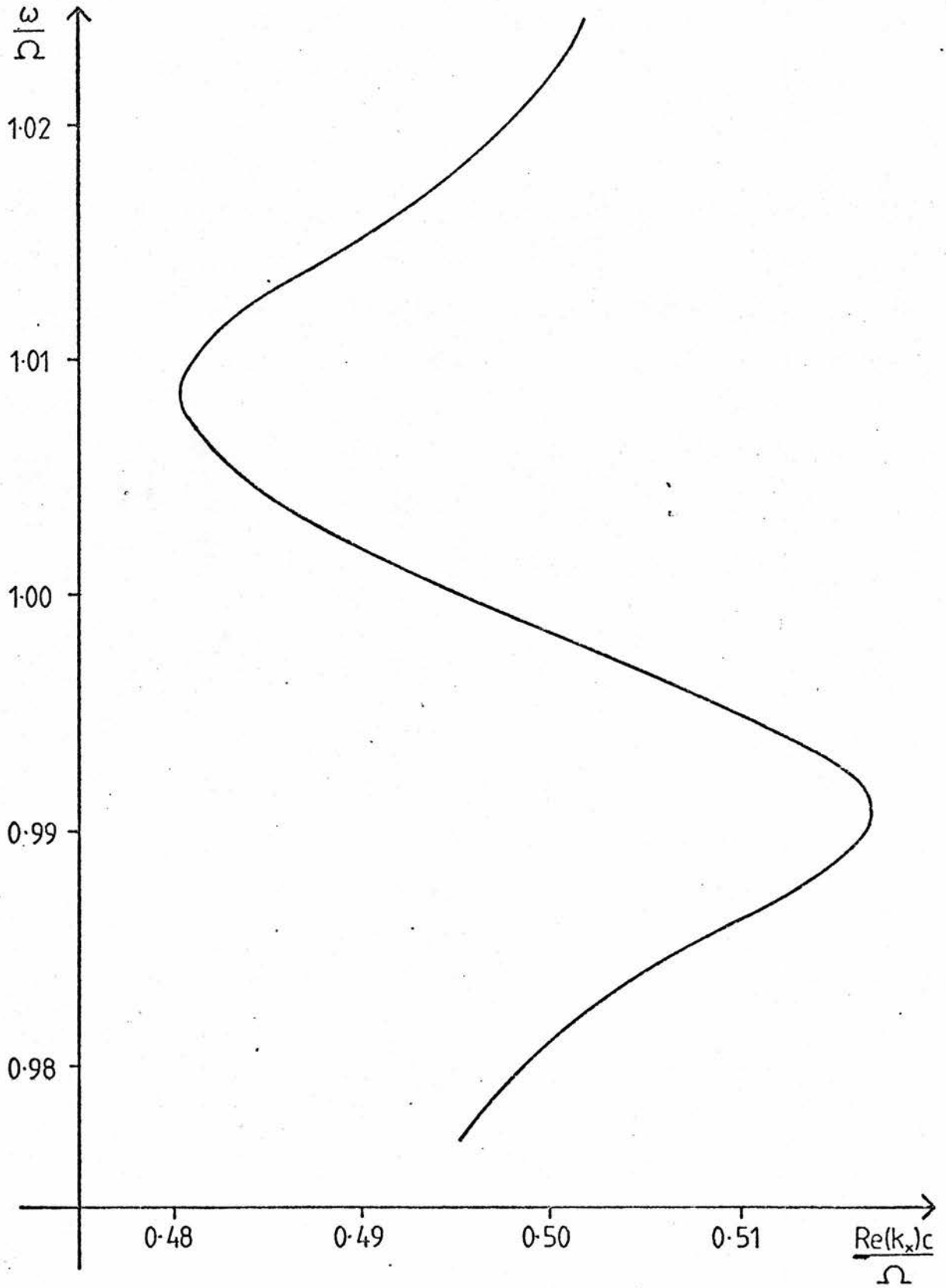

Figure 3.4

Dispersion curve for the O mode in the non-relativistic case with the same parameters as for Fig. 3.1.

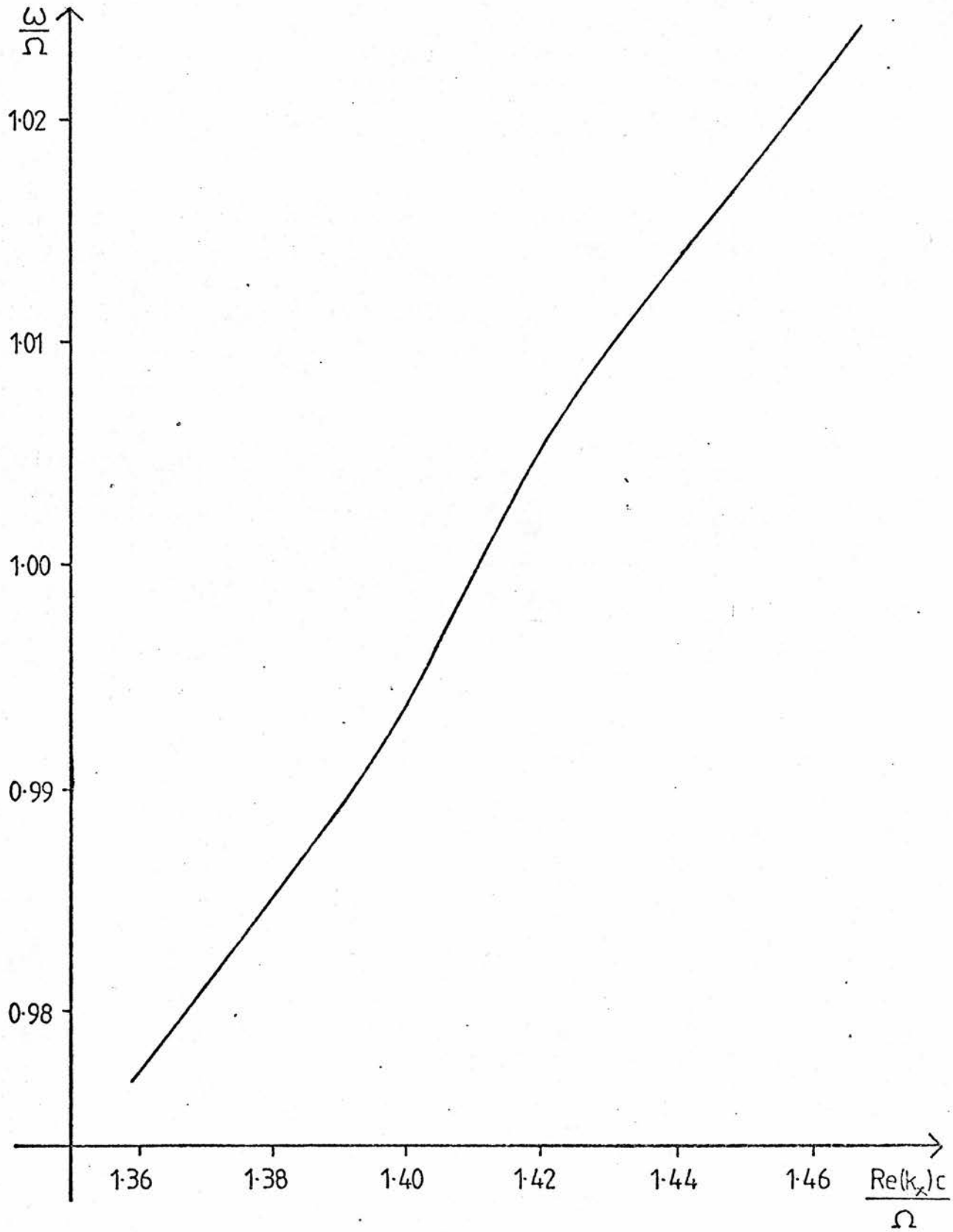

Figure 3.5

Dispersion curve for the X mode in the non-relativistic case with the same parameters as for Fig. 3.1.

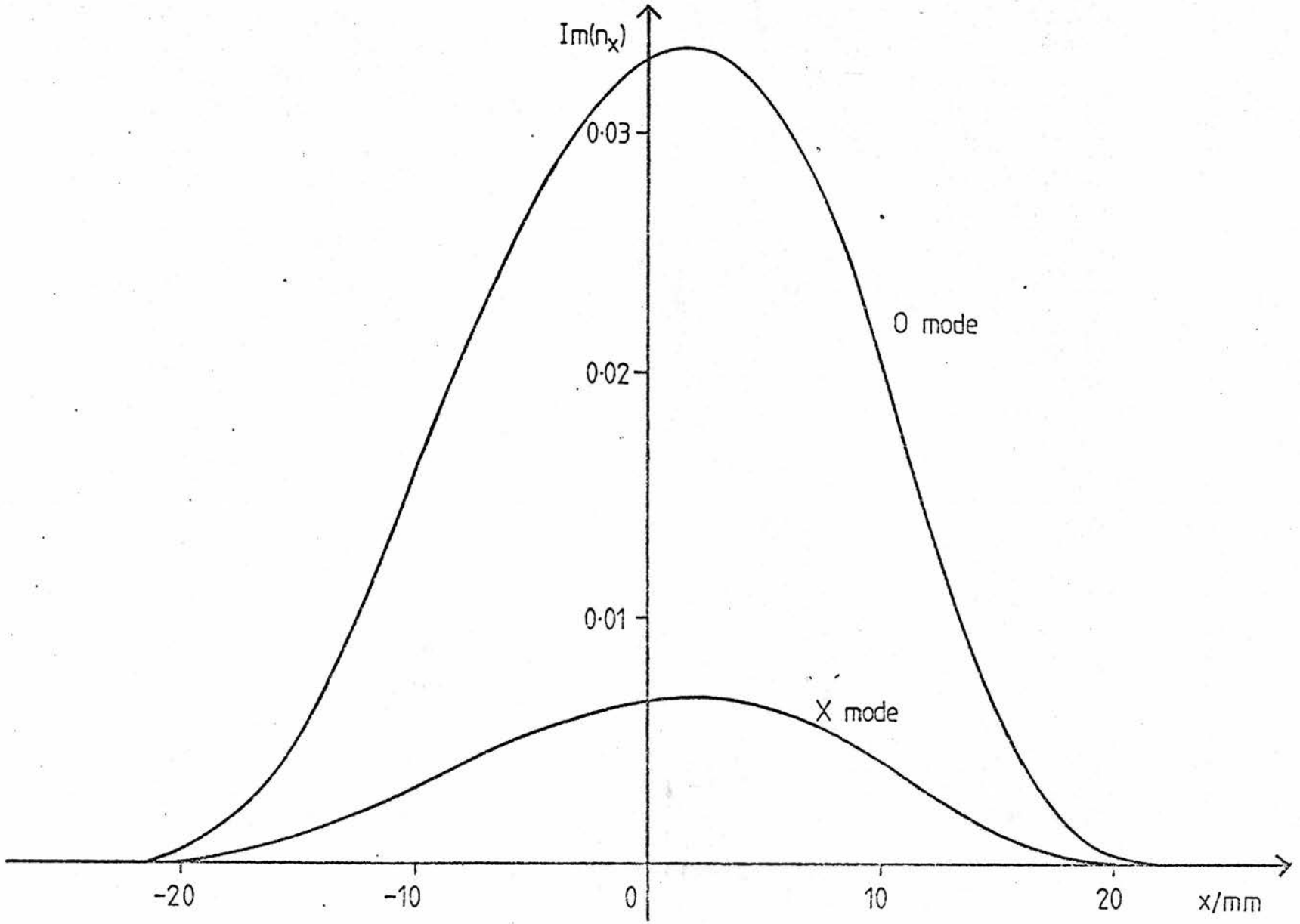

Figure 3.6

Variation of Im(n_x) with distance for the O and X modes in the non-relativistic case with the same parameters as for Fig. 3.1.

as far as the low density cut-off given by $\omega_p^2/\omega^2 = 1 - \Omega/\omega$, so that the cyclotron resonance is inaccessible from this side. There is no limit for the X mode on the high field side, except that in high density plasmas for which $\omega_p^2/\omega^2 > 2$, the high density cut-off given by $\omega_p^2/\omega^2 = 1 + \Omega/\omega$ will be encountered.

We see from Fig 3.3 that the O-mode is absorbed more strongly than the X-mode at the fundamental. This is generally true for a wide range of parameters. For instance, the variation in wave absorption with density has been investigated. The results are presented in Table 3.1. ω_p^2/ω^2 is proportional to the density and the other columns show the ratio of the wave intensity after the wave has passed through the plasma to the incident wave intensity. It is found that, in agreement with Hsu *et al.* (1983), the O-mode absorption increases with density (except for densities close to the O-mode cut-off) and the X-mode absorption decreases with density.

Table 3.1

Variation with density of total wave absorption of the O and X modes. We take T = 1keV, R = 1.2m, $n_z = 0.1$.

ω_p^2/ω^2	Wave intensity/Incident wave intensity	
	O mode	X mode
0.4	0.24	0.51
0.5	0.20	0.57
0.6	0.17	0.61
0.7	0.17	0.64
0.8	0.19	0.67

The results for the non-relativistic case are similar, but the absorption is now virtually symmetrical about $x = 0$, and there is no low field cut-off point. These results, together with the relativistic ones, have been compared with those of Fidone *et al.* (1978) and good agreement has been found.

Dispersion relation at the second harmonic

We combine equations (21) and (24) to obtain

$$(-n_x^2 + 1 + D)[(1 + A + B + Cn_x^2 - n_z^2)(1 + A + B + Cn_x^2 - n_x^2 - n_z^2) - (A - B + Cn_x^2)^2]$$
$$- n_x^2(E - F + Gn_x^2)[(1 + A + B + Cn_x^2 - n_z^2)(E - F + Gn_x^2) - (E + F + Gn_x^2 + n_z)(A - B + Cn_x^2)]$$
$$+ n_x^2(n_z + E + F + Gn_x^2)[(A - B + Cn_x^2)(E - F + Gn_x^2) - (n_z + E + F + Gn_x^2)(1 + A + B +$$
$$Cn_x^2 - n_x^2 - n_z^2)] = 0.$$

This becomes

$$n_x^8G^2 + n_x^6[C + 2G(-G - 2BG + Gn_z^2 + n_z + E + F)]$$
$$+ n_x^4[-2C + A - 4BC + B + 2Cn_z^2 + 1 - n_z^2 + (1+D)(-C) - 4EG - 8BGE + 4EGn_z^2$$
$$- 4CF^2 - 4CFn_z + (E+F)(n_z + E + F) + n_z(-4BG - n_zC + n_z + E + F + Gn_z^2) - 2Gn_z + Gn_z^3]$$
$$+ n_x^2[-1 - 2(A+B) + n_z^2 - 4AB + An_z^2 + Bn_z^2 + (1+D)(2C - A + 4BC - B - 2Cn_z^2 - 1 + n_z^2)$$
$$- 2E^2 - 4BE^2 + 2n_z^2E^2 - 2n_zBE - 2F^2 - 4AF^2 + 2F^2n_z^2 - 2n_zAF + 2(E+F)(-n_z + n_z^3)$$
$$- 2n_z(AF + BE)] + [(1+D)(1 + 2(A+B-n_z^2) + 4AB - 2An_z^2 - 2Bn_z^2 + n_z^4)] = 0.$$

This equation gives us four roots for n_x^2. We now consider the relative magnitudes of A, B, C, E, F and G. We find that E, F and G are in general much smaller than A, B and C. The reason is as follows. If we change the contour of integration for $\mathcal{F}_q$ and its derivatives as

in Fig 2.1, then the integrand will be exponentially decaying with t in each case. The greatest contribution to the integral will then come from $t << 1$. This is true for A, B and C which depend merely on $\mathcal{F}_q$. E, F and G, however, depend on the derivative of $\mathcal{F}_q$ with respect to $\mu\Omega/\omega$ or $2\mu\Omega/\omega$, and this brings an additional factor of - it into the integrand. This considerably reduces the contribution to the integral from $t << 1$, so that the magnitudes of E, F and G are much less than those of A, B and C.

Now the coefficient of n_x^8 is G^2, so this coefficient is small compared with the other coefficients, each of which contains an A, a B or a C. We will therefore always find a root for n_x^2 with a large magnitude. Not only is this physically unrealistic, but it is also inconsistent with our small Larmor radius approximation. We therefore ignore this root; this can be conveniently done by neglecting the $n_x^8 G^2$ term since its neglect will not significantly alter the other three roots. These three remaining roots correspond to the O-mode, the X-mode and the Bernstein mode (also known as the quasi-electrostatic mode (Lazzaro and Ramponi, 1981)).

At the second harmonic, both the O and X modes will propagate from the low field or the high field side provided that, in the case of the O mode, $\omega_p^2/\omega^2 < 1$ or, in the case of the X mode, $\omega_p^2/\omega^2 < \frac{1}{2}(1 - n_z^2)$ (Hui *et al.* 1980). The Bernstein mode can propagate on the low field side, but is evanescent on the high field side of the resonance (Hsu *et al.* 1983). Its propagation has been studied in detail by Bornatici *et al.* (1981).

In Fig 3.7 results for the imaginary part of n_x are plotted against x for the three modes. A logarithmic scale for $Im(n_x)$ is necessary because of the great disparity between the absorption of the different modes. The O mode is very weakly damped because it has a very small E_component, the E_component of the electric field being that component which rotates in the same sense as the electrons. In fact, the absorption of the O mode is so small that a large fraction of the incident power will pass straight through the plasma. The O mode is thus not of interest for heating and current drive at the second harmonic. The variation of wave absorption with density for the O and X modes is given in the following table.

Table 3.2

Variation with density of total wave absorption of the O and X modes. We take T = 1keV, R = 1.2m, n_z = 0.1.

ω_p^2/ω^2	Wave intensity/Incident wave intensity	
	O mode	X mode
0.1	0.988	0.14
0.15	0.983	4.7×10^{-2}
0.2	0.980	1.4×10^{-2}
0.25	0.977	3.7×10^{-3}
0.3	0.974	8.6×10^{-4}

As mentioned above, the Bernstein mode is evanescent on the high field side, and so is the most strongly damped of the three modes. This will ensure that there is no current reversal. It is

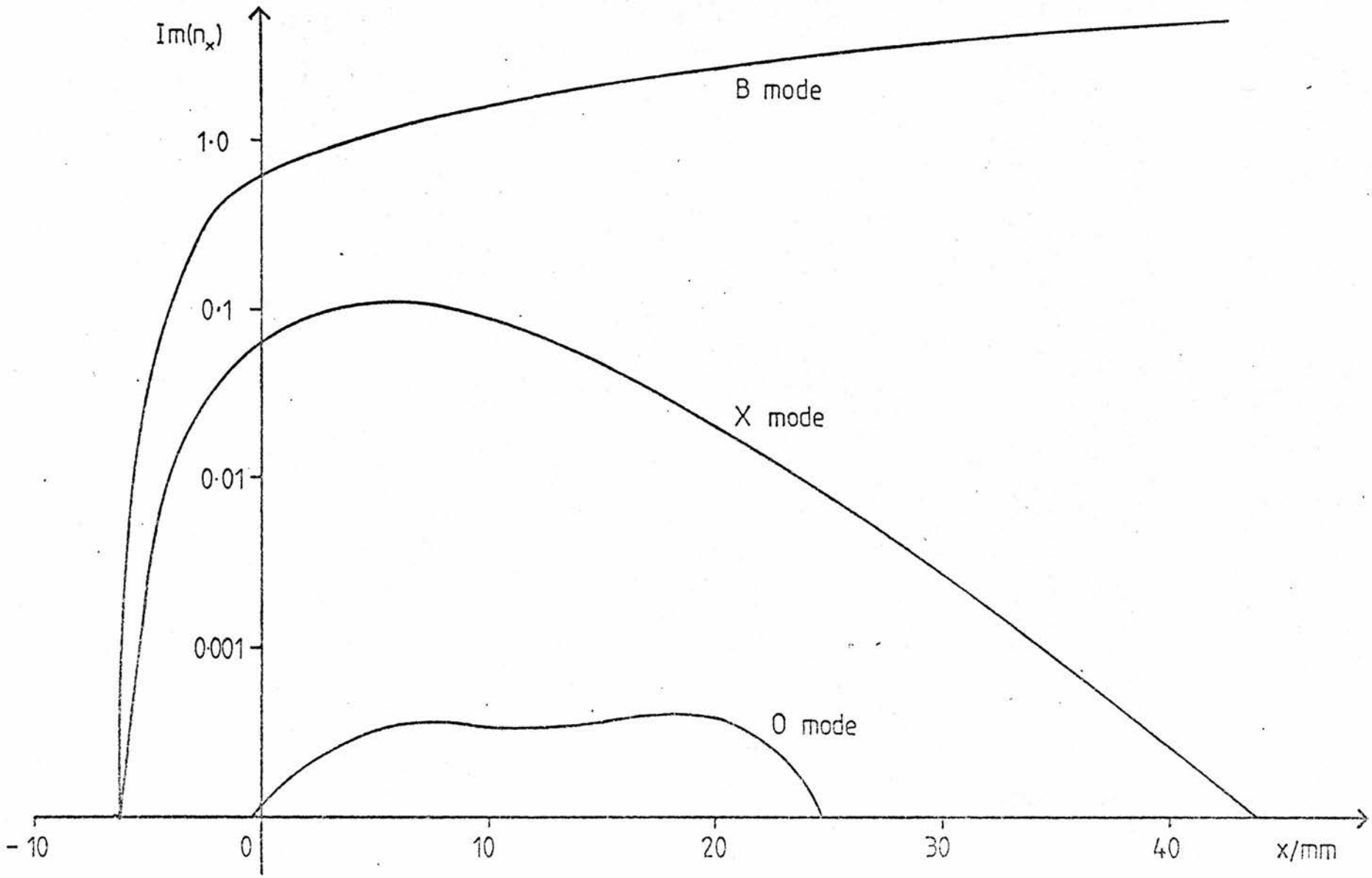

Figure 3.7

Variation of Im(n_x) with distance for the O, X, and Bernstein modes in the relativistic case with $T = 1$ keV, $\omega_p^2/\omega^2 = 0.2$, $n = 2$, $n_z = 0.1$, $R = 1.2$m.

heavily damped even far away from the resonance and this will allow absorption where the current drive efficiency is higher (see Chapters 4 and 5).

In Fig 3.8 we plot the real part of k_x in the form of a dimensionless ω-k diagram for all three modes. It can be seen that the X and Bernstein modes cross, indicating the possibility of coupling of the two modes and mode conversion between them. This is in fact the means by which we expect to excite the Bernstein mode. This will happen at the upper hybrid resonance layer (Lazzaro and Orefice, 1980) where $\omega_{UH}^2 = \omega_p^2 + \Omega^2$. The upper hybrid resonance layer is, however, inaccessible to the X mode propagating in from the edge of the plasma because of the evanescent region between the low density cut-off and the upper hybrid layer. It is thus necessary to launch the O mode in such a way that it can penetrate and propagate as an X mode by means of mode conversion. The mode conversion will take place if the O mode cut-off coincides with the X mode high density cut-off. This can only happen for a critical angle of incidence, where $n_z^2 = \Omega/(\omega+\Omega)$ (Weitzner and Batchelor, 1978). The sequence of events is then as follows (Hsu *et al.* 1983). The O mode is launched at an angle of about 35° to the perpendicular, it reaches the O mode cut-off, becomes a backward propagating mode and connects to the X mode. The X mode then propagates back to the upper hybrid resonance layer and transforms to the Bernstein mode.

We find, in agreement with Lazzaro and Ramponi (1981) that mode coupling of the X and Bernstein modes can only happen when the density (measured in terms of ω_p^2/ω^2) reaches a critical value which

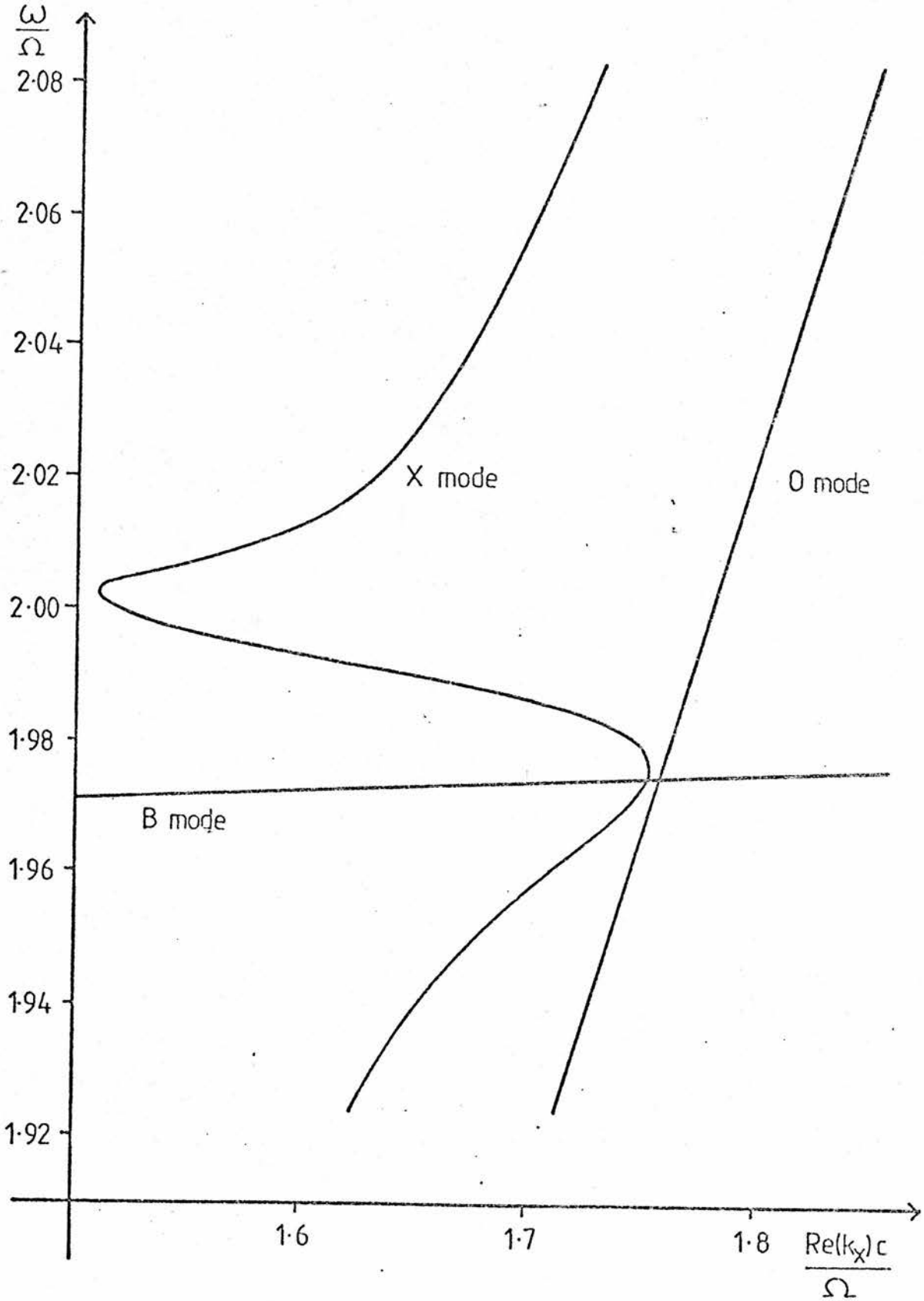

Figure 3.8

Dispersion curve for the O, X, and Bernstein modes in the relativistic case with the same parameters as for Fig. 3.7.

depends on the temperature and parallel refractive index. This critical value is plotted against n_z for several values of the temperature T in Fig 3.9. Lazzaro and Ramponi give a more detailed discussion of the conditions for coupling of the X and Bernstein modes.

Results for the solution of the relativistic dispersion relation have been compared with those of other authors. Hsu *et al.* (1983) do not use a relativistic dispersion relation, but present results for a large value of n_z (≈ 0.3) where the relativistic correction is not so important. Lazzaro and Ramponi use a relativistic dispersion relation but present results only for perpendicular propagation. In both cases, good agreement has been found with our results.

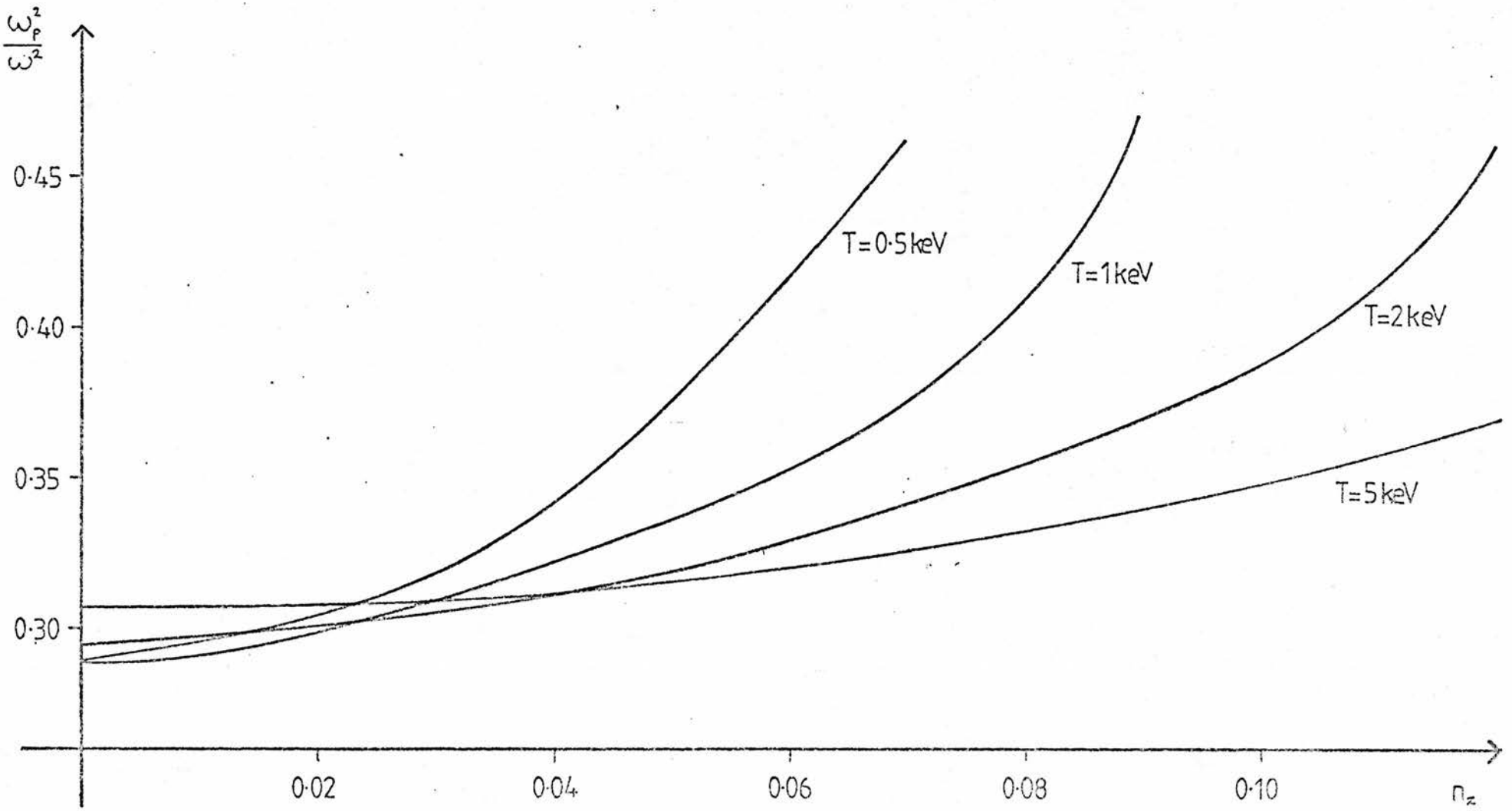

Figure 3.9

Critical values of ω_p^2/ω^2 for coupling of the X and Bernstein modes at the second harmonic.

CHAPTER 4

Current Drive Theory

ECRH current drive uses the following mechanism, which was proposed by Fisch and Boozer (1980). The idea is to preferentially heat electrons travelling in one direction along the magnetic field (to the left, say). Now the electron-ion collision frequency is proportional to $T^{-3/2}$, so that the heated electrons collide less often with the ions. Electrons travelling to the right are not heated and slow down by collisions with the ions at the normal rate. The net result is to produce a flow of electrons to the left, and a flow of ions to the right, i.e. a current.

Non-relativistic Resonance Condition

The mechanism for preferential heating of electrons is provided by the electron cyclotron resonance condition, which in the non-relativistic theory is

$$\omega - k_z v_z - n\Omega = 0. \tag{31}$$

This condition is just that the Doppler shifted frequency of the wave, as seen by an electron, must equal the electron cyclotron frequency or one of its harmonics. The geometry of the situation is as follows

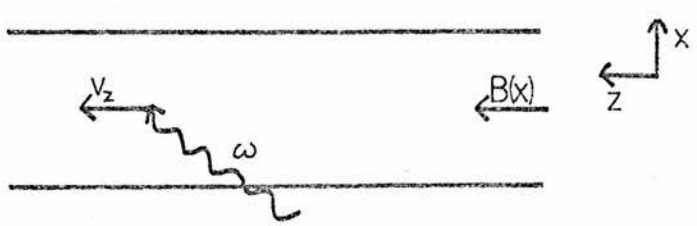

The resonance condition is plotted in Fig 4.1 for v_z as a function of distance, for a given value of n_z. We have again made the assumption of a linear magnetic field profile, as in equation (29). We see from Fig 4.1 that for $x < 0$, v_z is positive, so that the resonant electrons are moving to the left. The situation is reversed for $x > 0$. The result is that currents flow in opposite directions on opposite sides of the resonance point ($x = 0$). If, however, the wave is partially or completely absorbed before it reaches $x = 0$, then a net current may be generated.

Relativistic Resonance Condition

We now wish to consider the effect of including the relativistic mass variation of the electron. Since $\Omega = eB/m$ and $m = m_0(1 - v^2/c^2)^{-\frac{1}{2}}$, the resonance condition will be changed to

$$\omega - k_z v_z - n\Omega(1 - \tfrac{1}{2}v^2/c^2) = 0 \qquad (32)$$

where we have assumed that $v^2/c^2 << 1$, and $\Omega = eB/m_0$.

This condition is plotted in Fig 4.2. We find that for a given position, the resonant value of v_z now depends on the electron's perpendicular velocity, $v_\perp$, in the x-y plane. For a given value of $v_\perp$ the resonant velocities lie approximately on a parabola, the outermost parabola being for $v_\perp = 0$. We also find (as we did in Chapter 3) that there is a point on the low field side, given by $x/R = -n_z^2/2$, beyond which resonance, and hence wave absorption, is not possible.

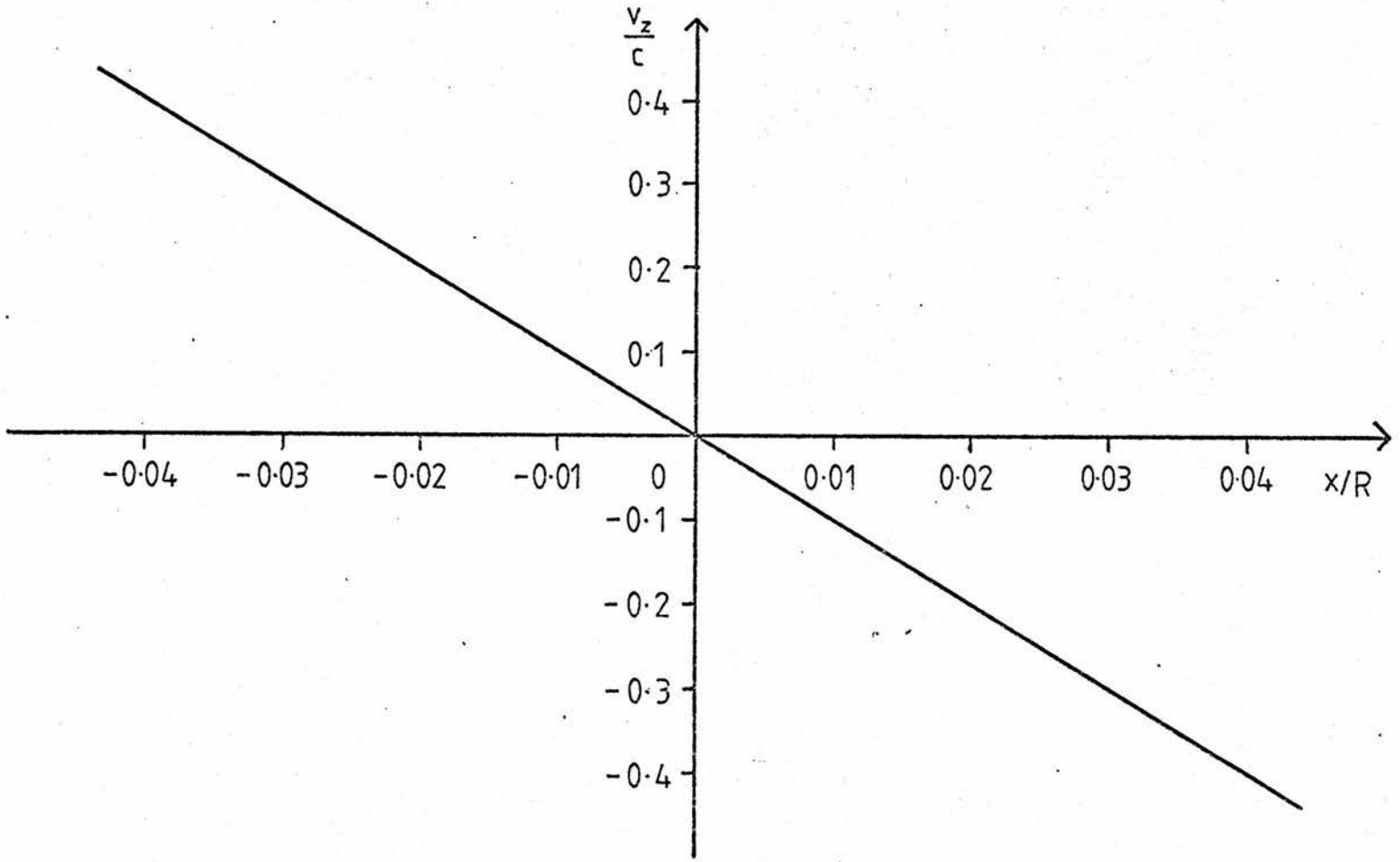

Figure 4.1

Non-relativistic resonance condition, $\omega - k_z v_z = \Omega$, with $n_z = 0.1$.

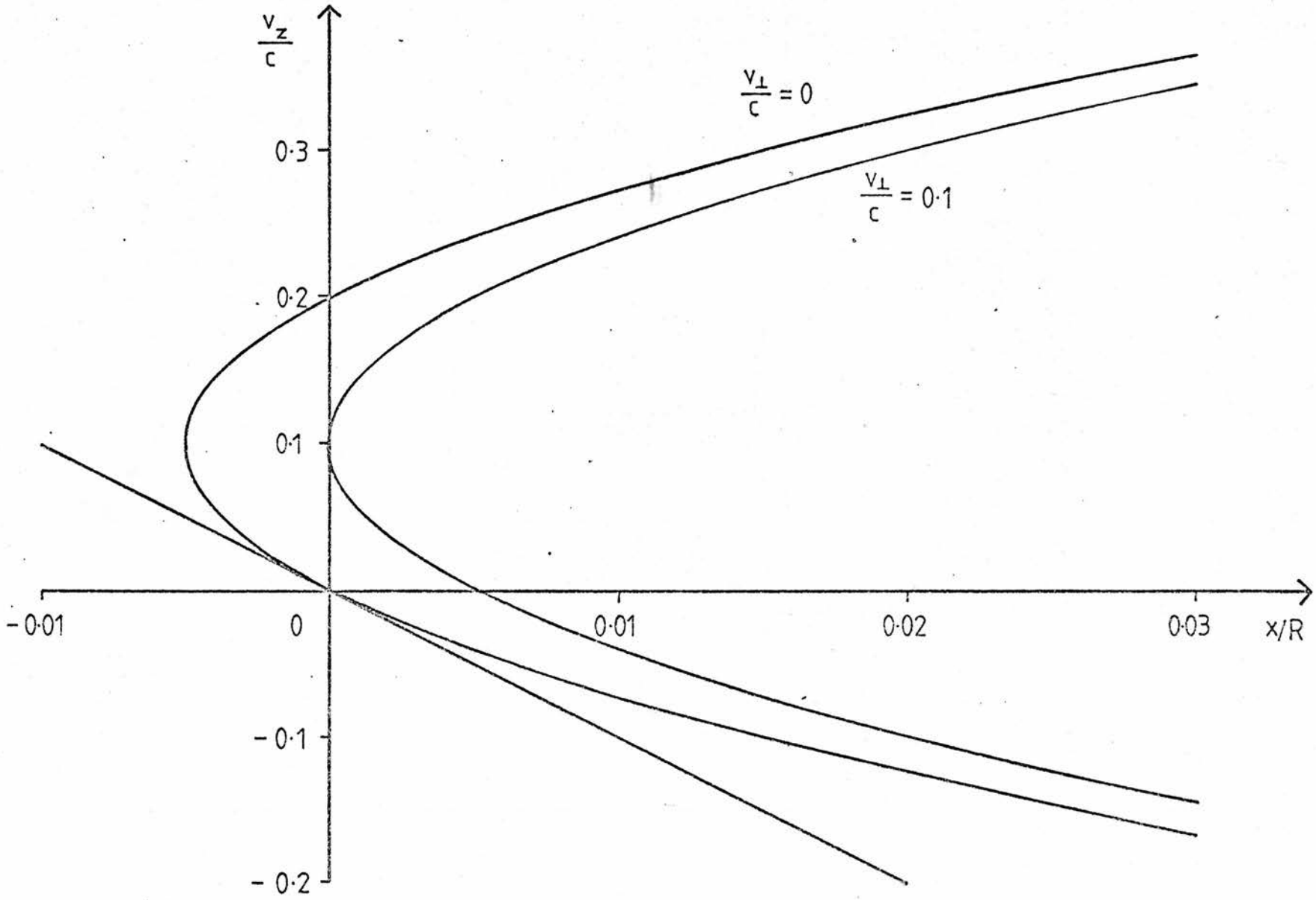

Figure 4.2

Relativistic resonance condition, $\omega - k_z v_z = \Omega\ (1 - \frac{1}{2}v^2/c^2)$, with $n_z = 0.1$.
The non-relativistic resonance condition is included for comparison.

The most significant feature, however, is that the resonance condition is now strongly asymmetric. We will no longer expect a reversal of the current at $x = 0$, but at some distance on the high field side, since around $x = 0$ the majority of resonant particles still have positive v_z. Only further out on the high field side will there be a sufficient number of resonant particles with negative v_z to give rise to a reversed current. Hence we can expect a net current to be generated even in the absence of strong absorption.

The non-relativistic straight line resonance condition has been included for comparison on the same graph. It will be seen that if the thermal velocity is low, then most particles will lie near the outermost parabola. If, in addition, the particles are near the origin, then the relativistic curve will approximate to the non-relativistic straight line. For this to be the case, we must have $v_t/c \ll n_z$ and $|x/R| \ll n_z^2/2$, since the nose of the parabola lies at $(-n_z^2/2, n_z)$. This can also be seen from a consideration of (32). We therefore expect our current drive results to be closer to the corresponding non-relativistic ones for larger values of n_z. The range of parameters over which relativistic effects are important has been discussed in more detail by Shkarofsky (1966).

Current drive calculation

This section outlines our current drive calculation which has already been described elsewhere (Cairns *et al.* 1983). The details are presented in the next section.

We first consider the effect of the waves on the distribution function. We take this to be described by a standard quasilinear diffusion term (Kennel and Engelmann, 1966) as follows

$$\left(\frac{\partial f}{\partial t}\right)_{waves} = \frac{1}{v_\perp}\frac{\partial}{\partial v_\perp}\left\{\frac{e^2 v_\perp}{4m^2}\left|E^- + \frac{k_x v_z}{\Omega}E_z\right|^2 \delta\left[\omega - k_z v_z - n\Omega\left(1 - \frac{1}{2}\frac{v^2}{c^2}\right)\right]\frac{\partial f_0}{\partial v_\perp}\right\} \tag{33}$$

We have used the small Larmor radius approximation and have included the relativistic correction to the cyclotron frequency in the δ function which expresses the resonance condition. $E^- = E_x - iE_y$ and f_0 is the equilibrium distribution which we take to be Maxwellian. We are thus using a linearised model in which the perturbation to the distribution function is assumed to be small. The validity of this assumption will be investigated in Chapter 6.

Also, we assume a monochromatic wave. A spread in wavenumbers, as would occur in practice, simply introduces an integral over k_z into (33). The current driven and power absorbed are also simply obtained from our results by integrating over the k_z spectrum.

Since, in our model, both the current driven and the power absorbed are proportional to the power input, through the $\left|E^- + \frac{k_x v_z}{\Omega}E_z\right|^2$ term in (33), there is a linear relation between the two quantities. We follow the approach of other authors (Fisch and Boozer, 1980; Eldridge, 1980; Cordey *et al.*, 1982) and calculate the ratio of current driven to power absorbed. To do this we use the theory of Fisch and Boozer.

The idea is as follows. A balance is assumed between the energy gained by an electron from the wave and the energy lost by collisions. A current arises from the fact that electrons with different energies collide at different rates. Now we consider the current due to the slowing down of a particular electron, averaged over a time Δt which is large compared with the reciprocal of the collision rate. This is just $\frac{1}{\Delta t}\int_0^{\Delta t} -ev_z dt$. The net current is just the change in this quantity produced by a wave impulse, i.e. $\delta\left(\frac{1}{\Delta t}\int_0^{\Delta t} -ev_z dt\right)$. The corresponding change in energy of the electron is $\delta(\frac{1}{2}mv_0^2)$, where v_0 is the initial velocity, so that the power dissipated in time Δt is $\frac{1}{\Delta t}\,\delta(\frac{1}{2}mv_0^2)$. The ratio of current to power is then

$$\frac{J}{P} = \frac{\delta\left(\int_0^{\Delta t} -ev_z dt\right)}{\delta(\frac{1}{2}mv_0^2)} \tag{34}$$

In order to evaluate J, we consider the slowing down process in more detail. From the Fokker-Planck equation written in the high velocity limit, Fisch and Boozer distinguish two collision rates: an energy loss rate $\nu_E = \frac{\nu_0 v_t^3}{Z_i v^3}$ and a parallel momentum loss rate $\nu_m = (2 + Z_i)\nu_E$, where Z_i is the charge state of the ions and $\nu_0 = \frac{\omega_p^4 \ell n \Lambda Z_i}{4\pi n_0 v_t^3}$, the Spitzer value of the collision frequency. Note that Fisch and Boozer employ a different value of ν_0 which is $\frac{2}{Z_i}$ times ours. The slowing down equations are then

$$\frac{dv}{dt} = -\nu_E v \quad \text{and} \quad \frac{dv_z}{dt} = -\nu_m v_z . \tag{35}$$

Hence

$$\frac{dv}{dv_z} = \frac{1}{2+Z_i} \frac{v}{v_z}$$

$$\therefore \frac{v}{v_0} = \left(\frac{v_z}{v_{z_0}}\right)^{\frac{1}{2+Z_i}} .$$

Also $v_z dt = -\frac{dv_z}{\nu_m}$, and we use the fact that in a time Δt, the parallel velocity of the electron goes from v_{z_0} to 0 (since Δt is large), so that

$$\int_0^{\Delta t} -ev_z dt = \int_{v_{z_0}}^{0} e \frac{dv_z}{\nu_m} = \frac{eZ_i}{(2+Z_i)\nu_0 v_t^3} \int_{v_{z_0}}^{0} v^3 dv_z$$

$$= \frac{eZ_i v_0^3}{(2+Z_i)\nu_0 v_t^3} \int_{v_{z_0}}^{0} \left(\frac{v_z}{v_{z_0}}\right)^{\frac{3}{2+Z_i}} dv_z = \frac{-eZ_i v_0^3 v_{z_0}}{(5+Z_i)\nu_0 v_t^3} .$$

Then

$$\frac{J}{P} = \frac{\delta\left(\frac{-eZ_i v_0^3 v_{z_0}}{(5+Z_i)\nu_0 v_t^3}\right)}{\delta(\frac{1}{2}mv_0^2)} . \tag{36}$$

If we now go from this single particle model to one based on the distribution function, in which the effect of the wave is to

produce a change δf in this function, we may drop the 0 suffices and obtain

$$\frac{J}{P} = \frac{-eZ_i}{m(5+Z_i)\nu_0 v_t^3} \frac{\int v^3 v_z \, \delta f \, d^3v}{\int \frac{1}{2} v^2 \, \delta f \, d^3v} .$$

We now envisage a steady wave giving a continuous change $(\partial f/\partial t)_w$ in the distribution function. Then

$$\frac{J}{P} = \frac{-en_0 v_t}{m n_0 v_t^2 \nu_0} \frac{Z_i}{5+Z_i} \frac{\int (v/v_t)^3 (v_z/v_t) (\partial f/\partial t)_w d^3v}{\int \frac{1}{2} (v/v_t)^2 (\partial f/\partial t)_w d^3v} . \qquad (37)$$

Other authors (Eldridge, 1980; Cordey *et al.*, 1982) have used a Lorentz gas model in which the quasilinear wave diffusion term is balanced against a collision term which is $\frac{\nu_0 v_t^3}{v^3} f_1$, where f_1 is the perturbation to the equilibrium Maxwellian distribution. In this model, the current density is given by

$$J = -n_0 e \int v_z f_1 \, d^3v \qquad (38)$$

and the power absorbed by

$$P = \int \tfrac{1}{2} m n_0 v^2 \left(\frac{\partial f}{\partial t}\right)_w d^3v. \qquad (39)$$

If we now substitute $\left(\frac{\partial f}{\partial t}\right)_w = \frac{\nu_0 v_t^3 f_1}{v^3}$ into (38) we obtain

$$\frac{J}{P} = \frac{-en_0}{m n_0 \nu_0 v_t^3} \frac{\int v_z v^3 (\partial f/\partial t)_w d^3v}{\int \frac{1}{2} v^2 (\partial f/\partial t)_w d^3v} \qquad (40)$$

It is easily seen that (40) is the same as (37) apart from a factor of $\frac{Z_i}{5+Z_i}$. Cordey *et al.* have compared the Fokker-Planck and Lorentz gas models, and have found that for $Z_i = 1$ they differ by a factor of 6 as we expect, except when the wave is resonant with electrons with small v_z. This is in agreement with the results of Karney and Fisch (1981), supporting their claim that in most circumstances the method of Fisch and Boozer is in good agreement with the numerical results of the Fokker-Planck equation. We may therefore use the integrals in (38) and (39) for the purposes of computation provided we remember to multiply the final current to power ratio by $Z_i/(5+Z_i)$.

Details of the Calculation

Using $\left(\frac{\partial f}{\partial t}\right)_w = \frac{\nu_0 v_t^3 f_1}{v^3}$ and equation (38), we have

$$J = - \frac{n_0 e}{\nu_0 v_t^3} \int v_z v^3 \left(\frac{\partial f}{\partial t}\right)_w d^3v.$$

The element of volume in velocity space is $d^3v = v\, dv\, dv_z\, d\phi$. We now change coordinates from v and v_z to v and ξ where $\xi = v_z/v$. The integral over ϕ introduces a factor of 2π and $dv_z = v d\xi$, so we obtain

$$J = \frac{-2\pi n_0 e}{\nu_0 v_t^3} \int_0^\infty dv \int_{-1}^{1} d\xi\ v^6 \xi \left(\frac{\partial f}{\partial t}\right)_w . \qquad (41)$$

Our procedure now is to write $\left|E^- + \frac{k_x v_z}{\Omega} E_z\right|^2$ in terms of a single electric field component, say E_y. We start from equation (1) which may be written as

$$(\underline{n}\cdot\underline{E})\underline{n} - \underline{n}^2\underline{E} + \underline{\underline{\varepsilon}}\cdot\underline{E} = 0.$$

Remembering that $n_y = 0$, this may be written in component form as

$$n_x n_z E_z - n_z^2 E_x + \varepsilon_{11}E_x + \varepsilon_{12}E_y + \varepsilon_{13}E_z = 0$$

$$-n_x^2 E_y - n_z^2 E_y + \varepsilon_{21}E_x + \varepsilon_{22}E_y + \varepsilon_{23}E_z = 0$$

$$n_x n_z E_x - n_x^2 E_z + \varepsilon_{31}E_x + \varepsilon_{32}E_y + \varepsilon_{33}E_z = 0.$$

We let $E_x - iE_y = E^-$. The last of these equations becomes

$$(n_x^2 - \varepsilon_{33})E_z = (n_x n_z + \varepsilon_{31})E^- + (\varepsilon_{32} + i\varepsilon_{31} + in_x n_z)E_y.$$

We write this equation as

$$AE^- + BE_z = \alpha E_y. \tag{42}$$

The first of the three equations is

$$(n_z^2 - \varepsilon_{11})E^- = (n_x n_z + \varepsilon_{13})E_z + (\varepsilon_{12} - in_z^2 + i\varepsilon_{11})E_y.$$

We write this as

$$CE^- + DE_z = \beta E_y. \tag{43}$$

Combining (42) and (43) we obtain

$$E^- = a E_y \quad \text{and} \quad E_z = b E_y$$

where $a = \frac{\alpha D - \beta B}{AD - BC}$ and $b = -\frac{\alpha C - \beta A}{AD - BC}$.

Then

$$\left.\begin{aligned} \left|E^- + \frac{k_x v_z}{\Omega} E_z\right|^2 = \left|a + \frac{k_x v_z}{\Omega} b\right|^2 |E_y|^2 = \left\{D_1 + D_2 \frac{v_z k_z}{\Omega} + D_3\left(\frac{v_z k_z}{\Omega}\right)^2\right\}|E_y|^2 \\ \text{where } D_1 = |a|^2,\ D_2 = \frac{a}{k_z}(k_x b)^* + \frac{k_x b}{k_z} a^* = 2\mathrm{Re}\left(\frac{abk_x}{k_z}\right),\ \text{and } D_3 = \left|\frac{bk_x}{k_z}\right|^2 \end{aligned}\right\} \quad (44)$$

Combining equations (33) and (44) we obtain

$$\left(\frac{\partial f}{\partial t}\right)_W = \left(\frac{e}{2m}\right)^2 \frac{1}{v_\perp} \frac{\partial}{\partial v_\perp} \left\{\left[D_1 + D_2 \frac{k_z v_z}{\Omega} + D_3\left(\frac{k_z v_z}{\Omega}\right)^2\right]|E_y|^2 \delta(\Delta\omega - k_z v_z) v_\perp \frac{\partial f_0}{\partial v_\perp}\right\}$$

where $\Delta\omega = \omega - \Omega(1 - \frac{1}{2}v^2/c^2)$.

On changing variables to ξ and v, this becomes

$$\left(\frac{\partial f}{\partial t}\right)_W = \left(\frac{\partial f}{\partial t}\right)_1 + \left(\frac{\partial f}{\partial t}\right)_2 \quad \text{where}$$

$$\left(\frac{\partial f}{\partial t}\right)_1 = \left(\frac{e|E_y|}{2m}\right)^2 \frac{1 - \xi^2}{v} \frac{\partial}{\partial v} \left\{\left[D_1 + D_2 \frac{k_z v\xi}{\Omega} + D_3\left(\frac{k_z v\xi}{\Omega}\right)^2\right]\delta(\Delta\omega - k_z v\xi) v \frac{\partial f_0}{\partial v}\right\}$$

and

$$\left(\frac{\partial f}{\partial t}\right)_2 = \left(\frac{e|E_y|}{2m}\right)^2 \left(\frac{-\xi}{v}\right) \frac{\partial}{\partial \xi} \left\{\left[D_1 + D_2 \frac{k_z v\xi}{\Omega} + D_3\left(\frac{k_z v\xi}{\Omega}\right)^2\right]\delta(\Delta\omega - k_z v\xi)(1 - \xi^2) \frac{\partial f_0}{\partial v}\right\}.$$

Now consider $\int_0^\infty dv \int_{-1}^{1} d\xi v^6 \xi \left(\frac{\partial f}{\partial t}\right)_1$. We integrate this by parts with

respect to v to obtain

$$\left(\frac{e|E_y|}{2m}\right)^2 \int_{-1}^{1} d\xi \left[\frac{v^6\xi(1-\xi^2)}{v} \left\{ \left[D_1 + D_2 \frac{k_z v\xi}{\Omega} + D_3 \left(\frac{k_z v\xi}{\Omega}\right)^2 \right] \delta(\Delta\omega - k_z v\xi)\, v \frac{\partial f_0}{\partial v} \right\} \right]_0^{\infty}$$

$$-5\left(\frac{e|E_y|}{2m}\right)^2 \int_0^{\infty} dv \int_{-1}^{1} d\xi\, v^5\xi(1-\xi^2) \left\{ \left[D_1 + D_2 \frac{k_z v\xi}{\Omega} + D_3 \left(\frac{k_z v\xi}{\Omega}\right)^2 \right] \delta(\Delta\omega - k_z v\xi) \frac{\partial f_0}{\partial v} \right\}.$$

The first expression vanishes at $v = 0$ and $v = \infty$ because of v^6 and $\frac{\partial f_0}{\partial v}$ respectively, so we are left with the second expression. We first perform the ξ integration. Since $|\xi| \leq 1$ and $\Delta\omega - k_z v\xi = 0$ for resonance, the limits of the velocity integral are changed to those within which $\left|\frac{\Delta\omega}{k_z v}\right| \leq 1$, say v_+ and v_-. Then

$$\int_0^{\infty} dv \int_{-1}^{1} d\xi v^6 \xi \left(\frac{\partial f}{\partial t}\right)_1 = -5\left(\frac{e|E_y|}{2m}\right)^2 \int_{v_-}^{v_+} v^5 \frac{\Delta\omega}{k_z v} \left(1 - \left(\frac{\Delta\omega}{k_z v}\right)^2\right)$$

$$\left[D_1 + D_2 \frac{\Delta\omega}{\Omega} + D_3 \left(\frac{\Delta\omega}{\Omega}\right)^2 \right] \frac{1}{k_z v} \frac{\partial f_0}{\partial v}\, dv. \qquad (45)$$

The factor $\frac{1}{k_z v}$ comes from the fact that the argument of the δ function is not ξ, but $\Delta\omega - k_z v\xi$.

Now consider $\int_0^{\infty} dv \int_{-1}^{1} d\xi\, v^6 \xi \left(\frac{\partial f}{\partial t}\right)_2$. We integrate by parts with respect to ξ to obtain

$$\left(\frac{e|E_y|}{2m}\right)^2 \int_0^\infty v^6 dv \left[-\frac{\xi^2}{v} \left\{ \left[D_1 + D_2 \frac{k_z v\xi}{\Omega} + D_3 \left(\frac{k_z v\xi}{\Omega}\right)^2 \right] \delta(\Delta\omega - k_z v\xi)(1-\xi^2) \frac{\partial f_0}{\partial v} \right\} \right]_{-1}^{1}$$

$$+ \left(\frac{e|E_y|}{2m}\right)^2 \int_0^\infty v^6 dv \int_{-1}^{1} d\xi \frac{2\xi}{v} \left\{ \left[D_1 + D_2 \frac{k_z v\xi}{\Omega} + D_3 \left(\frac{k_z v\xi}{\Omega}\right)^2 \right] \delta(\Delta\omega - k_z v\xi)(1-\xi^2) \frac{\partial f_0}{\partial v} \right\}.$$

The first expression vanishes at $\xi = -1$ and $\xi = 1$ because of the $1 - \xi^2$ term. Again we perform the ξ integration first, on the second expression. Then

$$\int_0^\infty dv \int_{-1}^{1} d\xi\, v^6 \xi \left(\frac{\partial f}{\partial t}\right)_2 = 2\left(\frac{e|E_y|}{2m}\right)^2 \int_{v_-}^{v_+} v^5 \frac{\Delta\omega}{k_z v} \left[1 - \left(\frac{\Delta\omega}{k_z v}\right)^2\right]$$

$$\left[D_1 + D_2 \frac{\Delta\omega}{\Omega} + D_3 \left(\frac{\Delta\omega}{\Omega}\right)^2 \right] \frac{1}{k_z v} \frac{\partial f_0}{\partial v} dv. \qquad (46)$$

We now combine equations (41), (45) and (46) to obtain

$$J = \frac{-2\pi n_0 e}{\nu_0 v_t^3} \left(\frac{e|E_y|}{2m}\right)^2 (-3) \int_{v_-}^{v_+} \frac{v^4}{k_z} \frac{\Delta\omega}{k_z v} \left[1 - \left(\frac{\Delta\omega}{k_z v}\right)^2\right]$$

$$\left[D_1 + D_2 \frac{\Delta\omega}{\Omega} + D_3 \left(\frac{\Delta\omega}{\Omega}\right)^2 \right] \frac{\partial f_0}{\partial v} dv.$$

Now introduce non-dimensional parameters as follows

$$y = v/v_t, \quad V^+ = v_+/v_t, \quad V^- = v_-/v_t, \quad u = \frac{\Delta_0}{k_z v_t},$$

$$\eta = \frac{1}{2}\frac{\Omega}{k_z v_t}\frac{v_t^2}{c^2}, \quad \text{and} \quad r = \frac{k_z v_t}{\Omega}$$

where $\Delta_0 = \Omega - \omega.$

Then

$$\frac{\Delta\omega}{k_z v} = \frac{-u + \eta y^2}{y}, \quad \frac{\Delta\omega}{\Omega} = r(-u + \eta y^2),$$

$$\text{and} \quad \frac{\partial f_0}{\partial v} = \frac{\partial}{\partial v}\left(\frac{n_0}{(2\pi v_t^2)^{3/2}} e^{-v^2/2v_t^2}\right) = \frac{-n_0 y}{(2\pi)^{3/2} v_t^4} e^{-y^2/2}.$$

So,

$$J = \frac{-2\pi n_0 e}{\nu_0 v_t^3}\left(\frac{e|E_y|}{2m}\right)^2 (-3)\left(\frac{-n_0 v_t}{k_z (2\pi)^{3/2}}\right)\int_{V^-}^{V^+} F1(y)\,dy \qquad (47)$$

where

$$F1(y) = y^5\left(\frac{-u + \eta y^2}{y}\right)\left(1 - \left(\frac{-u + \eta y^2}{y}\right)^2\right)\left[D_1 + D_2 r(-u + \eta y^2) + D_3 r^2(-u + \eta y^2)^2\right]e^{-y^2/2}$$

From (39), we find that the absorbed power density is

$$P = \tfrac{1}{2} m n_0 2\pi \int_0^\infty dv \int_{-1}^{1} d\xi\, v^4 \left(\frac{\partial f}{\partial t}\right)_w.$$

The calculation proceeds in exactly the same way as for J. We obtain

$$P = \tfrac{1}{2}mn_0 2\pi\left(\frac{e|E_y|}{2m}\right)^2(-2)\left(\frac{-n_0}{k_z v_t (2\pi)^{3/2}}\right)\int_{V^-}^{V^+} F2(y)\,dy \qquad (48)$$

where

$$F2(y) = y^3\left(1 - \left(\frac{-u+\eta y^2}{y}\right)^2\right)\left[D_1 + D_2 r(-u+\eta y^2) + D_3 r^2(-u+\eta y^2)^2\right]e^{-y^2/2}.$$

We now calculate V^- and V^+. These are the values of y for which $\left|\frac{\Delta\omega}{k_z v}\right| = 1$, i.e. $-u+\eta y^2 = \pm y$. This gives

$$y = \frac{\pm 1 \pm \sqrt{1-4u\eta}}{2\eta} \qquad (4 \text{ values}).$$

However, $y > 0$ since $v > 0$. Therefore

$$V^+ = \frac{1+\sqrt{1-4u\eta}}{2\eta} \quad \text{and} \quad V^- = \left|\frac{1-\sqrt{1-4u\eta}}{2\eta}\right|. \qquad (49)$$

We again stress that the quantity of interest is the ratio of the total current driven to the total power absorbed. We therefore have to integrate J and P through the resonance layer. Now both J and P depend on $|E_y|^2$ which varies with x, so we have to determine the behaviour of $|E_y|^2$. Since the wave frequencies used are high, we may use geometrical optics (Ginzburg, 1964) to describe the propagation of the wave, in which a WKB representation of the wave is used. We therefore make the following approximation

$$E_y = E_0\, e^{i\int \underline{k}.d\underline{r}} \quad \text{where } E_0 \text{ is independent of } \underline{r}.$$

Then $|E_y|^2 = |E_0|^2 \, e^{-2\int \mathrm{Im}(k_x)\,dx}$, since $k_y = 0$ and k_z is real, so that $\mathrm{Im}(k_x)$ gives the damping rate of the wave, as we saw in Chapter 3. We may now cancel $|E_0|^2$ out of the ratio of current to power, so that we never calculate the current and power densities absolutely, but merely their magnitudes relative to some electric field amplitude. We are then left with

$$\frac{\int J\,dx}{\int P\,dx} = \frac{n_0 e v_t}{n_0 m v_t^2 \nu_0} \; \frac{\int -3e^{-2\int \mathrm{Im}(k_x)\,dx} \left(\int F1(y)\,dy\right) dx}{\int e^{-2\int \mathrm{Im}(k_x)\,dx} \left(\int F2(y)\,dy\right) dx} . \qquad (50)$$

In order to get our final result in terms of Amps per Watt, we must compare the current density per unit area in the y-z plane, with the power absorbed per unit area in the y-z plane. Above, we have calculated the current density per unit length in the y direction. We now make the assumption that the effect of the absorbed radiation is smeared out around the tokamak due to rapid electron transport in the z direction, so the current density per unit is just $\frac{\int J\,dx}{2\pi R}$.

Now $\nu_0 = \frac{\omega_p^4 \ell n \Lambda Z_i}{4\pi n_0 v_t^3}$ and $\omega_p^2 = \frac{n_0 e^2}{m\varepsilon_0}$. We also remember to multiply our result by $\frac{Z_i}{5+Z_i}$, so that the final result is

$$\mathrm{I/P\ (Amps/Watt)} = \frac{6.11 \times 10^{18}}{5 + Z_i} \; \frac{T(\mathrm{keV})}{R(\mathrm{m})\, n_0(\mathrm{m}^{-3})\, \ell n \Lambda} \; \frac{\int -3e^{-2\int \mathrm{Im}(k_x)\,dx} \left(\int F1(y)\,dy\right) dx}{\int e^{-2\int \mathrm{Im}(k_x)\,dx} \left(\int F2(y)\,dy\right) dx} .$$

(51)

CHAPTER 5

Current Drive Program

This chapter describes the program that has been developed for calculating current drive, and presents some of the results that have been obtained. The procedure adopted is as follows. We first determine the limits, in terms of x, of the resonance region. For the relativistic case, the limit on the low field side is usually the low field cut-off point given by $x/R = -n_z^2/2$. For the high field side and the non-relativistic case, there is no such point, so the limits must be determined *a posteriori*. These will be the points beyond which current drive and power absorption are found to be negligible.

Having found these limits, we look at a series of 40 points spaced out through the resonance region. At each point we solve the dispersion relation, at either the fundamental or the second harmonic, to obtain n_x and therefore all the elements of the dielectric tensor. The diffusion coefficients D1, D2 and D3 of the last chapter are then calculated, using (44). The current and power densities at this point are calculated by means of (47) and (48). These are what will be referred to as the undamped current and power densities, since they are given in terms of the electric field component E_y which is reduced in magnitude as the wave passes through the plasma. They therefore indicate what the current and power densities would be in the case of very weak absorption.

We use the fact that $|E_y|^2 = |E_0|^2 e^{-2\int Im(k_x)dx}$ to obtain the actual current and power densities (though still in terms of E_0). The integral of $Im(k_x)$ is taken from the limit of the resonance region on the side from which the wave propagates, to the point under consideration. Once the current and power densities have been obtained at each point, they are integrated through the resonance region. The ratio of these two quantities is then multiplied by a factor, as in (51), to give the final result in terms of Amps per Watt. Profiles of current, power, perpendicular refractive index, and resonant parallel velocities may then be output graphically.

In the non-relativistic case a few changes have to be made. Firstly, we must use the non-relativistic dielectric tensor as given in equations (25) and (26). Secondly, we must use the non-relativistic resonance condition, so that $\Delta\omega = \omega - \Omega$. This means that the non-dimensional parameter η, which first appeared in (47), must be zero. In addition, the limits of the current and power integrals, V^+ and V^-, are changed. V^+ becomes infinity, so that a different integration routine is necessary.

Accuracy of Results

Before the results are presented, it should be mentioned that they are intended simply to illustrate the theory and demonstrate the importance of the relativistic correction to the electron mass in a hot plasma. A number of approximations have been made which will reduce the accuracy of the results. Some of these are as

follows

(1) The magnetic field is assumed to vary linearly with distance from the resonance point, rather than inversely as the distance from the centre of the tokamak.

(2) Temperature and density variation with distance has been neglected, although there is provision in the program for including temperature and density profiles.

(3) A slab model has been used in which the curvature of field lines is ignored. Other authors have included this in a ray-tracing code (Start and O'Brien, 1982; Edlington *et al.*, 1982; Start *et al.*, 1983).

(4) The effect of trapped electrons has been neglected. Cordey *et al.* (1982) have shown that this considerably reduces the current.

(5) In equation (3), f_0 is taken to be the equilibrium Maxwellian distribution of the plasma, which means that we are using a linearised model, in which the effect of waves on the particle distribution is not taken into account self-consistently. This point is dealt with in detail in the next chapter.

(6) We have assumed that E_0 is independent of $\underset{\sim}{r}$, whereas it varies slowly with $\underset{\sim}{r}$ in the space of one vacuum wavelength ($2\pi c/\omega$).

Results

Results are presented for the sets of parameters given below.

Table 5.1

	A	B	C	D	E	F
Temperature (keV)	1.0	1.0	5.0	1.0	1.0	5.0
ω_p^2/ω^2	0.75	0.75	0.75	0.2	0.2	0.2
Wave Frequency (GHz)	60	100	150	60	100	150
Major Radius (m)	1.2	3.0	5.0	1.2	3.0	5.0
Harmonic	1	1	1	2	2	2
Toroidal Magnetic Field (T)	2.1	3.6	5.3	1.1	1.8	2.7

We may regard parameters A as being typical of a laboratory machine such as the Culham DITE tokamak (Paul *et al.*, 1976), parameters B as being relevant to JET (Bickerton, 1979) and similar devices, and parameters C to proposed larger tokamaks like INTOR (INTOR Group, 1982). Parameters D, E and F correspond to the same machines as A, B and C, but run at the second harmonic. Because of the difficulty (at present) of generating very high frequency radio waves, the wave frequency will not simply be doubled in order to obtain the second harmonic resonance. Instead, the cyclotron frequency is reduced by lowering the magnetic field. In addition, we assume a lower density. This is for two reasons. First of all, the X mode has a cut-off at $\omega_p^2/\omega^2 = 0.5$ and secondly, there is a critical value of ω_p^2/ω^2 at which mode conversion between the X and Bernstein modes takes place. We therefore choose a value of ω_p^2/ω^2 which is sufficiently low that both the O and X modes propagate freely.

Fundamental Frequency

In Fig. 5.1, current density profiles are plotted for parameters A and the O mode with $n_z = 0.1$. The solid line represents the undamped current (as explained earlier) and the other lines show the current density profiles for incidence from the low and high field sides. The same profiles are plotted in Fig. 5.2 for $n_z = 0.4$. For comparison, the undamped current according to the non-relativistic calculation is plotted for $n_z = 0.1$ and 0.4 in Figs. 5.3 and 5.4 respectively. Note that the units of current density are arbitrary, and that the actual current densities in different figures are not necessarily directly comparable; the physical values can be gauged from the results for total current per unit power absorbed.

The strongly asymmetric nature of Fig. 5.1 is just as we expected in the discussion of the resonance condition in Chapter 4. The current reversal point is not at the origin as it is in the non-relativistic case (see Fig. 5.3), but is displaced by a significant amount to the high field side. In this case, current reversal will lead to a non-negligible reduction in the net current since the absorption is not strong enough for the wave to be absorbed almost completely on one side of the resonance.

The undamped current profile in Fig. 5.2 more closely resembles the corresponding non-relativistic one, Fig. 5.4, than did Fig. 5.1. This was again to be expected since relativistic effects are more important for smaller values of n_z. We also find that the region in which there is significant current drive is larger for $n_z = 0.4$: its

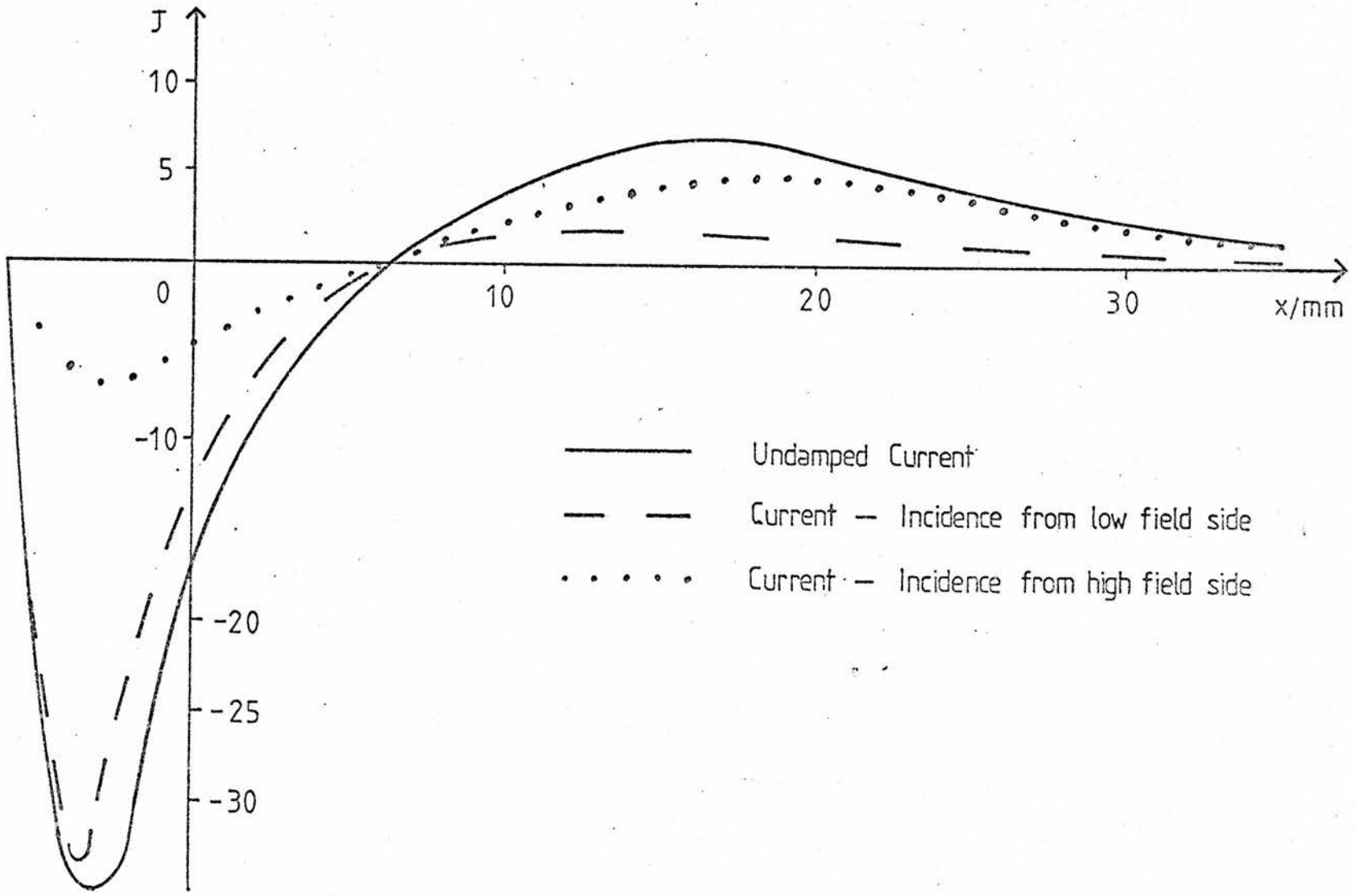

Figure 5.1

Current density profiles for the O mode in the relativistic case with parameters A, and $n_z = 0.1$. The units of current density are arbitrary.

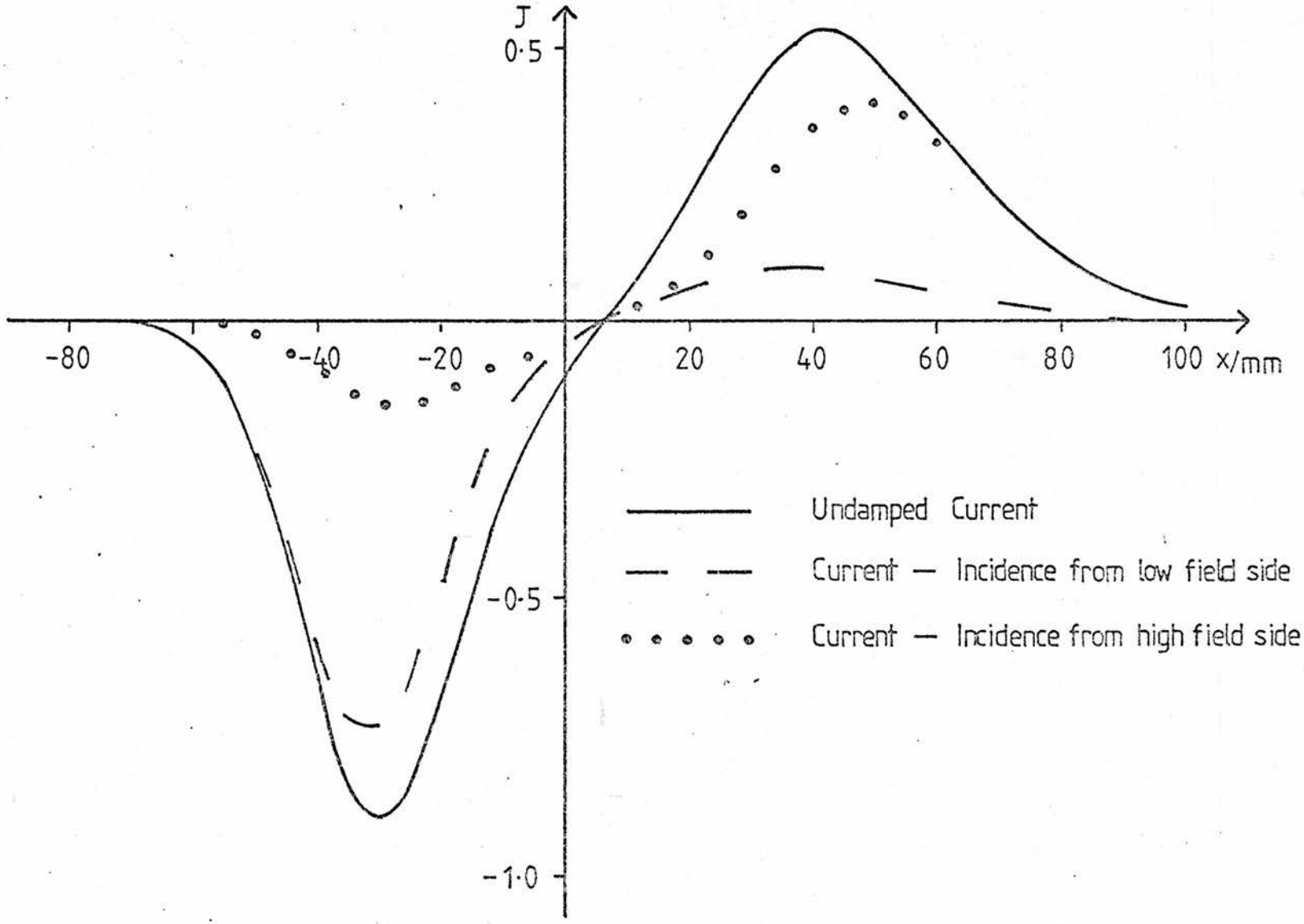

Figure 5.2

Current density profiles for the O mode in the relativistic case with parameters A, and $n_z = 0.4$. The units of current density are arbitrary.

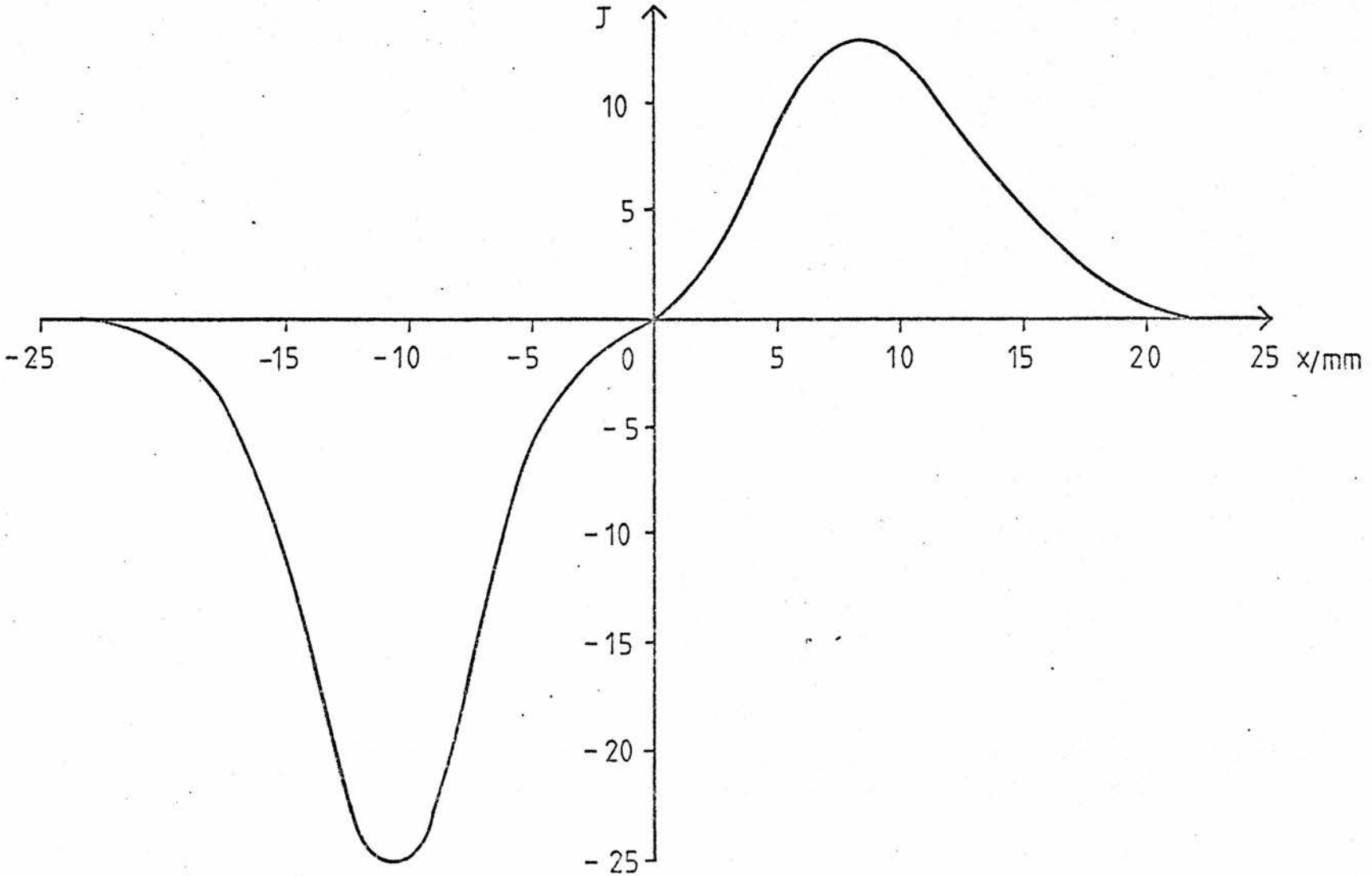

Figure 5.3

Undamped current density profile in the non-relativistic case for the O mode with parameters A, and $n_z = 0.1$. The units of current density are arbitrary.

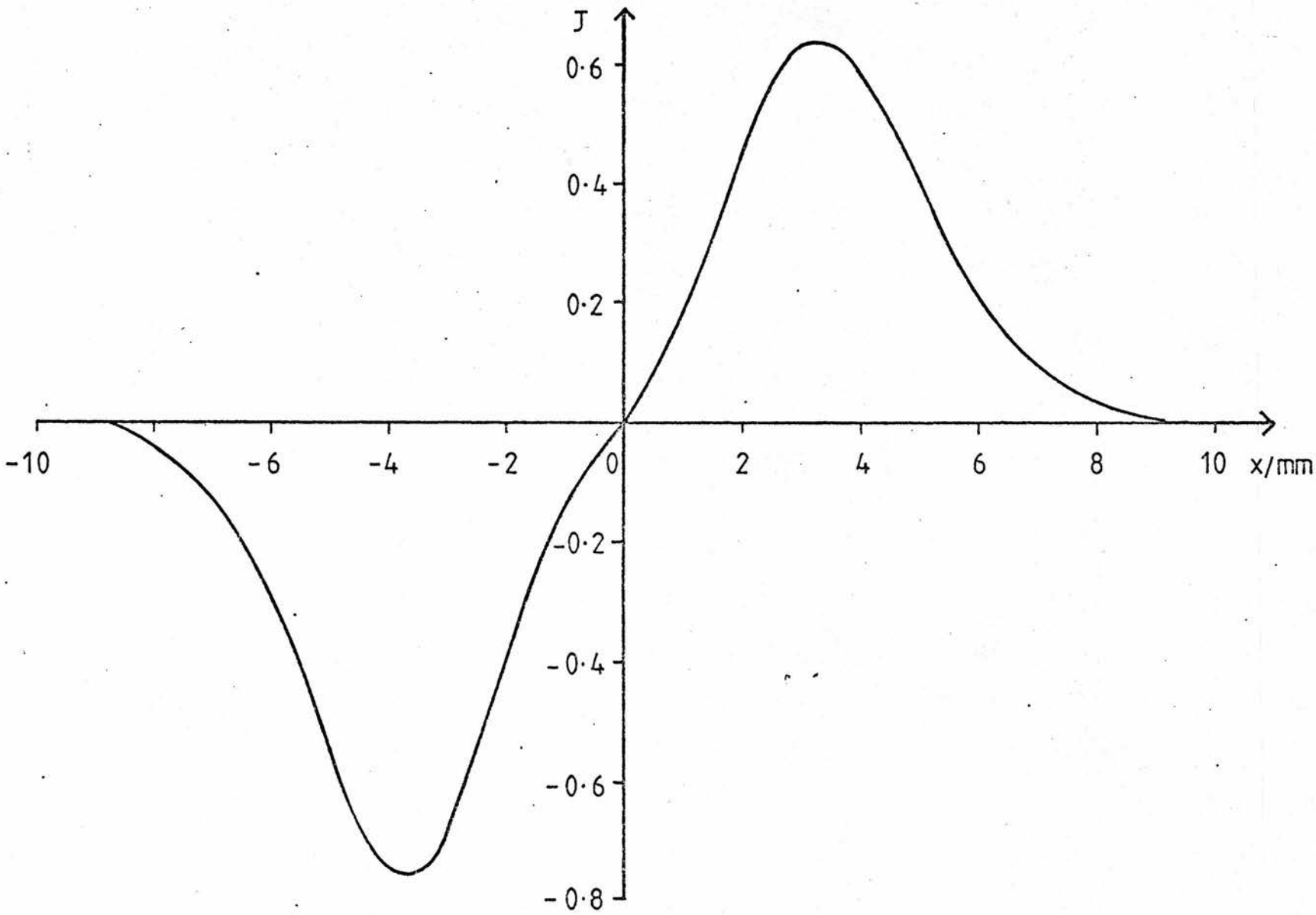

Figure 5.4

Undamped current density profile in the non-relativistic case for the O mode with parameters A, and $n_z = 0.4$. The units of current density are arbitrary.

width was about 4 cm in Fig. 5.1 and is about 16 cm in Fig. 5.2. The same is true in the non-relativistic case, and the reason can easily be seen from the non-relativistic resonance condition (31): particles of a given velocity are in resonance at a distance proportional to n_z.

In Fig. 5.5 the power absorption profiles are plotted for the same parameters with $n_z = 0.1$. There is one curve for each direction of propagation. The units for each curve were arbitrary, so one of the curves has been rescaled to allow comparison with the other. This was done using the fact that the total power absorbed is the same irrespective of the side on which the wave was incident. This fact is confirmed by the result that the wave intensity drops to the same fraction of the incident wave intensity on passing through the plasma in both cases.

It is evident from the curve for incidence from the high field side that there are two resonances, closely spaced, rather than a single one with the associated Gaussian broadening. This apparently strange result has been explained by Arunasalam *et al.* (1983) simply using linear absorption theory. It is seen only with the O mode.

In Figs. 5.6 and 5.7 we plot results for parameters C and the O mode, with $n_z = 0.1$. The most striking feature is that there is no current reversal in either case because the wave has been strongly damped, much more so than for parameters A. This is simply a consequence of the larger radius and wave frequency for parameters C. The other notable feature is that, for incidence from the high

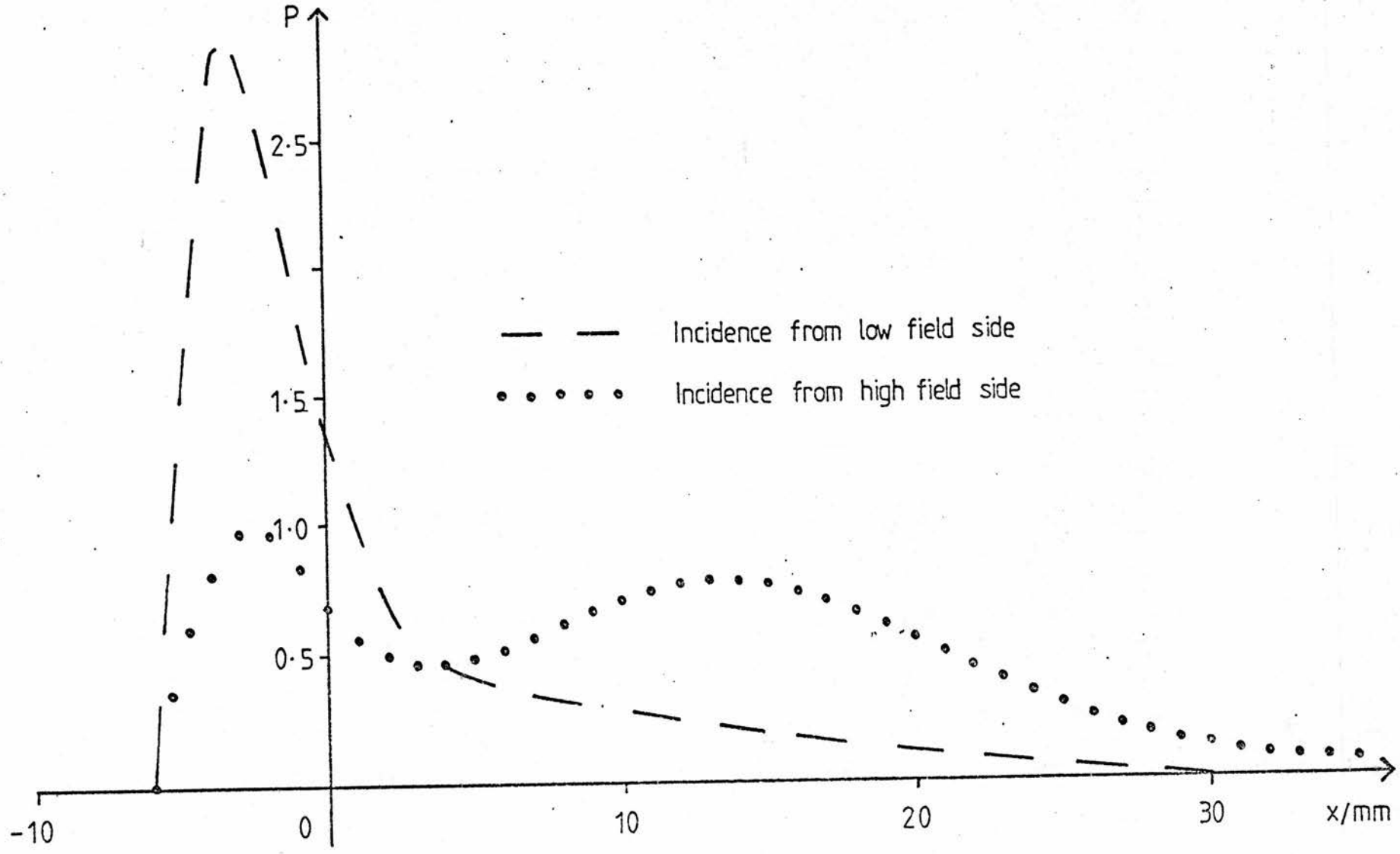

Figure 5.5

Power absorption profiles in the relativistic case for the O mode with parameters A, and $n_z = 0.1$. The units of power density are arbitrary.

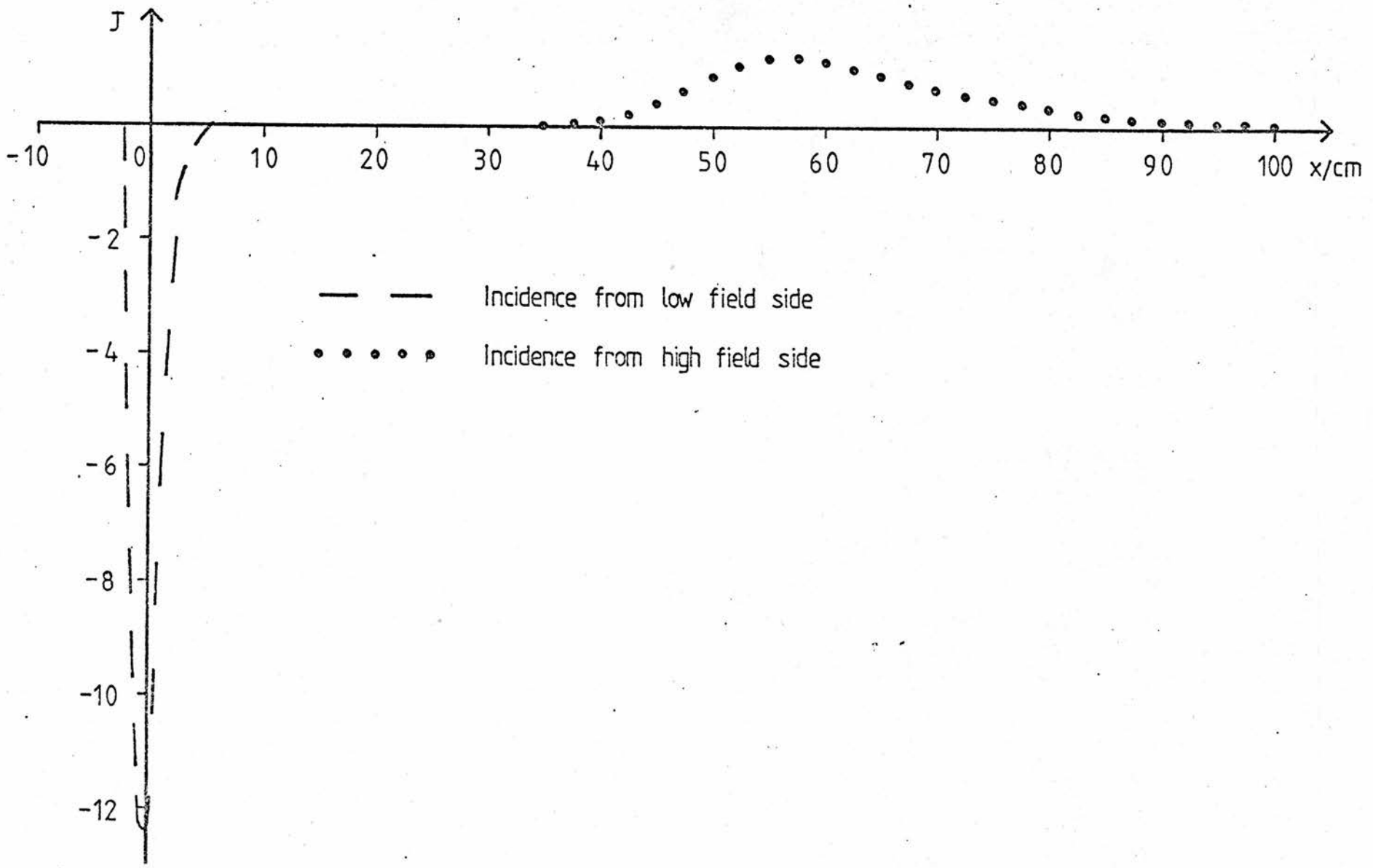

Figure 5.6

Current density profiles in the relativistic case for the O mode with parameters C, and $n_2 = 0.1$. The units of current density are arbitrary.

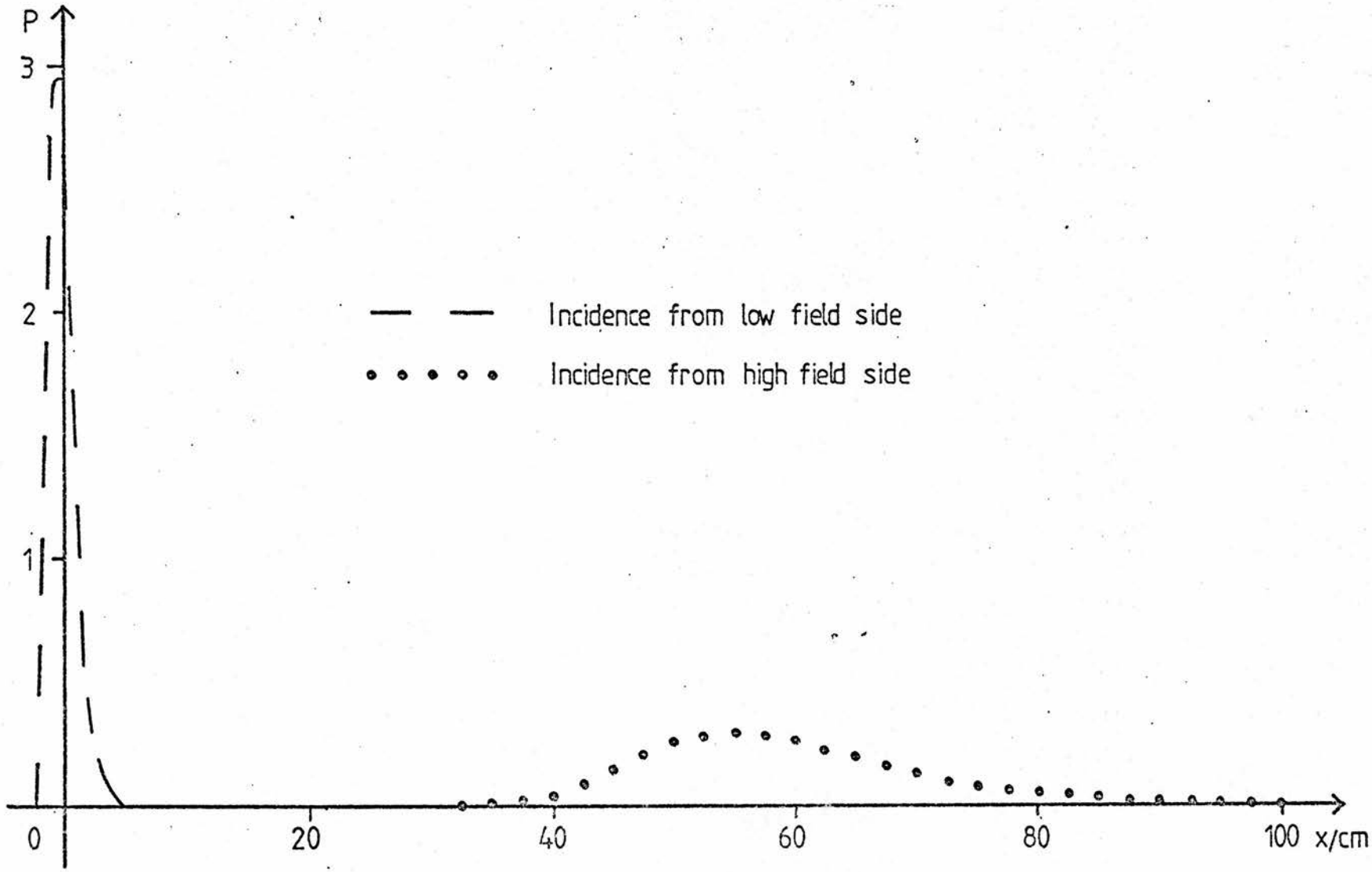

Figure 5.7

Power profiles in the relativistic case for the O mode with parameters C, and $n_z = 0.1$. The units of power density are arbitrary.

field side, the current layer is wider and is displaced a considerable distance from $x = 0$. The same is evident in Fig. 5.7 which shows the power profiles for the same two cases. For incidence from the high field side, both current and power densities fall to zero about 40 cm from the resonance, simply because the wave has been completely absorbed by then.

A comparison of Figs. 5.6 and 5.7 will reveal that, on the high field side, the current and power profiles are shifted very slightly with respect to one another. This also happens in the non-relativistic case. This is a consequence of the fact that the current to power ratio increases away from resonance. The reason for this is that, far away from the resonance, the wave resonates with electrons which have a higher speed. These electrons collide less frequently and so are more able to retain a directed current than slower electrons in the bulk of the distribution. The current drive efficiency is illustrated in Figs. 5.9 and 5.10 where the current to power ratio, in units of $n_0 e v_t / n_0 m v_t^2 \nu_0$, is plotted as a function of distance from the resonance point, in the relativistic and non-relativistic cases, respectively.

It will be seen that the ratio varies linearly with x for large x in the relativistic case, whereas it varies as x^2 in the non-relativistic case. Cordey *et al.* (1982) have discussed the non-relativistic case. The linear variation in the relativistic case has been explained by Cairns *et al.* (1983).

Fig. 5.8 gives power profiles corresponding to those in Fig. 5.7, but obtained using the non-relativistic theory. It is apparent

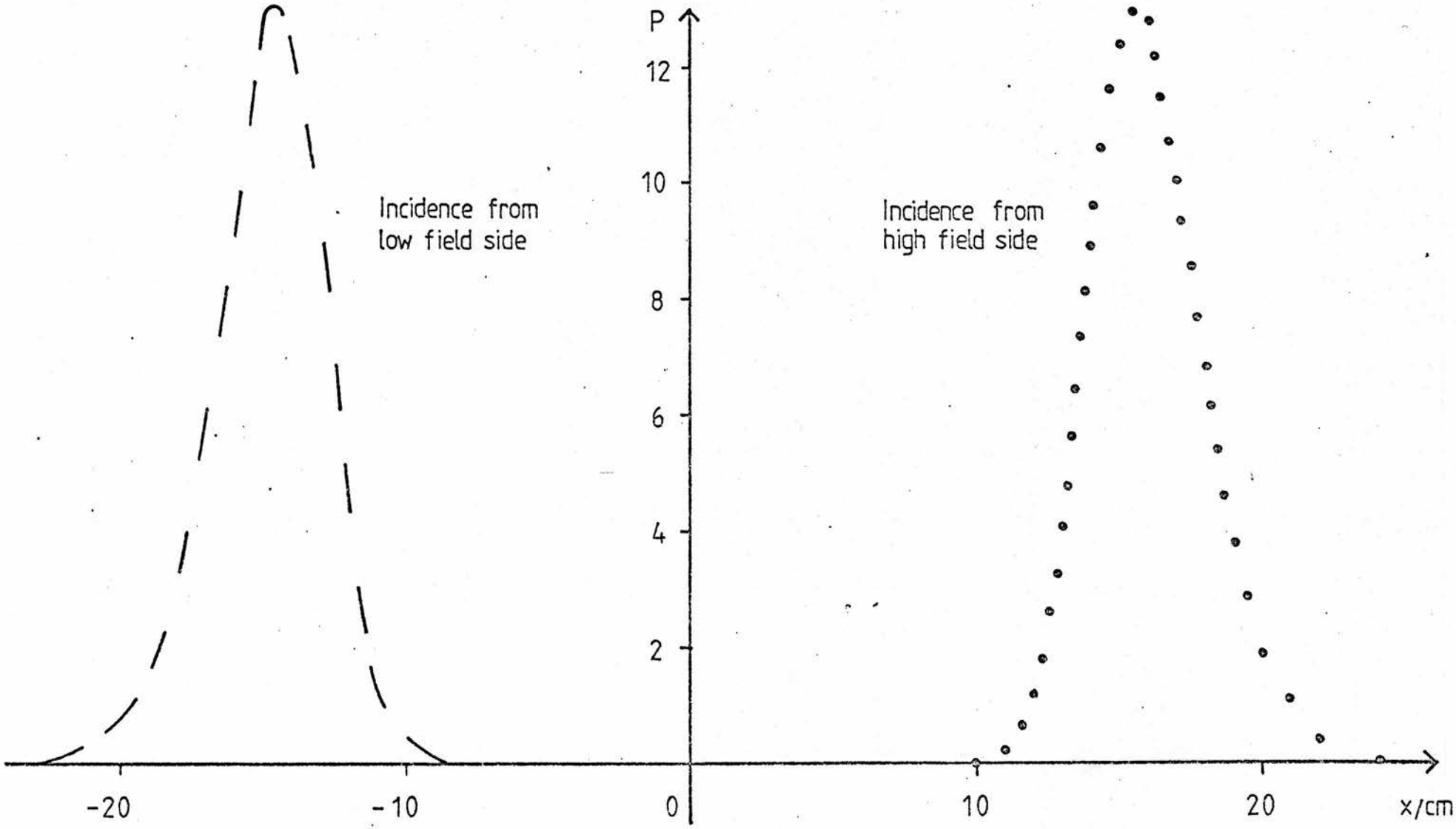

Figure 5.8

Power profiles in the non-relativistic case for the O mode with parameters C, and $n_z = 0.1$. The units of power density are arbitrary.

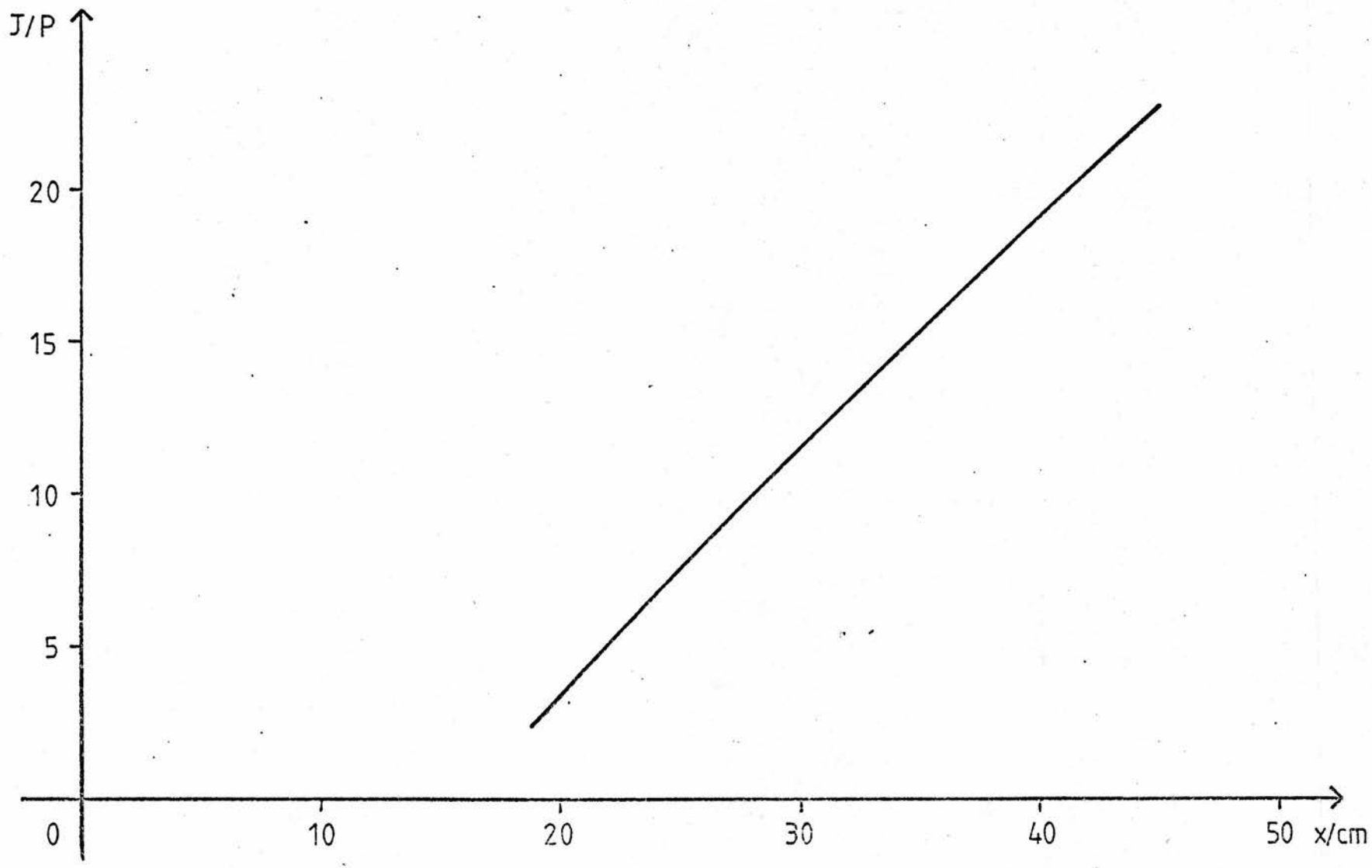

Figure 5.9

J/P in units of $n_0 e v_t / n_0 m v_t^2 \nu_0$ as a function of distance in the relativistic case with parameters C, and $n_z = 0.1$.

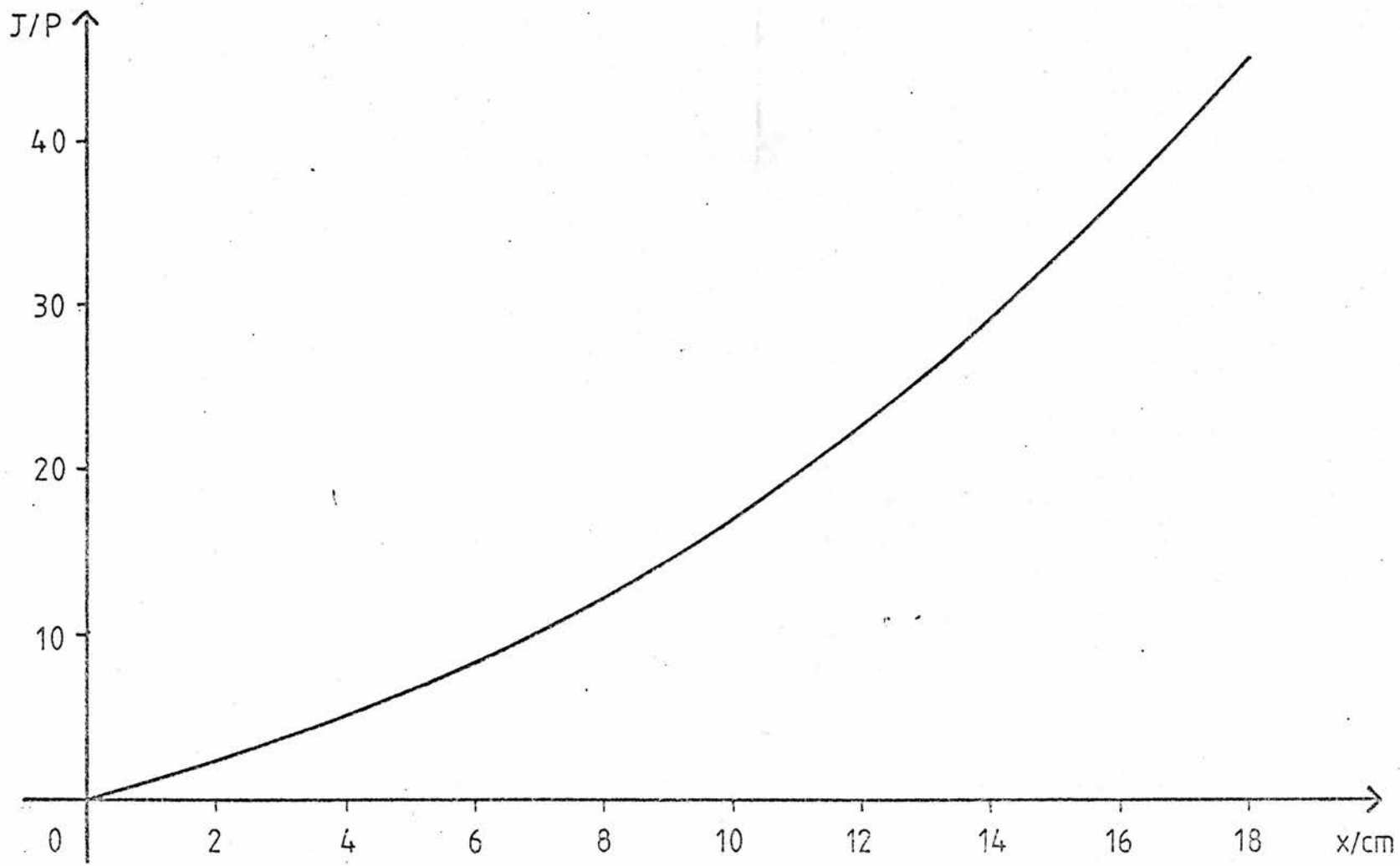

Figure 5.10

J/P in units of $n_0 e v_t / n_0 m v_t^2 \nu_0$ as a function of distance in the non-relativistic case with parameters C, and $n_z = 0.1$.

that, for incidence from the high field side, the inclusion of the relativistic correction shifts the predicted position of maximum power absorption by a substantial amount (in this case about 40 cm). Naturally, the same shift occurs for the current layer. The reason for this can be seen in Fig. 4.2: for a given value of v_z, resonance takes place farther from the resonance when the relativistic correction is included, since the resonant value of x goes as v_z^2 as opposed to v_z in the non-relativistic theory. This shift is of great importance, since one of the advantages of ECRH is that it may be used for accurately controlling the current profile in a tokamak (Lashmore-Davies *et al.*, 1982).

In Fig. 5.11 we give results for the ratio of total current to total power absorbed as a function of the angle of incidence for parameters A. Figs. 5.12 and 5.13 show the corresponding results for parameters B and C. It can be seen from the latter two Figures that the X mode or the O mode from the high field side are more efficient than the O mode from the low field side. This is simply a consequence of the fact that the current to power ratio is large away from the resonance on the high field side. In Fig. 5.11, however, the O mode from the low field side is more efficient. This is because the absorption is weaker for parameters A, so for incidence from the high field side, the power is not absorbed so far away from resonance, and there is also a larger reverse current, leading to a smaller net current. For parameters B and C, the reverse current is negligible.

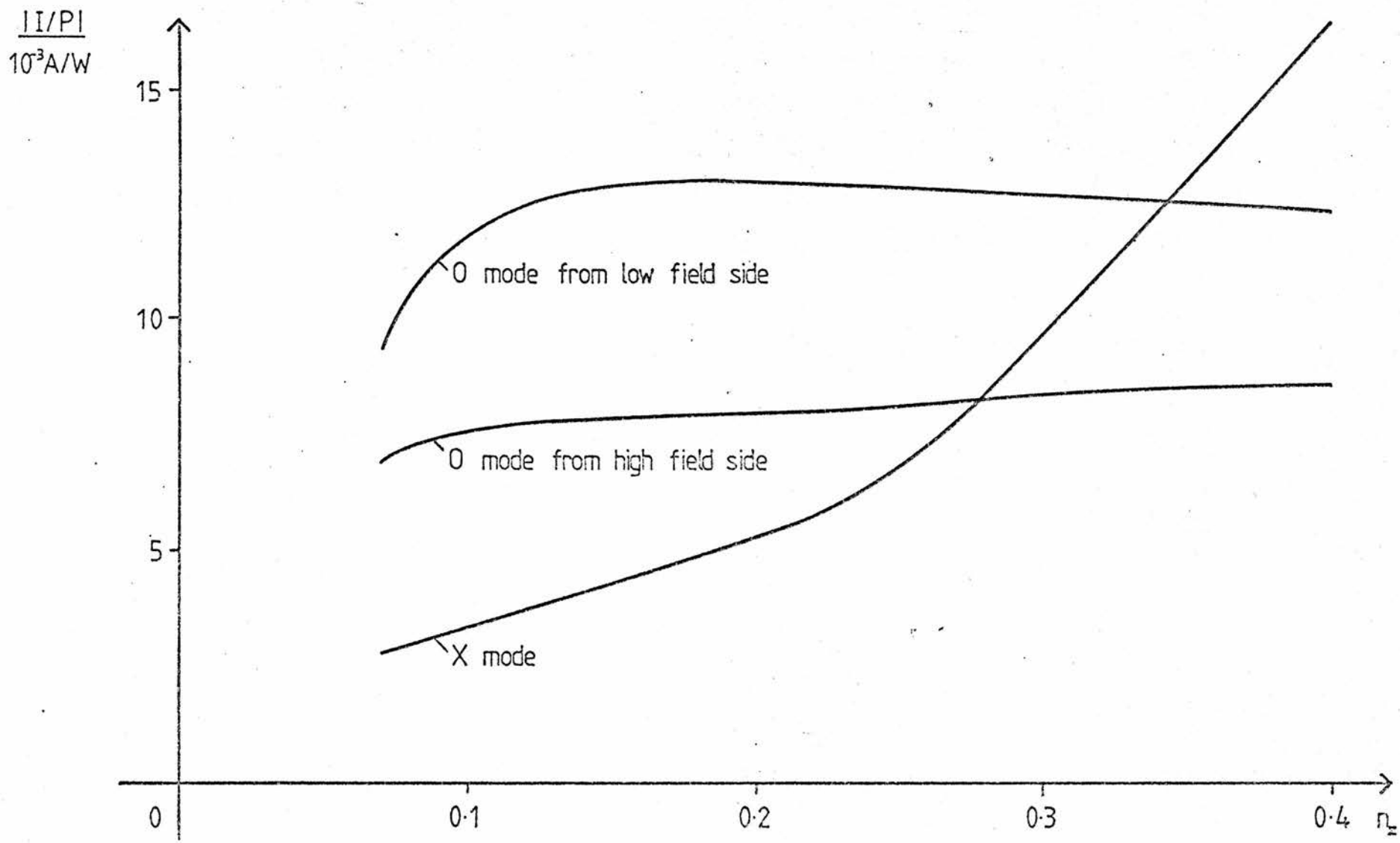

Figure 5.11

Current drive efficiency as a function of n_z in the relativistic case with parameters A.

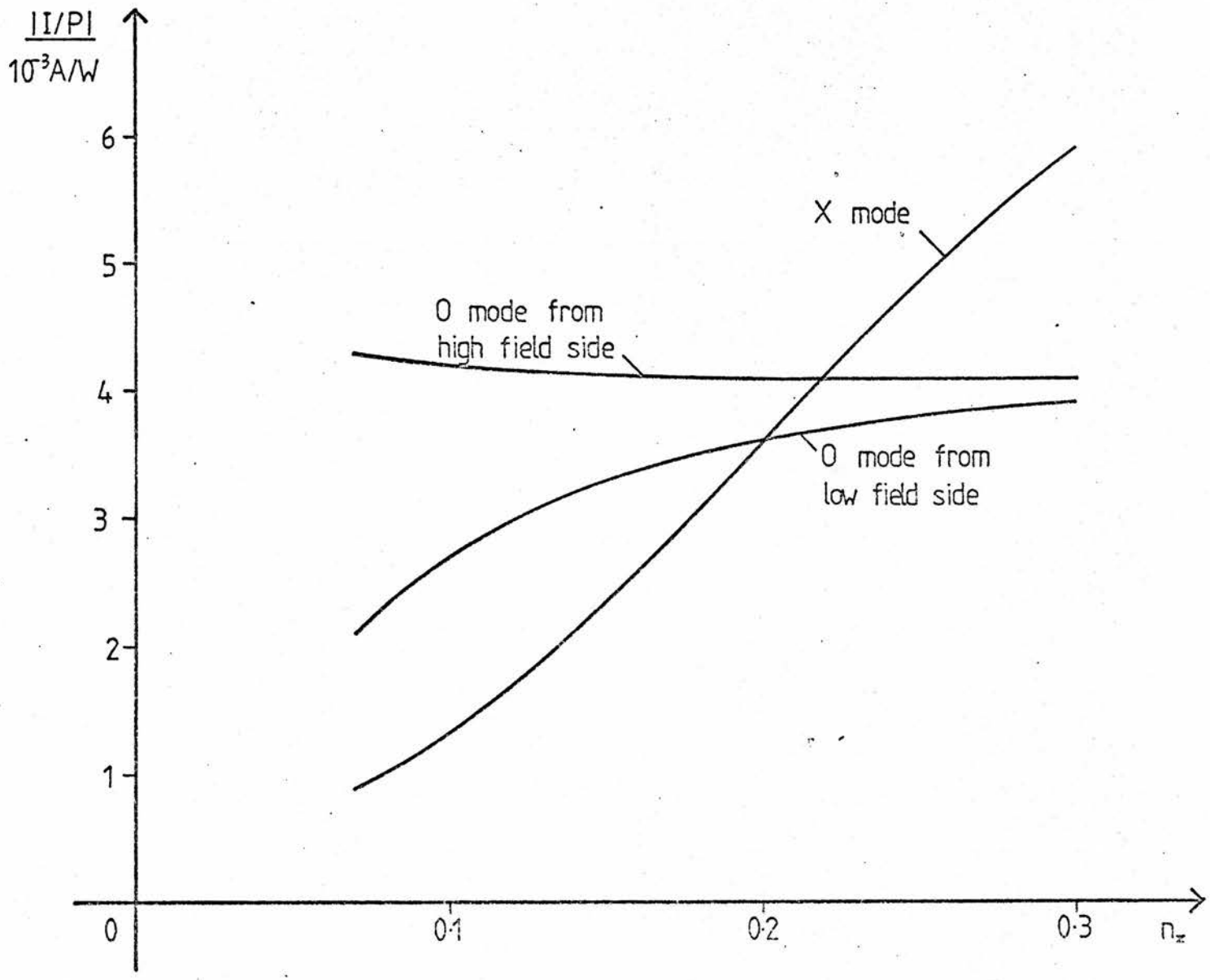

Figure 5.12

Current drive efficiency as a function of n_z in the relativistic case with parameters B.

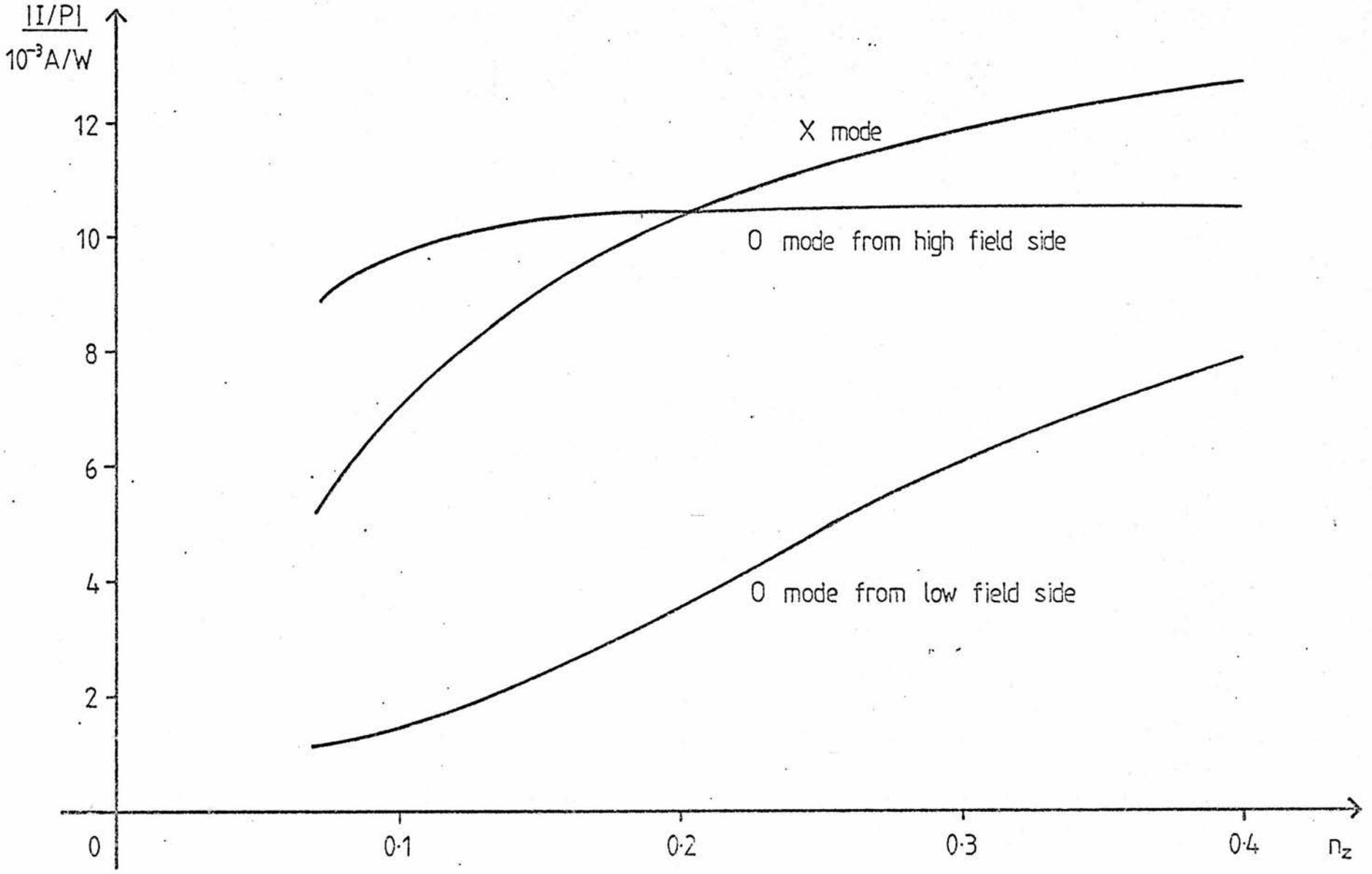

Figure 5.13

Current drive efficiency as a function of n_z in the relativistic case with parameters C.

One way to increase the efficiency of the O mode from the low field side is to reduce the wave frequency so that the resonance point is actually outside the plasma. Absorption must then take place on the high field side of the resonance where the efficiency is higher, but the drawback is that the absorption and current drive occur at the edge of the plasma.

The variation of current drive efficiency with n_z depends on a number of things. Firstly, the absorption of a particular mode will depend on n_z. This will affect the presence and strength of a reverse current and, for incidence from the high field side will affect the position at which current drive takes place. For incidence from the low field side, power absorption and current drive first take place at the nose of the parabola, at which $v_z/c = n_z$. Thus for larger values of n_z, resonance can take place with fast electrons on the low field side, leading to a higher efficiency, if the absorption is sufficiently strong.

For the X mode, the absorption is stronger for larger values of n_z, leading to current drive farther from the resonance point, and thus a greater efficiency. For the O mode, the absorption decreases with n_z, so the efficiency is no greater for larger values of n_z for propagation from the high field side. For incidence from the low field side, and parameters A, the absorption is weak enough to allow a substantial reverse current, even more so for larger values of n_z. For parameters B and C, however, the absorption is strong enough to allow current drive away from the resonance point

on the low field side and, as explained above, this leads to greater efficiency for larger values of n_z, as seen in Figs. 5.12 and 5.13.

Finally, we note that for larger values of n_z, the efficiencies of the O mode from the low and high field sides are similar. This was to be expected, since the behaviour for larger values of n_z should be similar to that of the non-relativistic current drive, which is antisymmetrical about the resonance point.

Second Harmonic

In Figs. 5.14 and 5.15, current profiles are plotted for the O and X modes and parameters D, with $n_z = 0.1$. As has already been said, the O mode is very weakly absorbed at the second harmonic, so it is necessary to plot only the undamped current in Fig. 5.15. It is interesting to note that the undamped current for the O mode is stronger on the high field side, which is not the case for the O mode at the fundamental, or for the X mode at either the fundamental or the second harmonic. There is no simple reason for this since the current depends not only on the velocity distribution of the electrons, but also on the wave diffusion coefficients.

Fig. 5.16 shows power absorption profiles for incidence from the low field side and the same parameters as above. It shows again the strong absorption of the Bernstein mode and the weak absorption of the O mode.

Figs. 5.17, 5.18 and 5.19 give results for the ratio of total current to total power for parameters D, E and F. The O and X modes

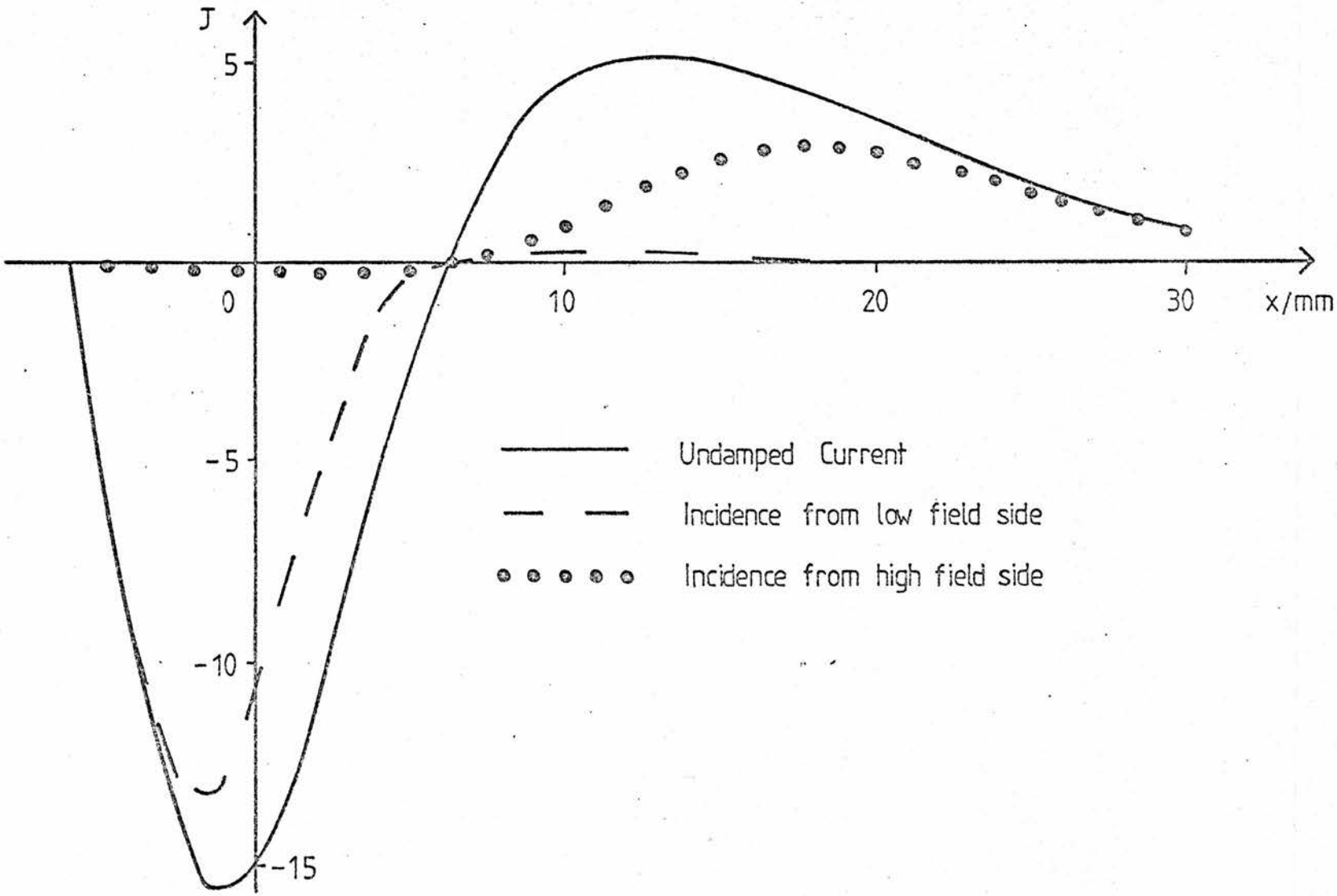

Figure 5.14

Current density profiles in the relativistic case for the X mode with parameters D, and $n_z = 0.1$. The units of current density are arbitrary.

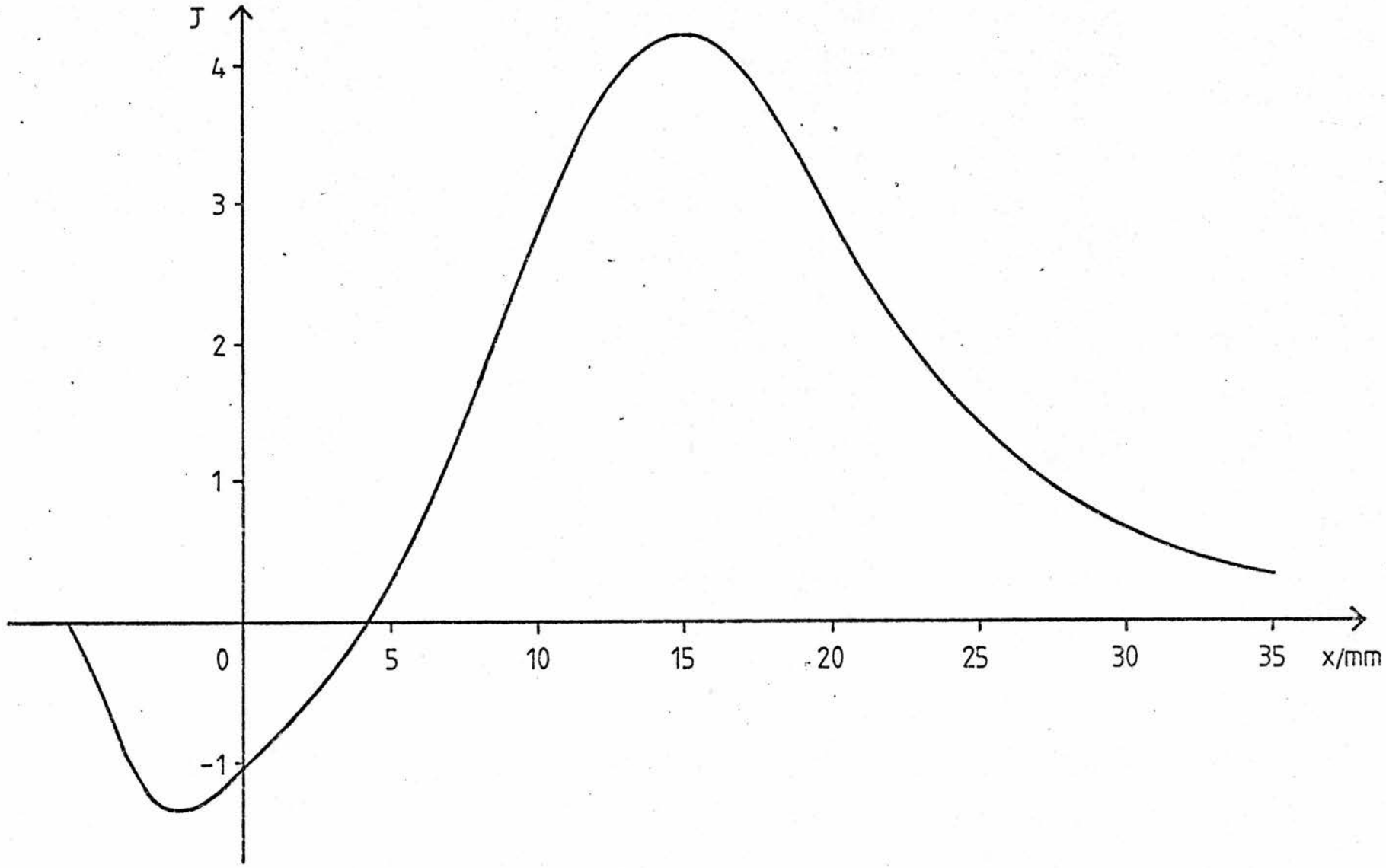

Figure 5.15

Undamped current density profile in the relativistic case for the O mode with parameters D, and $n_z = 0.1$. The units of current density are arbitrary.

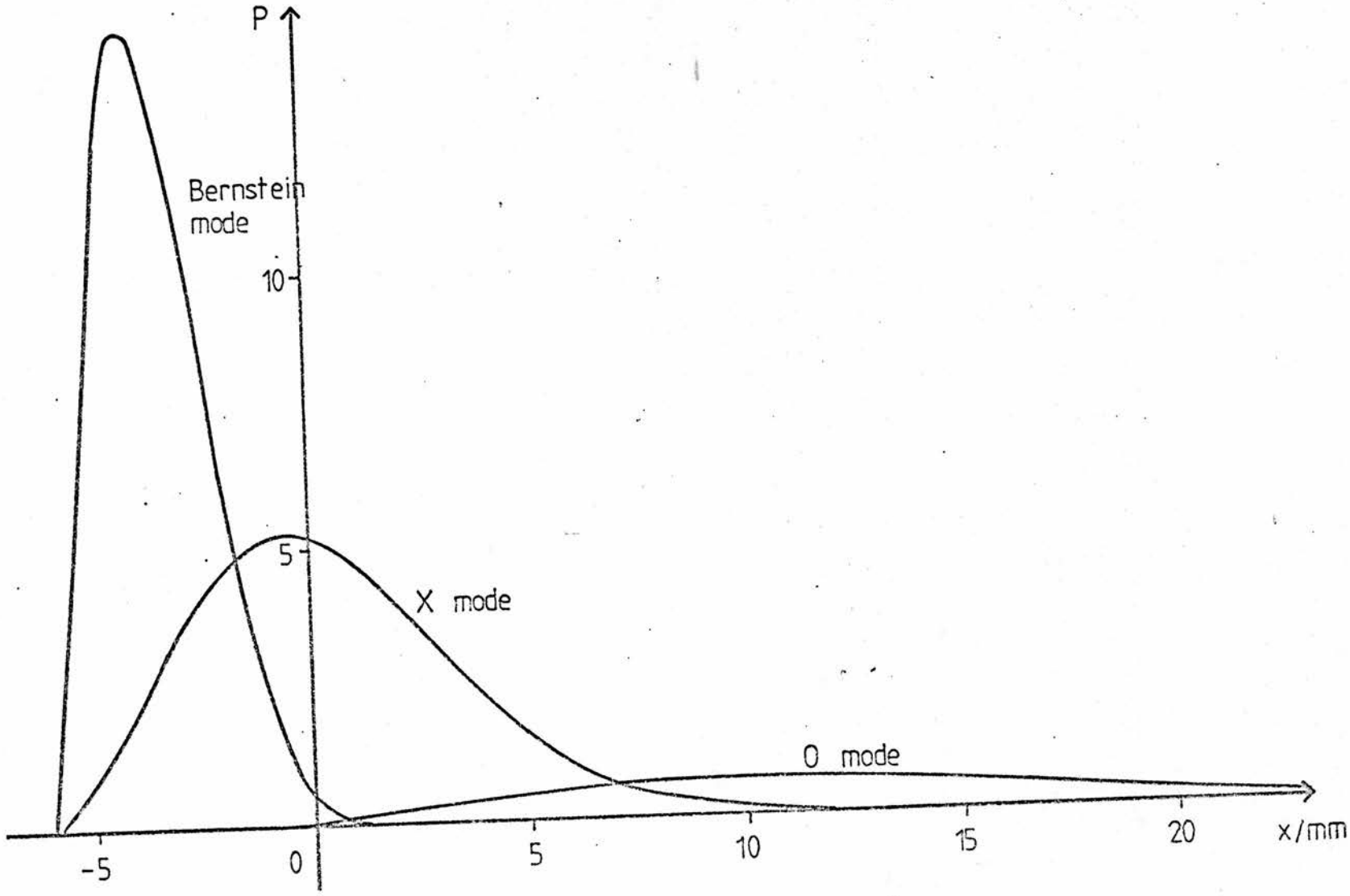

Figure 5.16

Power density profiles in the relativistic case for incidence from the low field side with parameters D, and $n_z = 0.1$. The units of power density are arbitrary.

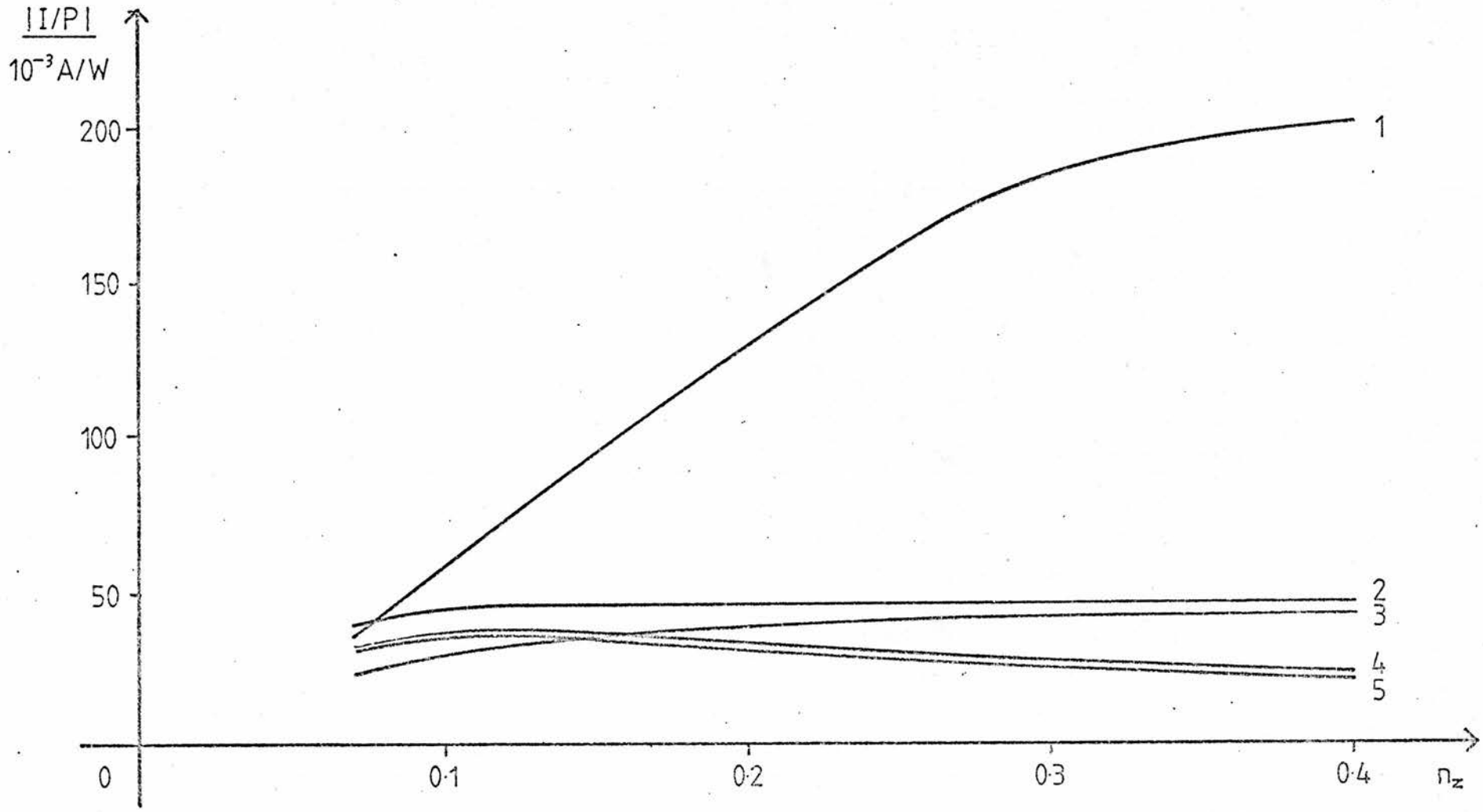

Figure 5.17

Current drive efficiency as a function of n_z in the relativistic case with parameters D.
Curve 1 refers to the Bernstein mode incident from the low field side.
Curves 2 and 3 refer to the X mode incident from the high and low field sides.
Curves 4 and 5 refer to the O mode incident from the high and low field sides.

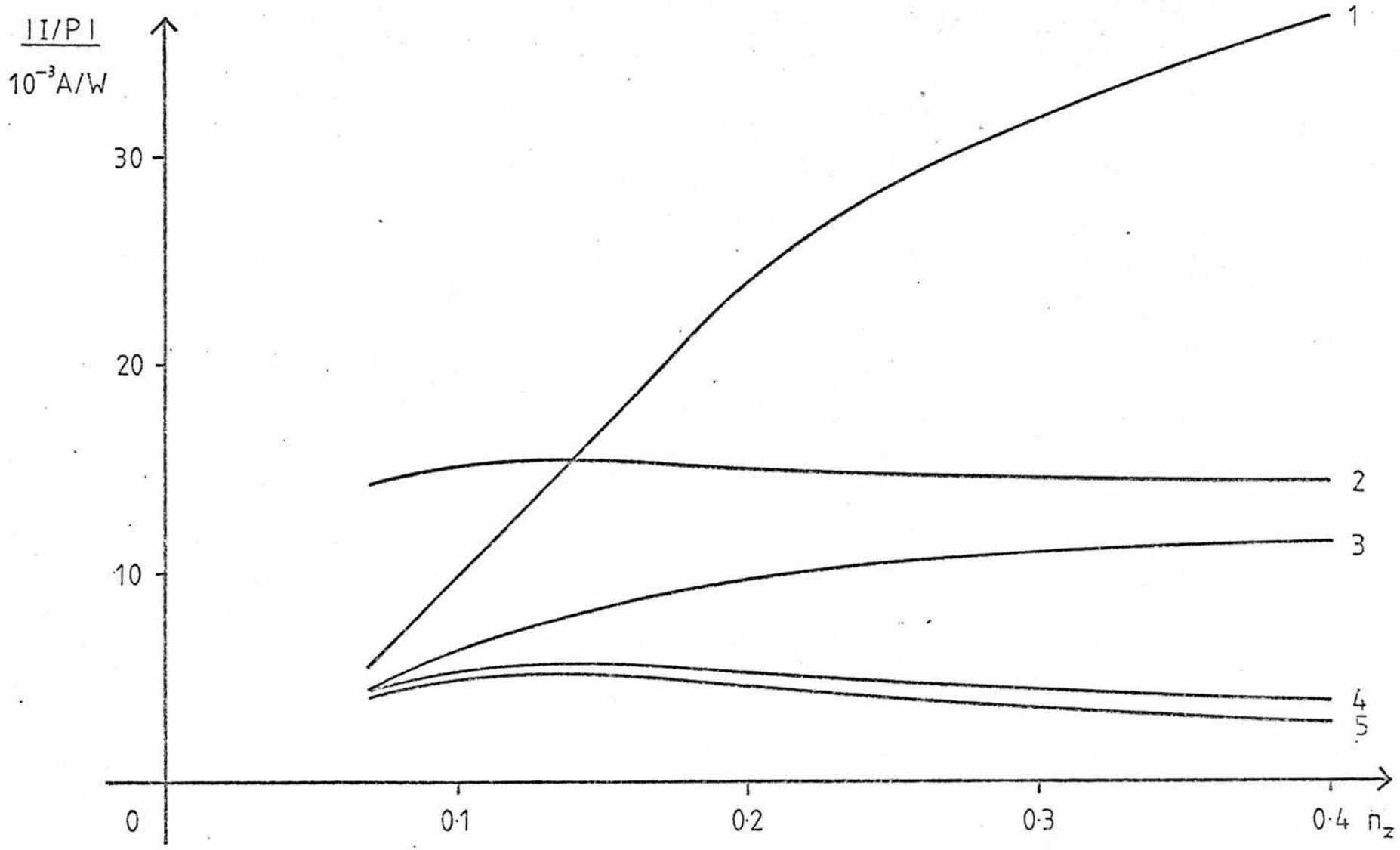

Figure 5.18

Current drive efficiency as a function of n_z in the relativistic case with parameters E. The numbering of the curves is the same as in Fig. 5.17.

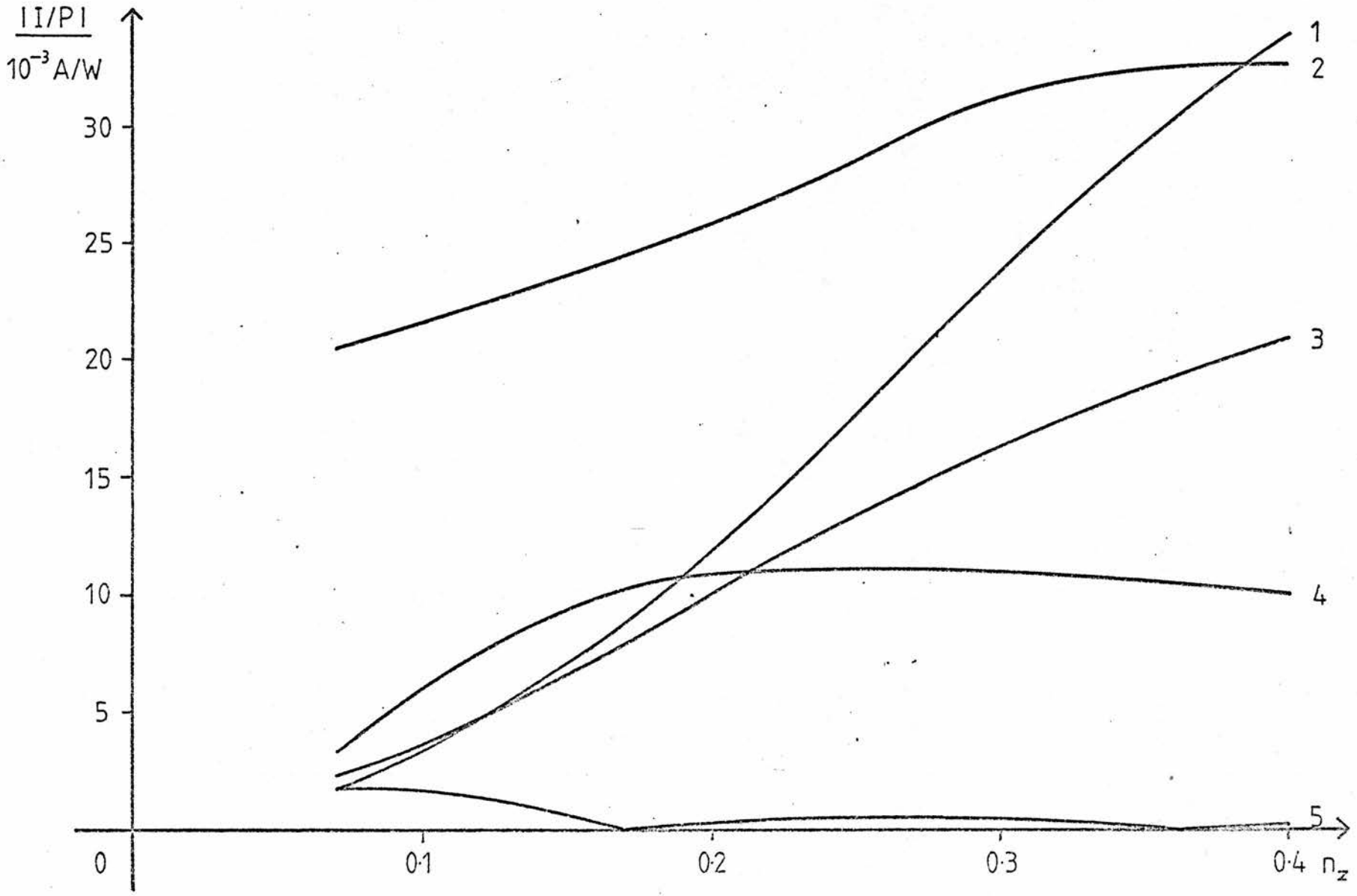

Figure 5.19

Current drive efficiency as a function of n_z in the relativistic case with parameters F. The numbering of the curves is the same as in Fig. 5.17.

can propagate from either the low or high field sides and results are given for each of these cases. As we saw in Chapter 3, a special combination of circumstances is required for the excitation of the Bernstein mode. In order to simplify matters, we ignore the question of whether or not the Bernstein mode can actually be excited for a given set of parameters. We then make the assumption that it has been excited on the low field side of the resonance, at or beyond the low field cut-off, and is propagating towards the resonance point. The results would be quite different if it was excited on the high field side of the resonance, in which case the current drive efficiency would be much higher.

The O mode is so weakly absorbed that the current and power profiles are virtually the same for incidence from the low and high field sides. This means that the current drive efficiencies will be the same. This is seen in Figs. 5.17 and 5.18. For parameters F, however, the absorption is sufficient to cause asymmetry, but not sufficient to prevent a substantial reverse current. Curve 5 in Fig. 5.19 shows the cancelling effect of the reverse current.

The results for the X mode are qualitatively similar to those for the O mode at the fundamental. The absorption of the X mode decreases with n_z, as does that of the O mode at the fundamental, and so the interpretation of the behaviour of current drive efficiency with n_z is the same. The only difference is that the absorption of the X mode is sufficient to prevent a significant reverse current, even for parameters D, so that incidence from the high field side is more efficient for all three sets of parameters.

For the Bernstein mode, the increase in current drive efficiency with n_z is simply due to absorption at a greater distance from the resonance on the low field side. The variation of absorption with n_z is not important since the absorption is total and is complete within a short distance (see Fig. 5.16).

It is appropriate to note here that a factor of $(v_\perp/v_t)^{2(n-1)}$ has been omitted from equation (33) after the $\frac{e^2 v_\perp}{4m^2}$ term. This means that at the second harmonic the current driven and power absorbed have been underestimated for large velocities. This will not affect the qualitative behaviour of the results.

CHAPTER 6

Validity of the Linear Approximation

In the Lorentz gas model, which gives current drive results proportional to ours, it is assumed that there is a balance between the effects of external waves and particle collisions on the distribution function, i.e.

$$\left(\frac{\partial f}{\partial t}\right)_W + \left(\frac{\partial f}{\partial t}\right)_C = 0$$

where

$$\left(\frac{\partial f}{\partial t}\right)_W = \frac{1}{v_\perp}\frac{\partial}{\partial v_\perp}\left\{\frac{e^2 v_\perp}{4m^2}\left|E^- + \frac{k_x v_z}{\Omega}E_z\right|^2 \delta\left(\omega - k_z v_z - \Omega\left(1 - \frac{1}{2}\frac{v^2}{c^2}\right)\right)\frac{\partial f}{\partial v_\perp}\right\}.$$

In the linear approximation, we write $f = f_0 + f_1$ where f_0 is the equilibrium electron distribution (taken to be Maxwellian) and f_1 is assumed to be a small perturbation. We then replace f by f_0 in the above expression for $\left(\frac{\partial f}{\partial t}\right)_W$. This expression may be rewritten as

$$\left(\frac{\partial f}{\partial t}\right)_W = \frac{\alpha}{v_\perp}\frac{\partial}{\partial v_\perp}\left\{\left[D_1 + D_2\frac{k_z v_z}{\Omega} + D_3\left(\frac{k_z v_z}{\Omega}\right)^2\right]\delta(\Delta\omega - k_z v_z) v_\perp \frac{\partial f_0}{\partial v_\perp}\right\}$$

where $\Delta\omega = \omega - \Omega(1 - \frac{1}{2}v^2/c^2)$, $\alpha = \frac{e^2|E_y|^2}{(2m)^2}$, and D_1, D_2 and D_3 are diffusion constants depending on the elements of the dielectric tensor.

Now, as before, $f_1 = \frac{v^3}{\nu_0 v_t^3}\left(\frac{\partial f}{\partial t}\right)_w$, so it can be seen that the perturbation f_1 is singular, because of the $\delta(\Delta\omega - k_z v_z)$ term in $\left(\frac{\partial f}{\partial t}\right)_w$. Thus, regardless of the value of α (which is proportional to the radio frequency power), it is difficult to justify the assumption that f_1 is small.

In practice, however, the wave will not be monochromatic, so there will be a spectrum of k_z values. All quantities of interest will then simply be integrated over this spectrum. Then $f_1 = \int \frac{v^3}{\nu_0 v_t^3}\left(\frac{\partial f}{\partial t}\right)_w S(k_z)dk_z$, where $S(k_z)$ gives the distribution of injected power over the k_z spectrum. For simplicity we take $S(k_z)$ to be a normalised step function, i.e.

$$S(k_z) = \begin{cases} \frac{1}{k_2 - k_1} & k_1 \leq k_z \leq k_2 \\ 0 & \text{otherwise} \end{cases}.$$

In order to evaluate f_1, we change coordinates to v and ξ where $\xi = \frac{v_z}{v}$. We get

$$f_1 = \int \frac{v^3}{\nu_0 v_t^3}\left\{\frac{\alpha(1-\xi^2)}{v}\frac{\partial}{\partial v}\left[\left(D_1 + D_2\frac{k_z v\xi}{\Omega} + D_3\left(\frac{k_z v\xi}{\Omega}\right)^2\right)\delta(\Delta\omega - k_z v\xi)\, v\,\frac{\partial f_0}{\partial v}\right]\right.$$

$$\left. - \frac{\xi\alpha}{v}\frac{\partial}{\partial\xi}\left[\left(D_1 + D_2\frac{k_z v\xi}{\Omega} + D_3\left(\frac{k_z v\xi}{\Omega}\right)^2\right)\delta(\Delta\omega - k_z v\xi)(1-\xi^2)\,\frac{\partial f_0}{\partial v}\right]\right\} S(k_z)dk_z$$

$$f_1 = \int_{k_1}^{k_2} \left\{ \beta v^2 (1-\xi^2) \frac{\partial}{\partial v} \left[\left(D_1 + D_2 \frac{k_z v\xi}{\Omega} + D_3 \left(\frac{k_z v\xi}{\Omega} \right)^2 \right) \delta(\Delta\omega - k_z v\xi) \nu \frac{\partial f_0}{\partial v} \right] \right.$$

$$\left. - \beta v^2 \xi \frac{\partial}{\partial \xi} \left[(1-\xi^2) \frac{\partial f_0}{\partial v} \left(D_1 + D_2 \frac{k_z v\xi}{\Omega} + D_3 \left(\frac{k_z v\xi}{\Omega} \right)^2 \right) \delta(\Delta\omega - k_z v\xi) \right] \right\} \frac{dk_z}{k_2 - k_1} \tag{52}$$

where $$\beta = \frac{\alpha}{v_t^3 \nu_0} .$$

Now

$$\int_{k_1}^{k_2} \left(D_1 + D_2 \frac{k_z v\xi}{\Omega} + D_3 \left(\frac{k_z v\xi}{\Omega} \right)^2 \right) \delta(\Delta\omega - k_z v\xi)\, dk_z = \frac{D}{|v\xi|}$$

where $D = D_1 + D_2 \frac{\Delta\omega}{\Omega} + D_3 \left(\frac{\Delta\omega}{\Omega} \right)^2$, provided that there is a value of k_z in $[k_1, k_2]$ such that $\Delta\omega = k_z v\xi$. If there is not, then the resonance condition is not satisfied, and f_1 is identically zero. Henceforth we assume that there is such a value of k_z. Then

$$f_1 = \frac{\beta v}{k_2 - k_1} \left[\frac{v(1-\xi^2)}{|\xi|} \frac{\partial}{\partial v} \left(\frac{\partial f_0}{\partial v} D \right) - \xi \frac{\partial f_0}{\partial v} \frac{\partial}{\partial \xi} \left(\frac{1-\xi^2}{|\xi|} D \right) \right]. \tag{53}$$

Now we use $f_0 = \frac{n_0}{(2\pi v_t^2)^{3/2}} e^{-v^2/2v_t^2}$ to obtain

$$f_1 = \frac{\beta v}{|\xi|(k_2 - k_1)} \frac{\partial f_0}{\partial v} \left[v(1-\xi^2) \left(- \frac{v}{v_t^2} D + D_2 \frac{v}{c^2} + 2D_3 \frac{\Delta\omega}{\Omega} \frac{v}{c^2} \right) + (1+\xi^2) D \right].$$

Then

$$\frac{f_1}{f_0} = \frac{-\beta v^2}{|\xi|(k_2-k_1)v_t^2}\left[(1-\xi^2)\left(-\frac{v^2}{v_t^2}D + D_2\frac{v^2}{c^2} + 2D_3\frac{\Delta\omega}{\Omega}\frac{v^2}{c^2}\right) + (1+\xi^2)D\right]. \tag{54}$$

Results are presented in Table 6.1 for parameters A of Chapter 5. We specify a central value of n_z and an angular spread in the wave of about 10°, which corresponds to $n_{z2} - n_{z1} = 0.17$. A value for $|E_y|^2$ of $5 \times 10^8 V^2 m^{-2}$ is specified, which corresponds to a power density of about 1 $kW cm^{-3}$. This is typical of present day tokamaks. The ratio in (54) is calculated for several values of x and v/v_t. The required value of ξ is obtained from the resonance condition, using the central value of n_z. If the magnitude of f_1/f_0 is small, then the linear approximation may be said to have been justified.

Table 6.1

Values of $|f_1|/f_0$ for parameters A with the O mode, $n_z = 0.17$, $n_{z1} = 0.09$ and $n_{z2} = 0.26$

v/v_t \ x	-0.01	-0.005	-0.001	0	0.001	0.005	0.01
0.5	-	-	4.60	16.7	7.02	-	-
1.0	-	20.3	6.49	3.12	22.0	1.13	29.3
2.0	114	122	167	195	249	5120	526

We point out that since the Lorentz gas model overestimates the current driven by a factor of $\frac{5+Z_i}{Z_i}$, we expect f_1 to be similarly overestimated. Also, when a full Fokker-Planck model is used, the resonance is broadened, so that (32) only needs to be satisfied approximately for there to be resonance. The effect of the waves is then spread over a greater region of velocity space, and this will reduce the value of f_1 for any particular point in velocity space.

Even so, we find that nowhere is f_1/f_0 small. f_0 is proportional to $e^{-v^2/2v_t^2}$, so for large values of v/v_t, a large value of f_1/f_0 is not important since the number of perturbed electrons will be very small. For $v/v_t \approx 2$, however, there will still be a significant number of resonant electrons, and these fast particles are most efficient for current drive, so that the large perturbation to f_0 cannot be ignored in this case.

We conclude that although we expect the qualitative features of our current drive results to be correct, the actual numbers cannot be relied on with any accuracy for conditions of interest in tokamaks.

CHAPTER 7

SUMMARY

This thesis has been concerned with the effect of the relativistic correction to the electron mass on ECRH current drive. In the introduction it was said that there has been a lot of experimental and theoretical work on ECRH, especially with the advent of the gyrotron. The reason for this is that ECRH has a number of advantages over other electromagnetic heating schemes. The interest in ECRH current drive is rather more recent, arising from the paper by Fisch and Boozer (1980) in which it was originally proposed. A number of theoretical studies were made and ECRH current drive was obtained experimentally. It was noted that the importance of relativistic effects on ECRH was well recognised. However, little or no work had been done on the corresponding relativistic effect on ECRH, namely the relativistic variation of the electron mass. The aim of the thesis, then, was to investigate the effect qualitatively, illustrating the theory with representative numerical results.

It was first necessary to investigate the propagation and absorption of electromagnetic waves by solving the relativistic dispersion relation. This relation is generally given in terms of the dielectric tensor. The relativistic form of the dielectric tensor was given by Trubnikov (1959), but his expression for it was exceedingly complicated. This expression was simplified in the weakly relativistic limit at and near electron cyclotron harmonics by Shkarofsky (1966), who used

a small Larmor radius approximation. He expressed the elements of the dielectric tensor in terms of a $\mathcal{F}_q$ function. This function was the subject of Chapter 2.

It was found that the $\mathcal{F}_q$ function was not well suited to direct numerical computation. This was because it involved an integral over an infinite range of an integrand which was oscillating rapidly. Further simplification was therefore desirable. Subject to certain conditions, Shkarofsky obtained what is referred to as the "tractable" expression for $\mathcal{F}_q$. Airoldi and Orefice (1982) showed that this expression is sufficient to obtain the most general dielectric tensor without any limitations. The expression was then used as a starting point for three methods of evaluating $\mathcal{F}_q$. The first of these was obtained by Krivenski and Orefice (1983). It involved simple expressions for $\mathcal{F}_{1/2}$ and $\mathcal{F}_{3/2}$ in terms of the plasma dispersion function and a recurrence relation with which $\mathcal{F}_q$ functions of higher order are obtained. It was found that the expressions for $\mathcal{F}_{1/2}$ and $\mathcal{F}_{3/2}$ were accurate, but that the use of the recurrence relation gave rise to numerical problems for small values of n_z. Two other methods were therefore given for use with small values of n_z. The first, which is valid for very small values of n_z, expresses $\mathcal{F}_q$ in terms of the F_q function of Dnestrovskii *et al.* (1964). The second method uses an infinite series of terms involving the F_q function.

As a test on the above three methods, a means of calculating $\mathcal{F}_q$ directly, using Simpson's rule, was given. Simpson's rule was also used in the case where $\mathcal{F}_q$ can be turned into a real integral.

Finally, the non-relativistic limit of $\mathcal{F}_q$ was given and some notes were made on the computation of $\mathcal{F}_q$ and its derivatives.

In Chapter 3, the relativistic dispersion relation was solved at the fundamental frequency and at the second harmonic. First of all, the small Larmor radius approximation was applied to the elements of the dielectric tensor as given by Shkarofsky, so that some simplification was possible. The non-relativistic limit of the dielectric tensor elements was also given.

At the fundamental frequency the dispersion relation becomes a quadratic equation for n_x^2, one root of which corresponds to the O-mode, and the other to the X-mode. It was found that for the Appleton-Hartree dispersion relation for a cold plasma, n_x is greater for the X-mode. This fact was used to distinguish the O and the X modes in our case of a hot plasma. Some dispersion curves were plotted, both for the relativistic and non-relativistic cases. It was noted in the relativistic case that absorption can only occur on the high field side of a particular point, known as the low field cut-off point. Limitations on the propagation of waves through the plasma were briefly mentioned. The variation with density of the absorption of the O and X modes was investigated and the results were found to be in agreement with those of other authors.

At the second harmonic the dispersion relation becomes a quartic equation for n_x^2. One of the roots was however ignored, leaving three roots which corresponded to the O, X and Bernstein modes. Dispersion curves were plotted for the three modes in the

relativistic case. The absorption of the X mode was found to be much stronger than that of the O mode. The Bernstein mode is the most strongly damped, since it propagates only on the low field side of the resonance. The possibility of coupling between the X and Bernstein modes was noted and the critical density at which this can take place was plotted.

Chapter 4 was concerned with ECRH current drive theory and the calculation of current drive efficiency. The mechanism for preferential heating of electrons was described and the non-relativistic resonance condition was then used to show how a current could arise. This would only happen in the case of strong wave damping. The relativistic resonance condition was considered next. Many features were evident simply from a graph of the resonant velocities against distance. There was, first of all, confirmation of a low field cut-off point beyond which wave absorption is not possible. More importantly, it was evident that the resonance condition is strongly asymmetric. The implications of this for current drive were discussed. The non-relativistic resonance condition was plotted on the same graph so that the conditions under which the relativistic correction is important could be seen.

The current drive calculation was then presented. The theory of Fisch and Boozer gives the current to power ratio in terms of $\left(\frac{\partial f}{\partial t}\right)_w$, for which the standard quasilinear diffusion term of Kennel and Engelmann is used. It was shown that the Lorentz gas model gives the same current to power ratio apart from a constant factor.

The details of the calculation were then given. Current and power densities at a particular point were found and these were then integrated through the resonance layer to find the total current driven and total power absorbed. The ratio of these was multiplied by a conversion factor to give the final result for current drive efficiency in terms of Amps per Watt.

Chapter 5 outlined the program that has been developed for calculating current drive and presented results obtained with it. The resonance region was defined and the current drive and power densities are integrated over 40 points in this region. Several approximations that have been made in the calculation were noted. At the fundamental, current density profiles were compared with the corresponding non-relativistic profiles. Power profiles were plotted and it was noted that the current and power profiles are shifted with respect to one another because of the fact that the current to power ratio increases away from resonance. Relativistic and non-relativistic power profiles were compared and it was shown that the inclusion of the relativistic correction significantly shifts the position of the current layer. Results for current drive efficiency versus angle of incidence were presented. Incidence from the high field side was found to give a higher efficiency in almost all cases.

At the second harmonic, similar results are presented for the relativistic case, but with the addition of the Bernstein mode incident from the low field side, and the X mode incident from the high field side. The O mode absorption is so weak that it is of no

interest for current drive. Of the others, the Bernstein mode gives the higher efficiency for propagation from the low field side.

In Chapter 6, the validity of the linear approximation was questioned. It was shown that for a monochromatic wave, the perturbation to the electron distribution function is singular. In practice there will be a spectrum of wave numbers, k_z, but the question remains as to whether the perturbation, f_1, is small compared to the equilibrium distribution function f_0. The ratio of these two quantities was taken, as a measure of the validity of the linear approximation. The results show that, for power densities typical of present day tokamaks, f_1 is in general much greater than f_0, thus making the linear approximation invalid.

Conclusions

We have shown that the relativistic correction to the electron mass affects ECRH current drive in a number of important ways. Firstly the resonance condition is now asymmetric. This means that the total current depends strongly on which side the wave is incident from. Also, in the case of weak absorption, currents on opposite sides of the resonance point no longer cancel. Secondly, there is a low field cut-off point beyond which no resonance is possible. This means that for incidence from the low field side the wave is resonant first of all with electrons in the bulk of the distribution which are ineffective for current drive. Finally, the scaling of the current to power ratio and resonant velocities with distance is changed,

allowing absorption at a greater distance than in the non-relativistic theory. This means that the position of the current layer will be significantly changed when the wave is strongly damped. We have also shown that, for power densities of interest, the linear approximation generally used for current drive calculations is not valid. This does not affect the qualitative conclusions, which follow from the resonance condition.

Further Work

As we have seen, the effects of the relativistic correction are important, and the correction must be included in any comprehensive model of ECRH current drive. As mentioned in the introduction, there are a number of other effects that have been included by other authors, namely trapped electrons, toroidal geometry, and relativistic dynamics. It would also be desirable to have self-consistent density and temperature profiles, and to use a full Fokker-Planck model (rather than one based on the high velocity limit, as we have used). The eventual aim, then, would be to carry out a nonlinear calculation, taking into account all the above effects. This has still to be done.

APPENDIX

Behaviour of the integrand of F_q for large t

We are interested primarily in the behaviour of the exponential part of the integrand in (2), that is

$$\exp \mu\left\{1 - [(1-it)^2 + n_z^2 t^2]^{\frac{1}{2}} - in\frac{\Omega}{\omega} t\right\} = \exp \mu\alpha(t), \text{ say}$$

$$\alpha(t) = 1 - \left[1 - t^2 - 2it + n_z^2 t^2\right]^{\frac{1}{2}} - in\frac{\Omega}{\omega} t$$

$$= 1 - t\left[\frac{1}{t^2} - 1 - \frac{2i}{t} + n_z^2\right]^{\frac{1}{2}} - in\frac{\Omega}{\omega} t$$

$$= 1 + it(1-n_z^2)^{\frac{1}{2}}\left[1 + \frac{2i}{t(1-n_z^2)} - \frac{1}{t^2(1-n_z^2)}\right]^{\frac{1}{2}} - in\frac{\Omega}{\omega} t.$$

We now expand the square root to order $\frac{1}{t}$.

$$\therefore \lim_{t\to\infty} \alpha(t) = 1 + it(1-n_z^2)^{\frac{1}{2}}\left[1 + \frac{i}{t(1-n_z^2)}\right] - in\frac{\Omega}{\omega} t$$

$$\lim_{t\to\infty} \alpha(t) = it\left[(1-n_z^2)^{\frac{1}{2}} + n\frac{\Omega}{\omega}\right] + 1 - \frac{1}{(1-n_z^2)^{\frac{1}{2}}}.$$

We draw two conclusions from this. Firstly, the real part of $\alpha(t)$ tends to a constant as $t \to \infty$, so there is no exponential decay of the integrand. Secondly, the substitution $y = -it$ will give exponential decay of the integrand if and only if $n\frac{\Omega}{\omega} < (1 - n_z^2)^{\frac{1}{2}}$.

REFERENCES

A C Airoldi and A Orefice (1982), *J. Plasma Phys.* 27, 515.

V V Alikaev, G A Bobroviskii, V I Poznyak, K A Razumova, V V Sannikov, Yu A Sokolov and A A Shmarin (1976), *Sov. J. Plasma Phys.* 2, 212.

V V Alikaev *et al.* (1978), "Heating on Toroidal Plasmas" (T Consoli, ed), Vol II, 339, Pergamon Press, Oxford.

T Antonsen and W M Manheimer (1978), *Phys. Fluids* 21, 2295.

V Arunasalam, P C Efthimion, J C Hosea, H Hsuan and G Taylor (1983), Princeton Plasma Physics Laboratory Report, PPPL-1986.

J M Berger *et al.* (1958), *Phys. Fluids* 1, 301.

R J Bickerton (1979), "Physics of Plasmas close to Thermonuclear Conditions", Varenna, Vol II, 725, published for the Commission of the European Communities by Pergamon Press, Oxford, 1981.

M Bornatici and F Engelmann (1979), *Radio Sci.* 14, 309.

M Bornatici, F Engelmann, C Maroli and V Petrillo (1981), *Plasma Phys.* 23, 229.

R A Cairns, J A Owen and C N Lashmore-Davies (1983), *Phys. Fluids* 26, 3475.

E Canobbio (1975), Proc. 5th Int. Conf. on Plasma Phys. and Contr. Nuclear Fusion Research, Tokyo, Vol III, 333, IAEA, Vienna.

V S Chan, S C Chiu, J Y Hsu and S K Wong (1982), *Nucl. Fusion* 22, 787.

J G Cordey, T Edlington and D F H Start (1982), *Plasma Phys.* 24, 73.

Yu N Dnestrovskii, D P Kostomarov and N V Skrydlov (1964), *Sov. Phys. - Tech. Phys.* 8, 691.

T Edlington, J G Cordey, M R O'Brien and D F H Start (1982), Proc. 3rd Joint Varenna-Grenoble Int. Symp. on Heating in Toroidal Plasmas, Grenoble, Vol III, 869.

O C Eldridge (1980), Oak Ridge National Laboratory Report, ORNL/M-7503.

Equipe TFR (1980), Proc. 8th Int. Conf. on Plasma Phys. and Contr. Nuclear Fusion Research, Brussels, Paper CN-38/D-3, IAEA, Vienna.

H Eubank *et al.* (1979), Proc. 7th Int. Conf. on Plasma Phys. and Contr. Nuclear Fusion Research, Innsbruck, Vol I, 167, IAEA, Vienna.

I Fidone, G Granata, G Ramponi and R L Meyer (1978), *Phys. Fluids* 21, 645.

I Fidone, G Granata and R L Meyer (1982), *Phys. Fluids* 25, 2249.

P J Fielding (1981), "Plasma Physics and Nuclear Fusion Research" (R D Gill, ed), 487, Academic Press, London.

N J Fisch (1978), *Phys. Rev. Lett.* 41, 873.

N J Fisch (1980), Proc. 2nd Joint Varenna-Grenoble Int. Symp. on Heating in Toroidal Plasmas, Como, Vol II, 1157.

N J Fisch and A H Boozer (1980), *Phys. Rev. Lett.* 45, 720.

N J Fisch (1981), *Phys. Rev. A* 24, 3245.

B D Fried and S D Conte (1961), "The Plasma Dispersion Function", Academic Press, New York.

H P Furth and S Yoshikawa (1970), *Phys. Fluids* 13, 2593.

V L Ginzburg (1964), "The Propagation of Electromagnetic Waves in Plasmas", Pergamon Press, Oxford.

J Hosea *et al.* (1980), Proc. 8th Int. Conf. on Plasma Phys. and Contr. Nuclear Fusion Research, Brussels, Paper CN-38/D-5-1, IAEA, Vienna.

J Y Hsu, V S Chan and F W McClain (1983), *Phys. Fluids* 26, 3300.

B Hui, K R Chu, E Ott and T Antonsen (1980), *Phys. Fluids* 23, 822.

INTOR Group (1982), International Tokamak Reactor : Phase One, Vienna 1980-81, 11, IAEA, Vienna.

H Jory *et al.* (1980), Proc. 2nd Joint Varenna-Grenoble Int. Symp. on Heating in Toroidal Plasmas, Como, Vol I, 269.

C F F Karney and N J Fisch (1981), *Nucl. Fusion* 21, 1549.

C F Kennel and F Engelmann (1966), *Phys. Fluids* 9, 2377.

V Krivenski and A Orefice (1983), *J. Plasma Phys.* 30, 125.

C N Lashmore-Davies, R A Cairns and J A Owen (1982), Culham Laboratory Report, CLM-R225.

E Lazzaro and A Orefice (1980), *Phys. Fluids* 23, 2330.

E Lazzaro and G Ramponi (1981), *Plasma Phys.* 23, 53.

D J Lees *et al.* (1972), Proc. 5th Euro. Conf. on Contr. Fusion and Plasma Phys., Grenoble, Vol II, 135.

W M Manheimer and V L Granatstein (1977), N.R.L. Memorandum Report 3493, Washington DC.

W M Manheimer (1979), "Infrared and Millimeter Waves" (K Button, ed), Vol 2, 299, Academic Press.

T Ohkawa (1970), *Nucl. Fusion* 10, 185.

F Parlange *et al.* (1978), "Heating in Toroidal Plasmas" (T Consoli, ed), Vol II, 183, Pergamon Press, Oxford.

J W M Paul, K B Axon, J Burt, A D Craig, S K Erents, S J Fielding, D H J Goodall, R D Gill, R S Hemsworth, M Hobby, J Hugill, G M McCracken, A Pospieszczyk, B A Powell, R Prentice, G W Reid, P E Stott, D D R Summers and C M Wilson (1976), 6th IAEA Conf. on Plasma Phys. and Contr. Nuclear Fusion Research, Bertchesgaden, Vol 2, 269, IAEA, Vienna, 1977.

N J Peacock *et al.* (1969), *Nature* 224, 448.

M Roberts (1979), Proc. 9th Euro. Conf. on Plasma Phys. and Contr. Nuclear Fusion Research, Vol 2, 197.

D C Robinson (1981), "Plasma Physics and Nuclear Fusion Research" (R D Gill, ed), 373, Academic Press, London.

J J Schuss *et al.* (1979), *Phys. Rev. Lett.* 43, 274.

I P Shkarofsky (1966), *Phys. Fluids* 9, 561.

D F H Start, N R Ainsworth, J G Cordey, T Edlington, W H W Fletcher, M F Payne and T N Todd (1982), *Phys. Rev. Lett.* 48, 624.

D F H Start and M R O'Brien (1982), Culham Laboratory Report, CLM-R225.

D F H Start, M R O'Brien and P M V Grace (1983), *Plasma Phys.* 25, 1431.

T H Stix (1975), *Nucl. Fusion* 15, 737.

V S Strelkov (1979), Proc. 9th Euro. Conf. on Contr. Fusion and Plasma Phys., Oxford.

N Suzuki *et al.* (1980), Proc. 8th Int. Conf. on Plasma Phys. and Contr. Nuclear Fusion Research, Brussels, Paper CN-38/T-2-3.

B A Trubnikov (1959), "Plasma Physics and the Problem of Controlled Thermonuclear Reactions" (M A Leontovich, ed), Vol III, 122, Pergamon Press, New York.

H Weitzner and D B Batchelor (1978), Oak Ridge National Laboratory Report, ORNL/TM-6462.

K-L Wong *et al.* (1980), *Phys. Rev. Lett.* 45, 117.

D J H Wort (1971), *Plasma Phys.* 13, 258.

T Yamamoto *et al.* (1980), *Phys. Rev. Lett.* 45, 716.